ULTRASENSITIVE MICROWAVE PLANAR METAMATERIAL SENSORS FOR MATERIALS CHARACTERIZATION

A Dissertation
Presented to
The Academic Faculty

by

Salem Ali Abdullah Alotaibi

In Partial Fulfillment
of the Requirements for the Degree
Doctor of Philosophy in the
School of Electrical and Computer Engineering

Georgia Institute of Technology
May 2020

ULTRASENSITIVE MICROWAVE PLANAR METAMATERIAL SENSORS FOR MATERIALS CHARACTERIZATION

Approved by:

Prof. Manos M. Tentzeris, Advisor
School of Electrical and Computer Engineering
Georgia Institute of Technology

Prof. Andrew F. Peterson
School of Electrical and Computer Engineering
Georgia Institute of Technology

Prof. Gregory D. Durgin
School of Electrical and Computer Engineering
Georgia Institute of Technology

Prof. Waymond Scott
School of Electrical and Computer Engineering
Georgia Institute of Technology

Prof. Karim Sabra
The George W. Woodruff School of Mechanical Engineering
Georgia Institute of Technology

Date Approved: February 18, 2020

To my beloved mother, the memory of my father,

my wonderful wife and the rest of my family

ACKNOWLEDGMENTS

All praise is to Allah (SWT), Lord of the Heavens and the Earths, and what they contain; most Beneficial, Most Merciful. I seek His benediction on our beloved Prophet, the best of humankind, Muhammad (SAW), his household and his companions, until the Day of Judgment. I thank Allah for His infinite bounties on me, one of which is the completion of this work; I seek His mercy and forgiveness, and indeed, I fear His wrath.

My gratitude, without reservation, goes to my mother for her endless support and prayers throughout my life. I will forever remain grateful.

I would like to convey my sincere gratitude to my advisor Prof. Manos M. Tentzeris for his support and guidance. I thank him for being available whenever I needed his assistance, and for being an exceptional advisor who helps each of his group members not to only perform his research but to be an independent researcher who is self-driven and who faces his future career with sharp research skills and boldness. Special thanks to the distinguished committee members Prof. Andrew F. Peterson and Prof. Gregory D. Durgin first, for accepting to be on my PhD committee, further, for their useful guidance, motivation, and professional contribution to my success and that of this work. I would like also to thank the other PhD exam committee members Prof. Waymond Scott and Prof. Karim Sabra for their positive comments.

Special thanks to the members of ATHENA research group for their support, friendship and fruitful discussions; my friends for their best wishes and help; and my sponsor Saudi Aramco, for the opportunity it gave me to study and accomplish this work.

I owe my deepest gratitude to my family for the continuous prayers and encouragement. Finally, special thanks to my wife who joined me in the middle of my PhD journey, for her unconditional support, companionship and sacrifices that eased the whole journey. To all, I remain grateful.

TABLE OF CONTENTS

LIST OF TABLES

LIST OF FIGURES

LIST OF SYMBOLS AND ABBREVIATIONS

MTL	Microstrip Line
CPW	Coplanar Waveguide
SNG	Single Negative
DNG	Double Negative
LH	Left Handed
SRR	Split Ring Resonator
CSRR	Complementary Split Ring Resonator
LH	Left Handed
RFID	Radio Frequency Identification
IoT	Internet of Things
MUT	Material Under Test
DGS	Defected Ground Structure
PCB	Printed Circuit Board
LCP	Liquid Crystal Polymer
VNA	Vector Network Analyzer

TEM	Transverse Electromagnetic
f_r	Resonance frequency
Δf_r	Shift in the resonance frequency
ε_0	The free space permittivity
μ_0	The free space permeability
$\Delta\varepsilon$	Change in the permittivity
$\Delta\mu$	Change in the permeability
$\mathbf{E_0}$	The original electric field
$\mathbf{H_0}$	The original magnetic field
$\mathbf{E}_1$	The perturbed electric field
$\mathbf{H}_1$	The perturbed magnetic field
$\boldsymbol{v}$	The perturbed volume
f_{MUT0}^{tmin}	The minimum transmission frequency with a 0-mm air gap
f_{free}^{tmin}	The free space minimum transmission frequency
Δf^{tmin}	The change in the minimum transmission frequency in GHz
$\Delta f^{tmin}\%$	The change in the minimum transmission frequency in %

L_{CSRR} The equivalent inductance of the loaded CSRR

C_{CSRR} The equivalent capacitance of the loaded CSRR

C_{MUT} The equivalent capacitance of the loaded MUT

SUMMARY

The objective of the proposed research is to design low power, miniaturized and ultrasensitive microwave transmission line based metamaterials, evaluate their performance then utilize them for bulk materials' constitutive parameters extraction and other practical applications with a narrower scope such as nondestructive and microfluidic sensing. Also, the research aims to introduce, model and verify a condition of sensitivity uniformity for permittivity and permeability sensors. Planar metamaterial-based sensors feature high measurement accuracy, excellent imaging capability, design simplicity and flexible design parameters. Moreover, one of their significant advantages is their compatibility with the printed circuit board (PCB) technology which eases their integration with passive and active microwave components. These features allow the designer to easily customize the sensor design to realize various sensing platforms that are suitable for a wide range of applications.

The research starts by revisiting the operational theory of CSRR based sensors to identify the influential factors that govern their performance. Then, the identified factors are going to be utilized to come up with sensing platforms with significantly improved and controlled sensitivity. As proof of concepts, the proposed platforms are going to be fabricated, tested and utilized for practical applications such as crack and microfluidic sensing.

CHAPTER 1. INTRODUCTION

1.1 Motivation

Future sensing networks will revolutionize numerous medical, agricultural and industrial applications. The envisioned role of these networks is to provide massive and instant data with high accuracy to big data processing units. Ambitious scientists and engineers strive to reshape current sensing networks based on the future demand and technology advancement by deploying millions of sensing spots that are synchronized and linked together to enable continuous and remote monitoring of several and crucial physical inputs. Examples of such inputs include but not limited to heartbeats of patients and elderlies, soil's moisture and fertility, corrosion rates and degradation of structural steels, toxic gas presence and spreading, instantaneousness weather conditions and global warming progression. In fact, traditional paradigms for the design and implementation of sensing networks are not going to be an option if the future Internet of Things (IoT) technology offers smart data acquisition, interpretation and immediate execution of necessary actions when needed. As the electrical and magnetic properties of materials are strong functions of the materials' configuration, electrical sizes, temperature and several other conditions, no doubt electromagnetic based sensors are going to be extensively utilized and will be indispensable elements in the future IoT technology.

IoT utilizes abundant spatially distributed sensing nodes that are linked to the processing unit(s) via predefined communication protocols. Each sensing node has its own controlled status which is a function of the interacting object/material properties and the node's sensing mechanism. Due to the expected huge amount of sensing nodes and the

finite network power, it is required to design each sensing node using a sensing platform that draws almost zero power from the interrogating signal [1]. Transmission line based metamaterials fulfill this requirement and consequently can be utilized as sensing nodes for IoT applications with high efficiency. The sensing node is the front end of any sensing network and almost the most vital element in the network. It affects the network integrity and suitability. Thus, such node should be thoroughly studied and properly design to attain the required performance.

This research utilizes a transmission line based metamaterials for the characterization of isotropic, low loss and nondispersive materials. One way to realize such metamaterial is to load microstrip line or coplanar waveguide with a substrate inclusion meta-resonator such as split ring resonator or a defected ground structure meta-resonator such as complementary split ring resonator. The following section provides a brief overview of metamaterials.

1.2 Metamaterials

Electromagnetic Metamaterial is an artificial structure with unusual properties that don't exist in nature [2]. An example of such structure includes a structure with negative permittivity, negative permeability or negative permittivity and permeability within RF and microwave frequency. A structure with negative permeability or negative permittivity is called a single negative (SNG) structure while one with negative permittivity and permeability is usually called double negative (DNG) or left-handed (LH) structure. LH materials were theoretically introduced in 1964 by the Russian physicist V. Veselago [3]. Three decades later a group of researchers was able to realize a 3D LH structure consisting

of conductive square split ring resonators and conductive wire strips deposited on fiberglass circuit board [4-5]. After that, two-dimensional metamaterial (widely known as planar metamaterials or metasurfaces) were realized using a meta-resonator loaded to conventional microwave transmission lines [6]. The introduction of such type of planar metamaterials was a remarkable advancement in the metamaterials field as it allows the realization of a metamaterial-based system using PCB technology and transmission lines. A transmission line based metamaterial is designed using a planar transmission line such as microstrip line (MTL) and Coplanar waveguide (CPW) loaded with a meta-resonator in the form of either defected ground structure (DGS) or surface substrate inclusion [7]. This structure can be utilized for various sensing applications as detailed in the next section.

1.3 Sensing with Transmission Line Based Metamaterials

The realization of planar metamaterials using planar transmission lines, allowed many researchers and engineers to utilize these metamaterials in different microwave devices such as passive filters, oscillators and phase shifters. They were also utilized for sensing applications due to their distinct features.

One of the advantages of a meta-resonator compared to conventional microwave resonator is that the earlier is an electrically small resonator and can be utilized for miniaturized systems. This implicitly means, at resonance meta-resonators store the resonating electrical and magnetic fields at a confined volume. These fields can interact with the electrically and/or magnetically close objects or fields and couple them to the resonating structure. Thus, the resonance frequency and the other associated resonance parameters change due to the presence of nearby samples which suggest that these types of

metamaterials can be utilized as microwave sensors. In 2012, a group of researchers utilized this type of metamaterials for the estimation of a dielectric sample's permittivity [8]. This research opened the door for others to utilize a similar type of sensors for the estimation of effective permittivity and permeability within specific sensing zones for a wide range of applications. Examples of such applications, include but not limited to microfluidic sensing, displacement and velocity estimation, crack detection and characterizations.

1.4 Problem Statement

Previous research in the field, focused more on the design and introduction of novel topologies of planar metamaterials for material characterization with little elaboration on the involved sensing mechanism or more precisely the factors that manipulate the sensor's sensitivity. The majority of the previous works utilized the discussed cavity perturbation theorem to explain the general behavior of the proposed metamaterials and how do they interact with dielectrics. Such theorem provides a basic idea on how planar metamaterials sense dielectrics however, it was developed based on a homogenous closed cavity assumption and hence doesn't provide a detailed insight into the structures under considerations. Also, previous works didn't discuss in detail the effect of various transmission line parameters, resonator's excitation schemes and resonator's order on the sensitivity of planar metamaterials. Thus, major research gaps and unanswered questions that need to be addressed and thoroughly investigated were identified by the researcher. This dissertation aims to address the following questions:

1- What are the influential factors that affect the performance of transmission line based metamaterials which are utilized for the characterization of isotropic, low loss and nondispersive materials? How do we interpret their influence based on the available electromagnetic theories and applicable system models and how can we control and optimize them?
2- What are the necessary conditions that need to be fulfilled by a permittivity and permeability sensors to obtain a uniform sensitivity over a large spectrum? How do we implement and interpret these conditions based on the planar metamaterials equivalent circuit model?

The rest of this dissertation is organized as follows: Chapter 2 provides a literature survey that summarizes the previous research efforts in the field. Chapter 3 presents the theoretical background and operation theory of transmission line based metamaterials. It also discusses the sensing mechanism of permittivity and/or permeability sensors. Chapter 4 presents a comprehensive sensitivity analysis that investigates the effect of the meta-resonator's excitation scheme, its order (i.e. single or double CSRR), and transmission line's substrate thickness on the sensitivity of transmission line based metamaterials. In addition the chapter proposes a condition of sensitivity uniformity and verifies it. The chapter includes also a design of a high sensitivity rectangular CSRR based sensor for relative permittivity measurement. Chapter 5 presents a comprehensive sensitivity analysis that investigates the effect of the meta-resonator path width and split length on the sensitivity of transmission line based metamaterials. It also presents a design of ultrasensitive sectorial CSRR based sensor for relative permittivity measurement and use for microfluidic and crack

sensing. The dissertation is concluded in chapter 7 which lists the major outcomes, contributions and future work.

CHAPTER 2. LITERATURE SURVEY

2.1 Overview

Electromagnetic wave propagation and scattering are controlled by materials configuration, electrical sizes, permittivity, and permeability. Precise identification of these parameters leads to accurate modeling and design of electromagnetic systems. Permittivity and permeability are, in general, functions of the interfering wave's frequency. However, permittivity has a stronger frequency dependence within RF and microwave frequency bands compared to permeability. Moreover, most dielectrics have poor magnetization properties within the same bands. Thus, the estimation of material permittivity is more significant than permeability for the design of most electromagnetic systems.

Several techniques have been utilized to estimate the electromagnetic properties of a material [9-36]. Material characterization using transmission line based metamaterials is one of the emerging techniques. This technique depends on the direct interaction between the material under test (MUT) and the transmission line's evanescent field which results in high measurement accuracy and excellent imaging capability [37-39]. The type of planar metamaterial in consideration in this dissertation is composed of a conventional transmission line loaded with a meta-resonator such as split ring resonator (SRR) or complementary split ring resonator (CSRR). Proper selection of the hosting transmission line as well as the resonating structure is an essential factor that controls the performance of the designed planar metamaterial (i.e. designed sensor).

Transmission line based metamaterials was introduced for relative permittivity

measurement in [8]. This paper utilized a microstrip line loaded with CSRR for the characterization of homogenous dielectric samples. It should be noted that the measurement of a permittivity within a specific sensing zone can be utilized to identify a material of interest when a homogenous material occupies the whole sensing zone, and/or utilized to measure a physical quantity of interest associated with a permittivity variation within a specified sensing zone. Numerous researchers have proposed different topologies of planar metamaterial for permittivity measurement [40-44] as well as other sensing applications with a narrower scope such as fluidic sensing [45-70], object's displacement and velocity [71-85], crack sensing [86-95]. The upcoming subsections discuss some of these applications in detail.

2.2 Permittivity Measurement of Homogenous Dielectric Samples

The first implementation of a metamaterial-based sensor using a planar transmission line was presented in [8]. This paper used a sensing platform composed of MTL loaded with a double CSRR. The passive structure is basically a passive stopband filter with a resonance frequency controlled by the MTL and CSRR design parameters. To estimate the relative permittivity of a homogenous dielectric sample using this setup, the authors loaded the loaded resonator (CSRR in this paper) with MUT. Fig.2.1 shows the used setup. Using a numerical solver, the whole setup was simulated where the relative permittivity of the loaded MUT was changed from 1 to 10 and the corresponding changes in the minimum transmission and minimum reflection coefficients were recorded and utilized to extract a mathematical relation between the change in the MUT's relative permittivity and the change in the sensing platform's scattering parameters.

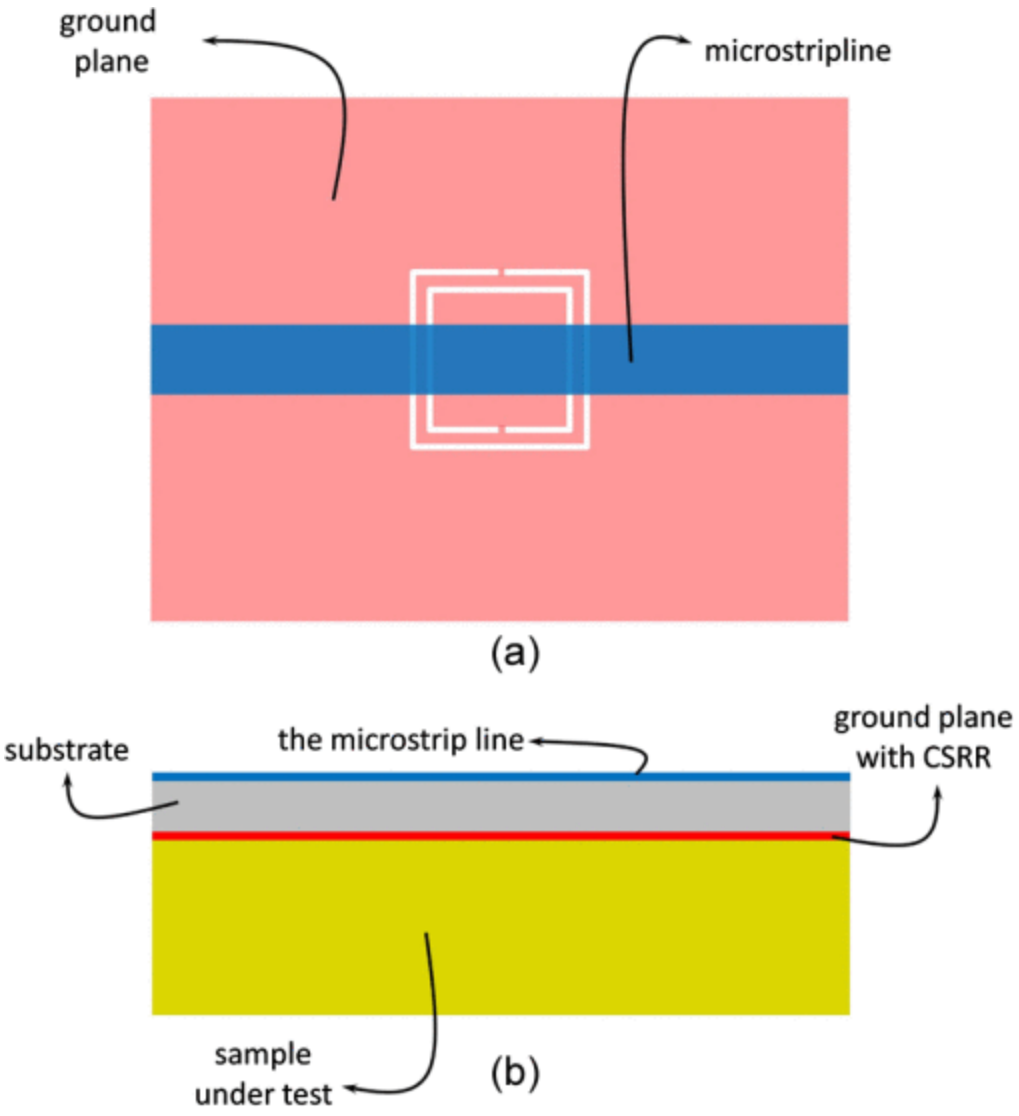

Figure 2.1 General setup of the used sensing platform in [8] (Reprinted from [8], © IEEE [2012])

The paper claimed that the CSRR based sensor is more sensitive than SRR based sensor for permittivity measurement. This claim was supported with a performed comparison between the performance of a double SRR and a double CSRR based sensors for permittivity measurement. The results of the comparison are shown in Fig.2.2. The presented procedure for this comparison overlooked critical details such as the used type of excitation, minimum transmission and minimum reflection frequency of the resonator

and whether the used MUT covers the whole resonator footprint or it only covers the area of the maximum electric field. Moreover, the presented comparison and details didn't clarify whether the obtained results could be generalized to higher or lower resonator order (single or triple SRR and CSRR resonator) or not. These notes are critical as each one of them changes the resultant equivalent MUT's capacitance and how it is coupled to the sensing platform.

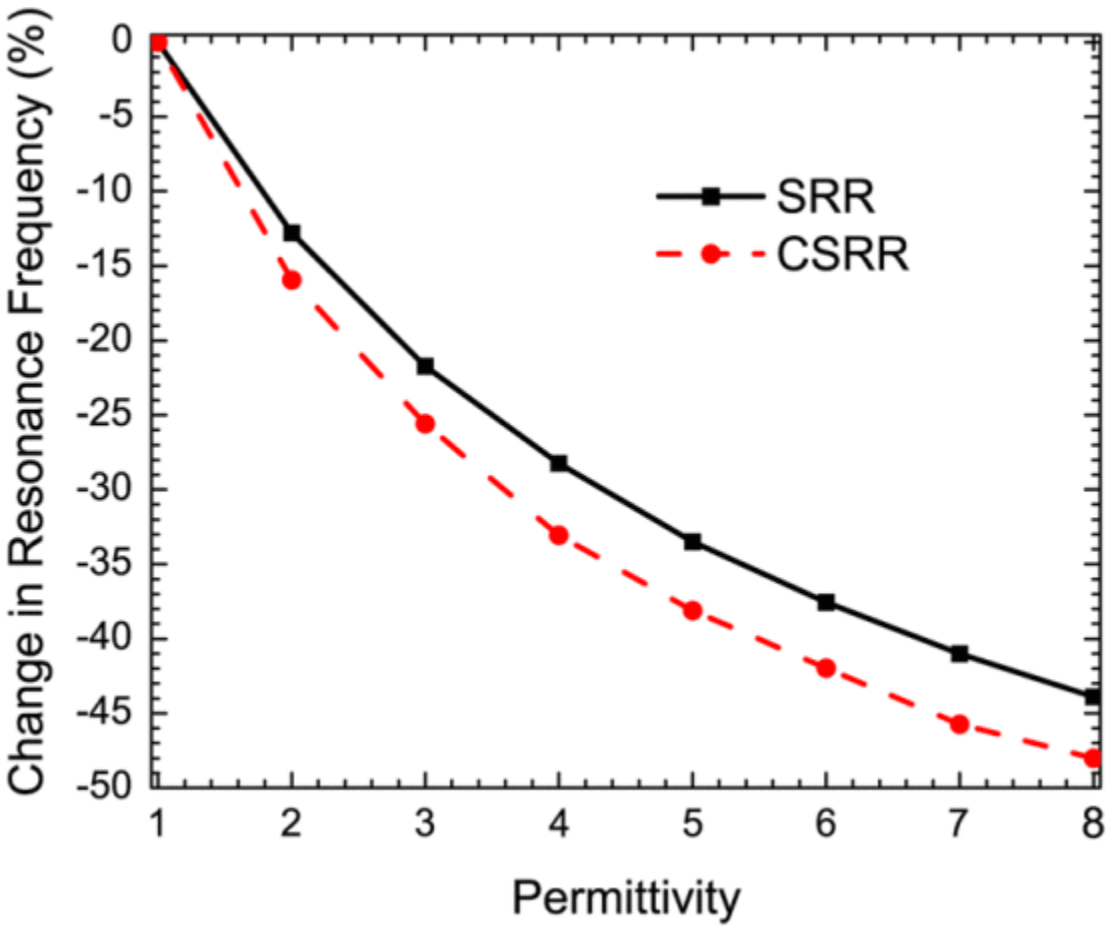

Figure 2.2 Behavior of the SRR and CSRR based sensors with respect to the permittivity of the surrounding medium. (Reprinted from [8], © IEEE [2012])

Based on the results of [8], the minimum transmission frequency of the sensing platform is more sensitive to the variation of the loaded MUT's permittivity compared to the minimum reflection frequency. Thus, many papers that have been published since 2012 utilized this parameter to estimate the effective permittivity of the sensing zone. In fact, many of the published papers have utilized even similar excitation schemes, resonator order and substrate thickness. As it is going to be seen in this dissertation, all of these factors play an essential role in the sensitivity of the sensing platform.

The previous paper was the first journal paper in the field and it paved the way for other researchers to develop similar or new designs with additional applications and specifications for material characterization. For example, in [40] the author utilized CSRR based sensors for the estimation of MUT's relative permittivity as well as its loss tangent. This feature is crucial at the presence of two regions within the sensing zone with different permittivity and conductivity. An example of such case includes anomaly detection of insulated metal surfaces or rusty metal surfaces. In such a case, the sensor will have a minimum transmission frequency shift due to permittivity variation as well as a variation in the magnitude of the minimum transmission and minimum reflection due to MUT's conductive and dielectric losses. Such sensors are good candidates for structural health monitoring systems.

It should be noted that a meta-resonator based sensor, interacts with the material's permittivity using its evanescent field at resonance. The extent of this field around the resonator is highly dependent on the resonance frequency. Thus, this type of sensor was used in [41] for the estimation of the relative permittivity of the MUT as well as its thickness.

2.3 Permittivity Measurement of Liquid (Microfluidic Sensing)

In 2013, a group of researchers published two journal papers where they utilized SRR based sensor [45] and CSRR based sensor [46] to estimate the complex permittivity of liquid samples. Fig. 2.3 and Fig. 2.4 show the setup of the proposed sensors in these papers. The proposed sensors validated the ability of the meta-resonator based sensors to distinguish between different microfluidics with different complex permittivity.

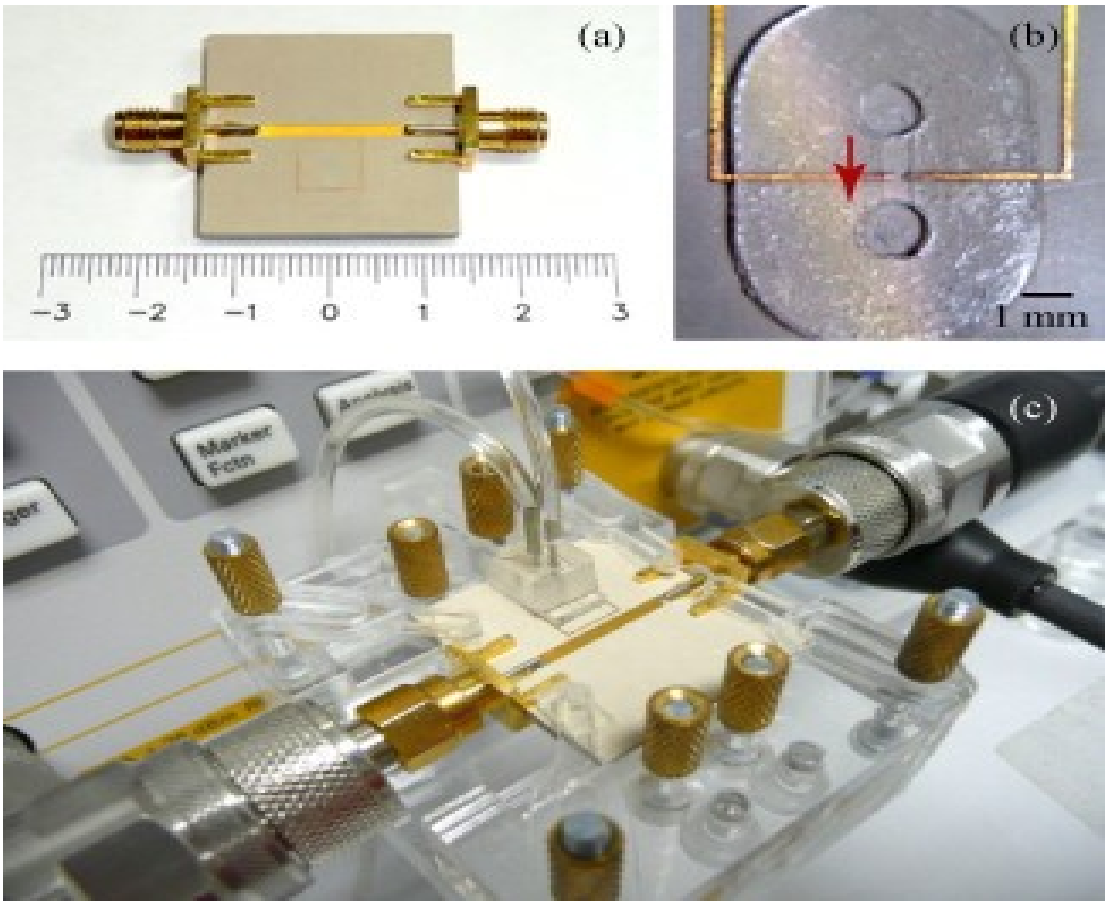

Figure 2.3 Setup of the proposed sensor in [45] (Reprinted from [45], © Elsevier [2013])

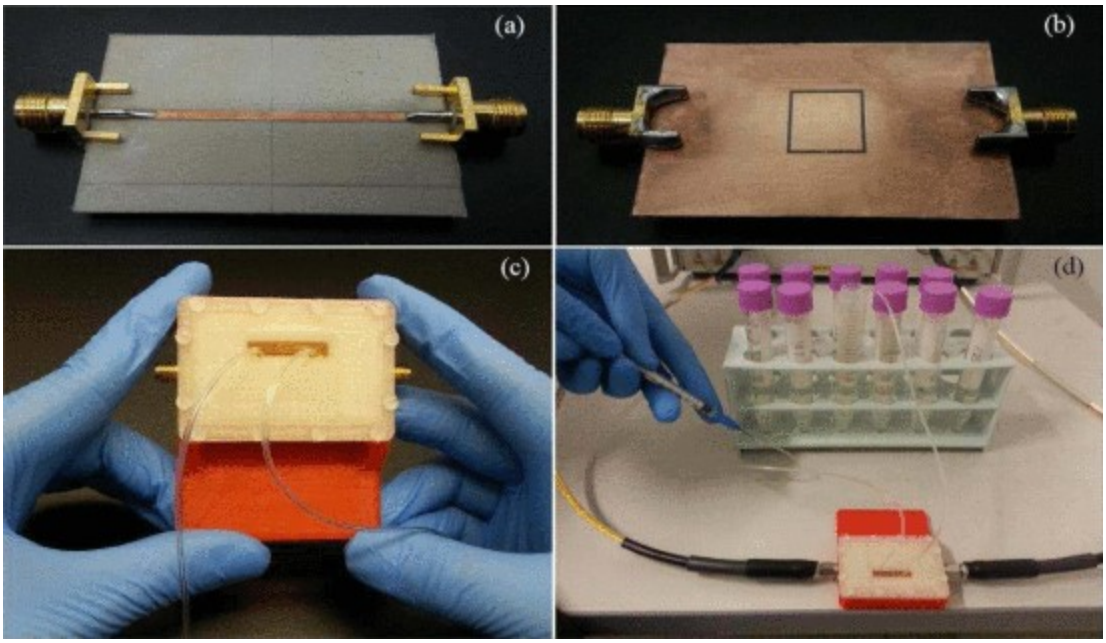

Figure 2.4 Setup of the proposed sensor in [46] (Reprinted from [46], © IEEE [2013])

The sensing platform of these sensors was designed using simple MTL loaded with a meta-resonator. In the SRR based sensor, the meta-resonator was deposited as a substrate surface inclusion with close proximity to the MTL strip. At resonance, this configuration ensures the development of a high electric field within the SRR split which basically defines the sensing zone for a permittivity sensor. For the CSRR based sensor, the meta-resonator was etched at the ground plane perpendicular to the MTL strip. At resonance, this configuration ensures the development of a high electric field within the CSRR circumference which is located at the opposite side of the resonator's split. Thus, the sensing zone of the CSRR based sensor is bigger than the sensing zone of the SRR based sensor. This fact doesn't mean that CSRR based sensor has a better performance than SRR based sensor as this is a general statement that needs to be restated based on the basis of comparison. For example, when the microfluidic channel of the two sensors was loaded with water, the minimum transmission frequency of the CSRR based sensor changed by

25% while the corresponding frequency of the SRR based sensor changed by almost 7.5% yet the later consumed less water than the earlier to come up with this result. Moreover, CSRR is optimally excited using MTL, while SRR is optimally excited using coplanar waveguide (CPW) [7]. In addition, for microfluidic sensing the design, dielectric constant and location of the microfluidic channel affects the sensitivity of the sensor as it changes the effective permittivity within the sensing zone. Thus, the equivalent channel's capacitance seen by the SRR based sensor which uses a confined channel around its split to trap the loaded liquid, is totally different than the equivalent channel's capacitance seen by the CSRR based sensor which uses broader channel that covers part of its circumference.

A modified SRR based sensor was used in [47]. The used sensor depends on the edge excitation of the utilized double SRR using two unconnected MTL strips. Fig. 2.5 shows the setup of the proposed sensor in this reference. Unlike previous design which uses a passive bandstop filter for sensing applications, this passive structure results in a passive bandpass filter. The microfluidic channel extends along the interface of the two SRRs. Two versions of this sensor were proposed. The microfluidic channel of each one of them was designed with different materials and sizes. When the microfluidic channel of each version was filled with water, the maximum transmission frequency of the first version which has a bigger channel changed by 2.4% while the corresponding change in the second version was 0.6%. Thus, despite the fact that the proposed two versions are relatively more complex than the conventional SRR ones, both of them have very limited sensitivity. The reason is that edge coupling is not the optimum excitation of SRR due to the loss of considerable part of the exciting electric and magnetic fields in the non-guiding medium above the MTL strip (i.e. the air). However, this design has an advantage as it

utilized a bandpass filter structure rather than a bandstop structure which allows the utilization of this setup as a microfluidic switch within a narrow band. In addition, the proposed sensor has a narrow microfluidic channel that was designed in the same plane of the substrate. This increases the sensor's compactness and increases the practicality of this sensor especially for applications where the afforded sensor space is limited in the third dimension.

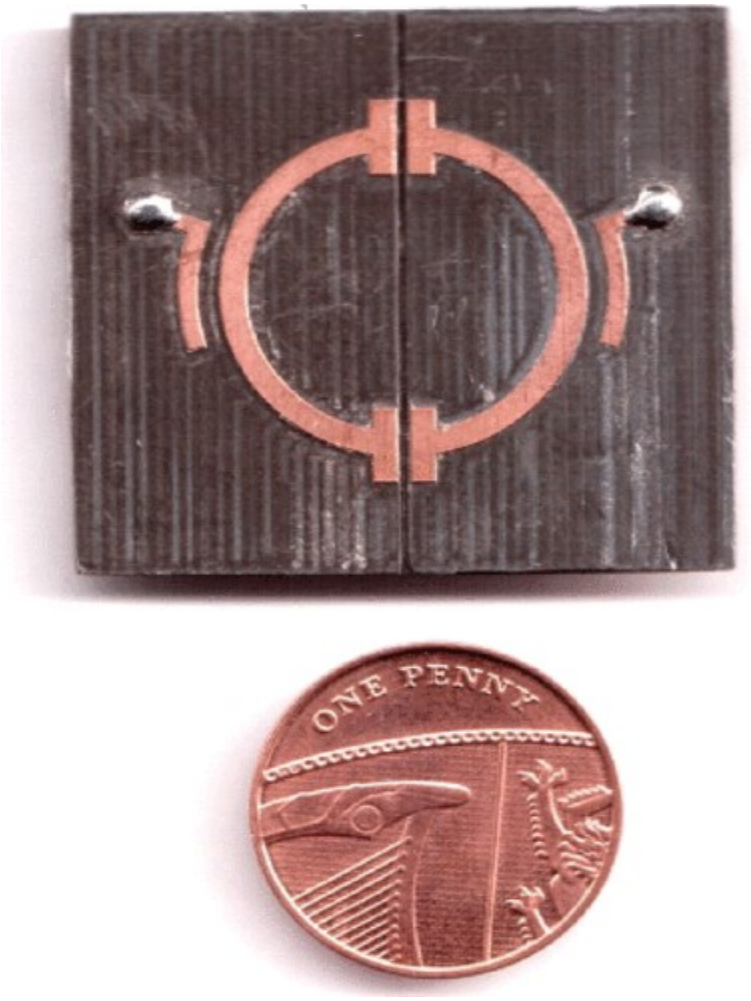

Figure 2.5 Utilized sensor in [47], the microfluidic channel extends between the two SRRs (Reprinted from [47], © IEEE [2014])

The previously discussed sensors, use two experimental steps to estimate the permittivity of a given sample. In the first step, the free space minimum transmission frequency of the sensor is measured. In this step the sensor's meta-resonator is unloaded and the measured frequency is the reference frequency that is needed for all subsequent measurements. In the second step, the minimum transmission frequency of the sensor is measured after loading its meta-resonator with the MUT. The minimum transmission frequency in this step is compared to the reference one which leads to the approximate permittivity of the loaded MUT. This traditional procedure is not immune to the possible stochastic noise from the testing equipment or environmental condition around the sensor. Moreover, re-utilization of a sensor may cause a slight shift in its minimum transmission frequency due to the accumulation of tiny particles above its most sensitive area (i.e. above the meta-resonator) or due to a slight deformation of the sensor surfaces. For this reason, a novel sensing platform based on differential sensing was proposed in [48].

The proposed microwave microfluidic differential sensor is composed of splitter/combiner MTL that is loaded with two identical double SRRs. The splitter splits the guided microwave signal evenly among the two branches. Each SRR is loaded to a single branch of the branched MTL and excited with equivalent power compared to its counterpart. In addition, each SRR is loaded with an identical microfluidic channel. Fig. 2.6 shows the design of the proposed differential sensor in [48].

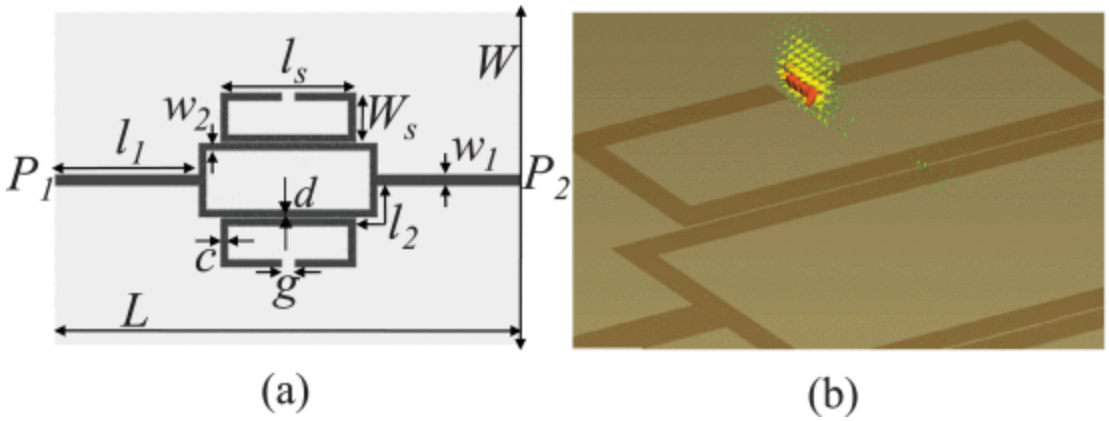

Figure 2.6 Proposed differential sensor in [48], the electric field at resonance is shown in (b) (Reprinted from [48], © IEEE [2017])

If the two meta-resonators are loaded with identical MUTs, the effective permittivity sensed by each resonator is going to be identical as well as the electrical length of the combined resonator/MUT structure thus, a single local minimum transmission frequency is going to be detected within the frequency band of operation. However, if there is a tiny difference between the loaded MUTs, the branched line will be unbalanced and two local minima are going to be detected within the frequency band of operation. Thus, differential sensing allows the designer to relax the required design's complexity to obtain permittivty estimations with more integrity by adapting splitter/combiner configuration which detects the variation between two MUTs under the same environmental and setup conditions. An example of the practically of this type of sensor is the detection of concertation variation among different microfluidic. Fig. 2.7 shows the measured transmission coefficient for different microfluidics that were tested using the discussed sensing platform. It should be noted that differential sensing can be implemented using different meta-resonators and different transmission lines as long as the branched lines are

split and combined with two different ports. Additional differential sensors for microfluidics and other sensing applications can be found in [96-102].

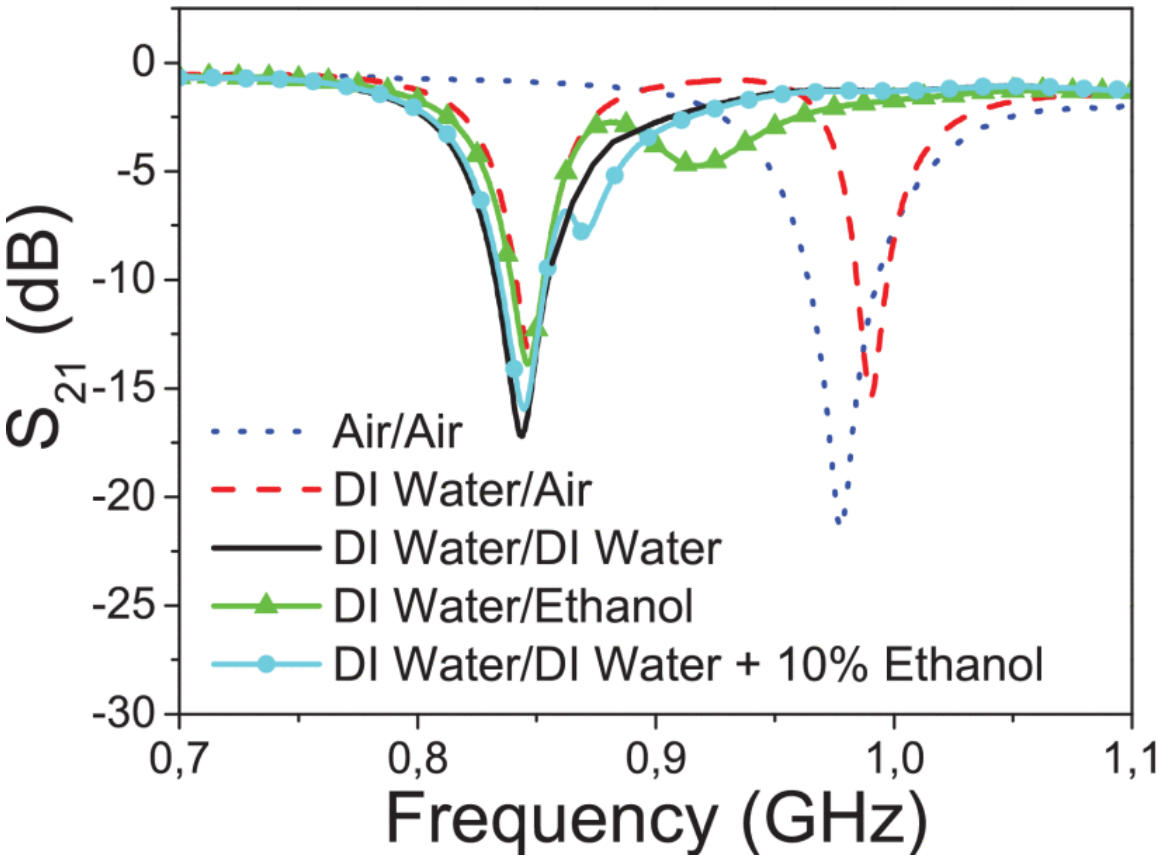

Figure 2.7 Measured transmission coefficient of the differential sensor presented in Fig. 2.6 for different channels loading (Reprinted from [48], © IEEE [2017])

Despite the fact that the differential sensor is able to detect a very small difference between two MUTs, the sensitivity of this sensor itself depends on the sensitivity of the two sub-sensors that compose it. Thus, the differential sensor that is composed of two sensors that have low resolution might not be able to produce distinct local minima when the loaded MUTs are not electrically and/or magnetically similar. For this reason, the introduction of the differential sensor doesn't eliminate the need for the enhancement of the existing meta-resonator based sensors sensitivity.

2.4 Crack Sensing

Crack detection using a meta-resonator based sensor was first proposed in [86]. The proposed sensor composed of MTL loaded with double CSRR. It was used to detect straight fine crack that was artificially created in the upper surface of an aluminum cube. The CSRR footprint and the MTL ground plane was covered with a Teflon sheet to reduce the conductivity between the ground plane and the aluminum cube. It was also used to mimic the presence of a paint layer above the cracked surface which is usually the case in practice. The used CSRR is a square resonator with a 3-mm side. Such resonator provides high intensity and highly confined sensing fields that can detect tiny cracks at an early stage. Fig.2.8 shows the proposed sensor and scanning direction. The minimum transmission frequency of the proposed sensor shifts by 240 MHz for a crack with 0.1mm width.

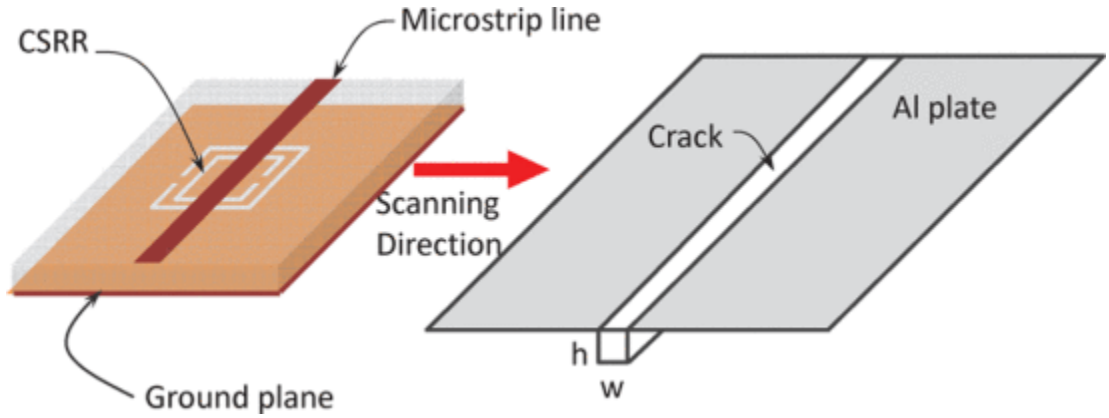

Figure 2.8 Proposed crack sensor in [86] and scanning direction (Reprinted from [86], © IEEE [2012])

The same research group published a paper that discussed in detail the proposed sensor and utilized it for the detection and characterization of surface cracks in both metallic and non-metallic surfaces [87]. The paper explained the detection mechanism

based on both metallic and non-metallic surfaces. At resonance the loaded CSRR has its maximum electric field at one side of the CSRR opposite to the CSRR's split as shown in Fig. 2.9 while the maximum surface current appears at the CSRR's split as shown in Fig. 2.10. For optimized crack detection and characterization in non-metallic (dielectric) MUT, the CSRR side with the dominant electric field needs to be parallel to the crack. Similarly, for optimized crack detection and characterization in metallic MUT, the CSRR split which has the dominant surface current needs to be parallel to the crack.

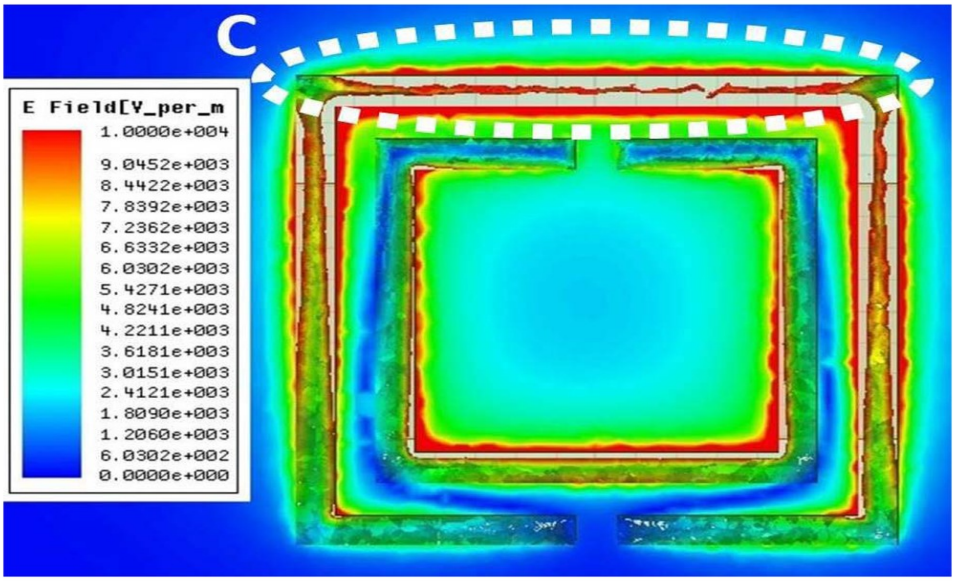

Figure 2.9 Electric field profile of the loaded CSRR at resonance, (Reprinted from [87], © *Sensors* [2014])

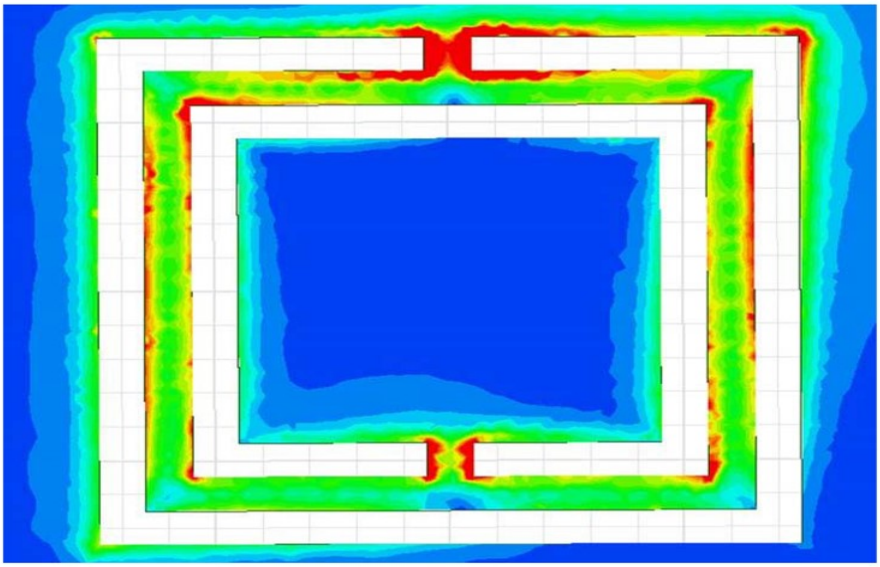

Figure 2.10 Surface current profile of the loaded CSRR at resonance, (Reprinted from [87], © Sensors [2014])

Previously discussed sensors were designed using conventional double CSRR. This type of resonator is basically an unclosed rectangular path etched in the ground plane. When this type of sensor is used to detect a crack in a metallic MUT, the internal island of the CSRR and the metallic surface of the MUT compose an equivalent coupling capacitance that degrades the performance of the sensor. Thus, a modified CSRR design was used to reduce the coupling capacitance between the crack sensor and the metallic MUT [92]. The used CSRR has many rectangular strips within its internal island which dramatically decreases the conductivity of the internal surface and consequently reduces the equivalent CSRR-MUT electrical coupling. Fig.2.11 shows the proposed sensor topology. Compared to previous designs, the proposed sensor has a higher dynamic range and consequently higher frequency resolution. The minimum transmission frequency of the proposed sensor has a frequency shift of 1.5 GHz for a surface crack with a 0.2mm width and 2mm depth. The paper discussed the influence of the standoff distance (a gap

between the sensor and MUT) on the integrity of the sensor outcomes. As the sensor senses with the evanescent field, the sensed crack needs to be within the sensor's sensing zone which extends few microns below the loaded meta-resonator. Thus, as the standoff distance increases, the integrity of the sensor outcomes decreases. In addition, it should be noted that the integrity of the sensor outcomes depends on the crack orientation with respect to the sensing elements within the loaded meta-resonator [92]. For example, using the proposed sensor with the proposed meta-resonator orientation, the existing MUT crack needs to be parallel to the MTL strip for optimized detection.

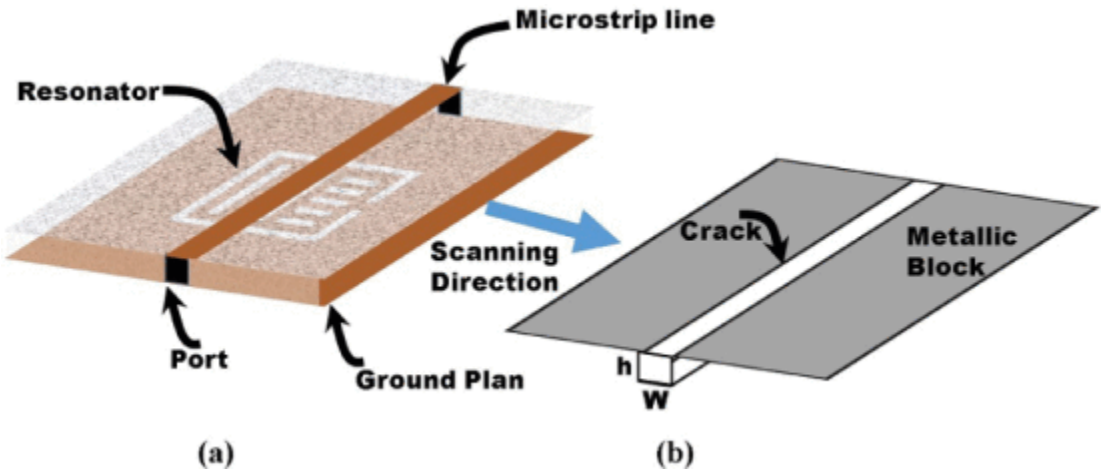

Figure 2.11 Proposed crack sensor in [92] and scanning direction (Reprinted from [92], © IEEE [2017])

2.5 Permeability and Permittivity Measurement of Magneto-dielectrics

Magneto-dielectric substrates are substrates with non-unity permeability and permittivity. Non-unity permeability and permittivity increase the magnetic and electric energies storage within the substrates. They also reduce the electrical lengths of microwave systems as they allow more control over the wave velocity within the guiding structure

compared to conventional substrates. For these reasons, these types of substrates are utilized for the design of high efficiency electrically small antennas [106].

As discussed previously, the permittivity of a dielectric can be measured using the resonating electric field of the meta-resonator based sensor. The resonating electric field polarizes the molecules of the dielectric and stores electric energy within the MUT which can be modeled with an equivalent capacitance loaded to the meta-resonator. For permeability measurement, the resonating current within the meta-resonator is utilized to induce a current within the loaded MUT. The induced current is directly proportional to the resonating current. The induced current within the MUT stores part of the resonating energy in the form of magnetic energy, thus the MUT in this case can be modeled with equivalent inductance. Based on the discussed mechanism, it should be noted that the resonating electric field as well as the resonating currents contribute to the resonance frequency variation. Thus, for better estimation, the sensing zone of the MUT permittivity and the sensing zone of the MUT's permeability should not be closely located. It should also be noted that, as magnetic charges don't exist and utilized only as an analogy to the presence of electric charges, the losses determined by the complex permeability of a given magneto-dielectric is essentially associated with the magnetic losses caused by the induced current polarity oscillations (i.e. magnetic dipoles oscillations).

A single meta-resonator based sensor for complex permeability and complex permittivity measurement was proposed in [107]. The sensor was designed using modified double CSRR loaded to MTL. Two tests were performed for each MUT, one test to measure the MUT's permittivity while the other is used to measure the MUT's permeability. In each test, the loaded MUT was placed at the location of the maximum

field/current of interest (i.e. maximum electric field for permittivity measurement and maximum surface current for permeability measurement). Fig.2.12 shows the proposed sensor topology and the resonating fields' profile.

A key advantage of the proposed sensor is the clear difference between the locations of the two sensing zones. Loading the MUT to meta-resonator at the permittivity sensing zone causes a frequency shift based on the material's permittivity only. Similarly loading the MUT to meta-resonator at the permeability sensing zone causes a frequency shift based on the material's permeability only. Thus, the two quantities are estimated with high accuracy.

The provided study didn't discuss the optimized excitation scheme for high sensitivity. It didn't also estimate the error related to the air gap presence for permeability and permittivity measurement. The air gap is a common source of error for a near field sensor. The presence of such gap influences the impedance seen by the meta-resonator and consequently varies the impedance of the loaded MUT which may results in a serious fluctuation in the obtained reading. As this sensor has two different sensing zones, air gap error should be molded using two different formulas where each one is related to a specific sensing zone and specific material's parameter (i.e. permeability and permittivity).

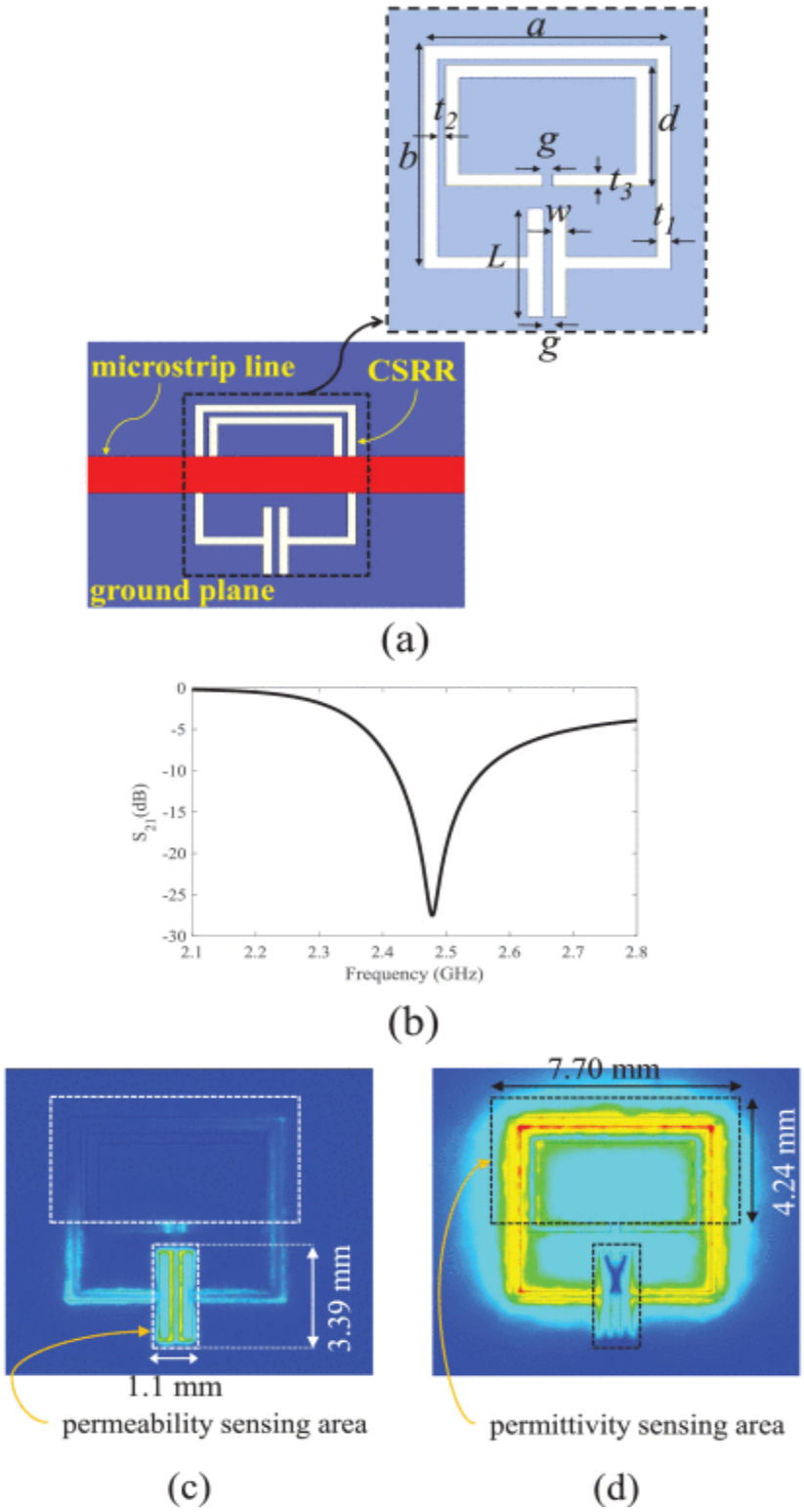

Figure 2.12 Proposed sensor for Magneto-dielectric MUTs (Reprinted from [107], © IEEE [2018])

2.6 Remarks on the Platform's Practicality and Sensitivity Comparison

CSRR based sensing platforms are two-port networks where a change in the minimum transmission frequency is utilized to extract unknown permittivity of a loaded MUT. Such setup is suitable for a test at an equipped laboratory using a vector network analyzer. However, the planar metamaterial based sensors can be utilized as sensing spots in a wireless sensing network when they are integrated with RFID tags for IoT applications. For example, for a chip-less RFID, the loaded resonator will interact with the interrogating electromagnetic wave and introduces a change in the tag load impedance based on the variation of the permittivity within the sensing zone. One way to realize such a scheme with a chip-less RFID tag, is to excite the resonator with MTL strip within the RFID internal circuitry [108].

To measure material's permittivity with a sensor composed of a planar resonating structure, MUT should be brought into the sensing zone which is characterized by the presence of high resonating electric field intensity. Key performance enhancement for a relative permittivity sensor is to enlarge its sensing zone and strengthen its resonating electric field while maintaining uniform sensitivity over a large band of frequency. Proper selection of the hosting transmission line as well as the resonating structure is an essential factor to attain such enhancement.

The sensitivity of various sensors can be compared using the relation between the minimum transmission frequency and the MUT's relative permittivity. Previously proposed sensors had different operational bands and minimum transmission frequencies. It is expected that a sensor with a high free space minimum transmission frequency to have a higher shift magnitude (i.e. shift measured in GHz) compared to a sensor with a lower

one when they are loaded with identical MUTs. Thus, to have a consistent sensitivity comparison irrespective of shift magnitude (i.e. irrespective of the resonator's size), it is recommended to compare the percentage of the minimum transmission frequency shift rather than the magnitude of minimum transmission frequency shift.

MUT's relative permittivity range is another crucial factor for consistent comparison. The MUT's equivalent capacitance is inversely proportional to the minimum transmission frequency shift increment. Consequently, as the permittivity of the loaded MUT's increases, the increment in the magnitude and percentage of the minimum transmission frequency shift with respect to free space minimum transmission frequency decreases. For large permittivity, the corresponding increment starts to be negligible. For this reason, the sensitivity of a permittivity sensor with a free space minimum transmission frequency less than 10 GHz could be evaluated efficiently using MUTs with a variable relative permittivity between 1 and 10. Table 2.1 shows a sensitivity comparison based on the percentage of the minimum transmission frequency shifts as the MUT's relative permittivity changes from 1 to 10 for previous studies that used CSRR based sensors for permittivity measurements. The basic configuration of the compared sensors is similar where a coaxial line is used to feed a microstrip transmission line (MTL) loaded with a CSRR. These studies used the same alignment of single or double CSRR with respect to the MTL strip (i.e. the resonator's slit is oriented perpendicularly to the MTL strip). The used orientation ensures resonance excitation with pure electric excitation through the time-varying electric field between the MTL strip and the ground plane.

Table 2-1 Sensitivity Comparison between Recent CSRR Based Sensors

Ref.	Freq. Band (GHz)	Resonator	Freq. Shift
[8]	0.8-1.3	Double CSRR	38 %
[40]	1.8-2.8	Double CSRR	36%
[41]	1.08-1.63	Single CSRR	34%
[41]	2.16-3.33	Single CSRR	35 %
[42]	1.75-2.7	Double CSRR	35%
[43]	5.23-8.45	Double CSRR	38%

CHAPTER 3. CSRR BASED SENSORS: OPERATION THEORY

To develop a microwave sensor we need to design a microwave system that has a tangible variation in at least one of its characterizing parameters caused by a corresponding variation in the permittivity and/or permeability of a given MUT. The optimum performance of a sensor is attained when the interaction between the sensor and the MUT is maximized which consequently maximizes the variation of the characterizing parameter or parameters.

Each proposed sensor in this research is designed using a microwave planar transmission line (MTL) that is loaded with a passive resonator (CSRR). Every transmission line has its unique electric and magnetic field profiles within and around its spatial extent. The resonance of a passive resonator can be optimally excited using optimum alignment between the resonator and interacted electric and/or magnetic fields. Therefore, it is necessary for a sensor designer to understand transmission lines' propagating modes and fields' profiles as well as resonator excitation requirements to be able to select a transmission line that better fits the resonator's optimum excitation scheme. The following subsections provide a smooth background that rationalizes the utilization of microstrip line loaded with a CSRR in this dissertation to realize high sensitivity relative permittivity sensors.

3.1 Sensing with Two-Port Network

Unlike low-frequency electrical systems, microwave systems or networks can be characterized using the network's scattering parameters. This is due to the fact that the wavelength of a microwave signal is too small compared to the physical dimensions of the

system which makes it difficult to measure the voltage and current variations within its physical extent with high accuracy [109]. Microwave network has at least two ports. A scattering parameter between two ports in a microwave network could be either a transmission or a reflection parameter. Each scattering parameter is represented by a complex number with a magnitude and phase. The magnitude and phase of a given scattering parameter are functions of the microwave network and the feeding network impedances. Consequently, they are functions of the frequency band of operation. For ideal and matched two ports network, the magnitudes of the normalized transmission and reflection coefficients are unity and zero, respectively. However, in practice these coefficients have slightly different values due to the presence of a non-preventable mismatch between the impedance of the two-port network and the corresponding impedance of the feeding network. The subsequent discussion in this chapter, is focused on a transmission line based two-port network as it is the utilized network in this dissertation.

In principle, the variation in the magnitude and/or phase of one or more scattering parameters could be utilized to estimate the permittivity and/or permeability of the medium through which the wave propagates. Thus, for a given transmission line the mentioned variation could be utilized to estimate the permittivity and/or permeability of the line's substrate. Moreover, if a dielectric material has a direct electric and/or magnetic coupling with the line's substrate and/or the propagating wave, scattering parameters could be utilized to estimate the permittivity and/or permeability of the interacting dielectric material (MUT). For example, when a simple planar transmission line is loaded with MUT (i.e. a slab of dielectric material is placed on top of a straight MTL signal strip), the velocity

of the microwave signal within the network decreases compared to the unloaded case which consequently varies the phase of the scattering parameter. In addition, if the loaded MUT is a lossy dielectric, the magnitude of the scattering parameter is also going to be changed. Yet, for both examples, the expected changes in the magnitude and phase might be insignificant/unidentifiable especially for a low loss dielectric sample with dielectric constant close to the dielectric constant of the transmission line's substrate. A recent study proposes a permittivity sensor using a planar transmission line with a meandered strip[114]. The proposed sensor has better sensitivity compared to a transmission line with a straight strip as the variation in the signal velocity (i.e. variation in the electrical length of the line) is higher.

The prior discussion considers using a simple transmission line as a microwave sensor. The magnitude of the transmission and reflection coefficients of such line is almost flat and in general doesn't have an easily identified characteristic features such as local minima and/or local maxima which mandate the use of a high precision measurement system if they are utilized for sensing applications. To reduce the need for such measurement system, microwave sensors are usually designed using a two-port network that exhibits minimum and/or maximum transmission and/or reflection within the frequency band of operation. This minimum/maximum changes its location within the frequency band of operation based on the properties of a loaded MUT. It should be noted that it is also preferred to have other characteristic features such as the bandwidth variation which is utilized to estimate the relative permittivity of a dielectric MUT in chapter five of this dissertation.

To design a two-port network with a scattering parameter that has at least one local minima and/or local maxima, the designer needs to purposely break the matching condition between input and output port of the two-port network by inserting an object with different impedance within the transmission medium. One way to realize such network (or sensor in our case) is to load a transmission line with a resonator. In such case, at a specific frequency (or frequencies) the system resonates and the energy of the injected wave is trapped within the resonator in the form of oscillating electric and magnetic energy, a case at which the transmission coefficient of the network reaches its minimum value (for bandstop configuration) or its maximum value (for bandpass configuration) within the frequency band of operation. Loading the loaded resonator with MUT, changes the resonator impedance which consequently changes the position of the minimum/maximum transmission coefficient.

To optimize the design of a microwave sensor for permittivity measurement, we need to determine the optimum resonator that better fit a transmission line with a given propagating mode for sensing applications. The upcoming section revisits the most popular types of transmission lines and their propagating modes.

3.2 Types of Transmission Lines Propagating Modes

The mode of a propagating wave can be classified as transverse electromagnetic (TEM), transverse electric (TE), transverse magnetic (TM) or hybrid mode. In the TEM mode the electric and magnetic fields are both orthogonal to each other as well as to the direction of the wave propagation. On the contrary, the TE (TM) mode has only electric (magnetic) field orthogonal to the direction of wave propagation. Hybrid mode is a combination of TE and TM propagating modes.

Electromagnetic waves propagate in a bounded or unbounded mediums. They propagate in unbounded homogenous medium with a TEM mode. On the other hand, when the EM waves are bounded within nonhomogeneous materials (i.e. conductors and/or dielectrics) the boundary conditions may alter the mode of the propagating waves. For example, EM propagates within coaxial cable with TEM mode however, single-conductor rectangular waveguide supports either TE or TM modes while MTL supports hybrid mode [109]. The question is which mode is better for passive resonator excitation.

At resonance, electric and magnetic fields induce magnetic (fictitious) and conduction current, respectively within a passive resonator that is composed of dielectric and conductive materials. They also induce displacement magnetic and electric currents. To maximize the resonance strength, these currents should be synchronized to increase the corresponding constructive interferences and reduce the destructive ones. For a given symmetric resonator loaded to a planar transmission line, this can be reasonably achieved by placing the resonator at a confined zone where almost all vector components of electric and magnetic fields that exist within the homogenous guiding medium (i.e. dielectric substrate) are perpendicular to each other as well as to the corresponding wavevector components. Thus, TEM mode is the preferred mode of excitation for passive resonator loaded to a planar transmission line.

A TEM transmission line with two conductors, has uniquely defined voltages, currents and characteristic impedances along its length. This type of line can be modeled by series inductors and shunt capacitors. The series inductances and shunt capacitances account for the strength and orientation of the magnetic and electric fields', respectively. Strictly speaking this model is valid for a perfect TEM transmission line. The series

inductances and shunt capacitances in the model indicate that at each electrically small section within the transmission line, all magnetic fields (electric fields) vector components are orthogonal to the corresponding electric fields (magnetic fields) vector components as well as to the corresponding wave vector components. This model fits more a coaxial cable where all transmitted wave is guided through a homogenous tubular dielectric which is sandwiched between central and circumferential conductors. However, it doesn't fit precisely planar transmission lines where the guided wave is transmitted in a non-homogeneous medium composed of a dielectric substrate and non-uniform layers of the surrounding medium (i.e. air). In such case, the planar transmission line has a propagating wave that is composed of a dominant TEM mode and a fractional TE-TM mode [109]. This mode is called the quasi-TEM mode. The propagating mode of a coplanar waveguide (CPW) and MTL is a quasi-TEM mode [109]. At a confined volume within their substrates, a CPW has a TEM mode with a parallel magnetic field with respect to the hosting substrate surface plane vector while MTL has a TEM mode with a parallel electric field with the same reference. Thus, the selection of either line for sensing applications depends on the optimum orthogonal excitation requirements of the loaded passive resonator. It also should take into account the type of circuit components that share the same transmission line. For example, CPW might be a preferred choice for a microwave sensor that shares the substrate with circuit elements that need easy access to the transmission line's ground.

3.3 Defected Ground Structure and Substrate Inclusion

MTL and Coplanar waveguide (CPW) are two of the most popular planar transmission lines. Both lines are used primarily for low power signal transmission. However, their function could be altered by changing their configurations or by adding

other passive or active elements to realize numerous microwave circuit components such as resonator-based sensors, filters and antennas. This dissertation proposes sensors that are designed using a planar transmission line loaded with scalable resonators. One way to realize such device, is to load the transmission line with either a conductive substrate inclusion or a ground plane defect.

Defected ground structure (DGS) and conductive substrate inclusions have been extensively utilized for various sensing and filtering applications. Ground defects and substrate inclusions are coupled to the quasi-TEM mode of the MTL or CPW. TEM mode is intense within a limited volume of the substrate of these transmission lines [109]. This limitation restricts the designer's choice of ground defect/substrate inclusion position within the hosting transmission line for proper coupling (excitation) purposes. Ground defect and substrate inclusion form mismatched loads, therefore they enforce new boundary conditions that change the profile of the original fields and induced currents within the hosting transmission line, which consequently causes a wave reflection and possibly a resonance at specific frequency band. For this reason, these two structures are considered as resonators.

Resonance occurs when a system stores an oscillating and balanced electric and magnetic energy. When a microwave circuit resonates, electric and magnetic energy oscillates between each other. The resonance frequency of the microwave resonator changes when the distribution of the electromagnetic fields within the resonator vicinity perturbs. This is due to the variation of the overall system's effective permittivity and permeability. The word system is referred to the resonator and the surrounding environment which includes interacted electromagnetic fields and/or electrically close

objects. Accordingly, when MUT brought into direct contact or close proximity to a resonating structure or when it interferes with the guided waves within a resonating structure, it perturbs its electromagnetic field distribution and consequently its resonance frequency changes. The change in the resonance frequency and the MUT properties can be related to each other using cavity perturbation relation in (1) [8].

$$\frac{\Delta f_r}{f_r} = \frac{\int_v (\Delta\varepsilon \mathbf{E_1} \cdot \mathbf{E_0} + \Delta\mu \mathbf{H_1} \cdot \mathbf{H_0}) \boldsymbol{dv}}{\int_v (\varepsilon_0 |\mathrm{E}_0|^2 + \mu_0 |\mathrm{H}_0|^2) \boldsymbol{dv}} \qquad (1)$$

where Δf_r is the shift in the resonance frequency f_r , $\Delta\varepsilon$ and $\Delta\mu$ are the change in the permittivity and permeability, respectively. ε_0 and μ_0 are the free space permittivity and free space permeability, respectively. $\mathbf{E_0}$ and $\mathbf{H_0}$ are the original fields. $\mathbf{E_1}$ and $\mathbf{H_1}$ are the fields with perturbation. $\boldsymbol{v}$ is the perturbed volume.

For extremely low power resonator with negligible variation in the magnitude of the electric and magnetic fields before and after the resonance, the relation can be simplified to (2)

$$\frac{\Delta f_r}{f_r} = \frac{\int_v (\Delta\varepsilon |\mathrm{E}_0|^2 + \Delta\mu |\mathrm{H}_0|^2) \boldsymbol{dv}}{\int_v (\varepsilon_0 |\mathrm{E}_0|^2 + \mu_0 |\mathrm{H}_0|^2) \boldsymbol{dv}} \qquad (2)$$

For sensing applications, the design and parameter selections of the planar transmission line as well as the defect/inclusion should be optimized to maximize the resonance strength and to optimally confine the resonating electrical (magnetic) fields within permittivity (permeability) sensing area. Moreover, the resonator's selection should consider the available excitation power by the feeding network. For example, it is expected that numerous sensing spots will be utilized for the emerging internet of things (IoT)

applications where each point will have very low power [1]. Thus, the utilization of electrically small resonators with almost zero power is a preferred choice for such applications.

3.4 Resonator Type

Split ring resonator (SRR) and its complement (CSRR) are electrically small structures with circular current paths which in turn develop tightly spaced inductance(s) and capacitance(s) at resonance. Such structures reduce the length of the current path required by conventional transmission line resonators which allow the realization of miniaturized resonator-based devices [8]. Fig.3.1 shows a layout of double square SRR and CSRR. Single SRR or CSRR can be obtained by simply removing the inner or outer ring of the double counterpart.

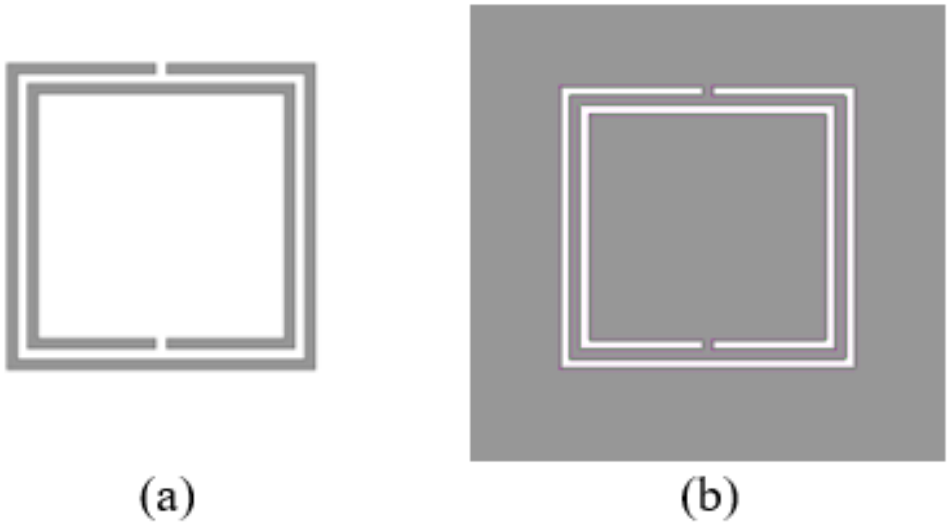

Figure 3.1 The layout of double (a) SRR (b) CSRR. Gray color designates conductive material. (Reprinted from [110], © IEEE [2019])

In principle, SRR and its complement can be magnetically and/or electrically excited. However, the normal time-varying magnetic (electric) field is considered as the dominant SRR (CSRR) excitation. For this reason, to ensure proper excitation of these resonators when loaded to a transmission line, SRR is placed as a substrate conductive inclusion in the bottom of a CPW substrate centered at the narrow gap between one of the ground strips and the central signal strip. On the other hand, CSRR is placed as a ground defect in the MTL ground plane normal to the MTL strip [7]. This excitation schemes force, conduction current circulation within the SRR circumference and magnetic current (fictitious) circulation within the CSRR circumference. It should be noted that a CSRR loaded to a transmission line is not a perfect complement of its counterpart due to the presence of the dielectric substrate and finite ground plane [7]. However, the overall expected response of the exact CSRR is slightly affected by these two factors especially for a thin substrate with low permittivity.

For electrically small resonators, the size of the sensing zone determines which resonator to be utilized as the captured energy is relatively low for both resonators. At resonance, CPW loaded with SRR concentrates the resonating electric field within its slit while MTL loaded with CSRR has a larger concentration area within its circumference. Therefore, each proposed sensor in this research is designed using MTL loaded with a CSRR.

CHAPTER 4. RECTANGULAR CSRR BASED SENSOR

4.1 Introduction

This chapter proposes miniaturized, lightweight and high sensitivity planar metamaterial based sensors for relative permittivity measurement within [0.9-10.9] GHz band. Each proposed sensor is designed using a thin-substrate microstrip line loaded with a single complementary split ring resonator (CSRR). The loaded resonator is excited using maximum electric/magnetic (cross-polarization) excitation to maximize the sensors' sensitivity. Each proposed sensor operates at different frequency ranges within [0.9-10.9] GHz band based on the size of the loaded resonator. Compared to similar state-of-the-art sensors, the proposed ones are at least (30)% more sensitive. The minimum transmission frequency shifts (50)% as the sample's relative permittivity changes from 1 to 10. The chapter proposes a condition of sensitivity uniformity to maintain a uniform sensitivity over the specified band irrespective of the resonator size. Utilizing the proposed condition, the sensitivity of all sensors remains uniform throughout [0.9-10.9] GHz band for all dielectric samples with relative permittivity between 1 and 10. This vital feature allows the practical realization of resonant probes with less computational operations and consistent measurements over a wide dynamic range of the sensing-related frequency. Experimental measurements are in good agreement with the numerical findings. The chapter includes a comprehensive sensitivity analysis that investigates the effect of resonator's excitation scheme, resonator's order (i.e. single or double CSRR) and substrate thickness on the sensitivity of CSRR based sensors. The proposed sensing platforms are recommended for

the development of highly sensitive, consistent and reliable planar sensors such as microfluidics, displacement, nondestructive and biomedical sensors.

The chapter is organized as follows. Section 4.2 provides a comprehensive sensitivity analysis where the effect of the excitation scheme, resonator's order, and substrate thickness on the sensors' sensitivity are thoroughly investigated. This section also presents a condition of sensitivity uniformity with the required proof of concept. Section 4.3 summarizes the sensors' design and outlines the measurement procedure. The experimental results are presented in section 4.4. The air gap effect is numerically studied in section 4.5.

4.2 Sensitivity Analysis

A comprehensive sensitivity study was conducted to investigate the effect of various excitation schemes, CSRR's order (i.e. single or double) and substrate thickness on the sensitivity of a CSRR based sensor. Throughout this chapter the considered cases were numerically studied using full-wave numerical simulation package ANSYS HFSS. The simulation setup consists of a planar sensor loaded with a variable permittivity MUT positioned underneath the MTL ground plane in direct contact with the etched CSRR. For all cases, the used CSRR is a square CSRR with a path width of 0.2mm. The split length as well as the separation between inner and outer rings for double CSRR are also 0.2mm for all cases. The used MUT is a rectangular dielectric cube with a 5-mm height. The width and length of the MUT are identical and assumed to be two times higher than the side length of the square CSRR. The planar center of the CSRR and the interfaced MUT's surface coincide. Except for the air gap study at the end of this chapter, the MUT is assumed to be in direct contact with the etched CSRR. Fig.4.1(a) and Fig.4.1(b) show the

general sensors' setup. For each studied case, the general structure was changed based on the case-specific excitation scheme, CSRR's order (single or double), substrate thickness and CSRR side length (CSRR's size).

Minimum transmission frequency was used to define the sensitivity of the proposed sensors. The minimum transmission frequency of MTL loaded with a CSRR is given by (4.1) [111]. The change in the minimum transmission frequency was calculated based on (4.2). The sensitivity of a CSRR based sensor at each studied case was calculated based on the percentage change in the minimum transmission frequency as given by (4.3).

$$f_{MUT0}^{tmin} = \frac{1}{2\pi\sqrt{L_{CSRR}(C_{CSRR} + C_{MUT})}} \qquad (4.1)$$

$$\Delta f^{tmin} = f_{MUT0}^{tmin} - f_{free}^{tmin} \qquad (4.2)$$

$$\Delta f^{tmin}\,\% = \left(\frac{f_{MUT0}^{tmin} - f_{free}^{tmin}}{f_{free}^{tmin}}\right) \times 100 \qquad (4.3)$$

where f_{MUT0}^{tmin} is the minimum transmission frequency at the presence of MUT with a 0-mm air gap . L_{CSRR} and C_{CSRR} are the equivalent inductance and capacitance of the loaded CSRR, respectively. C_{MUT} is the equivalent capacitance of the loaded MUT. f_{free}^{tmin} is the free space minimum transmission frequency (i.e. $f_{free}^{tmin} = f_{MUT0}^{tmin}$ with $C_{MUT} = 0$) Δf^{tmin} is the change in the minimum transmission frequency in GHz. Δf^{tmin} % is the percentage change in the minimum transmission frequency.

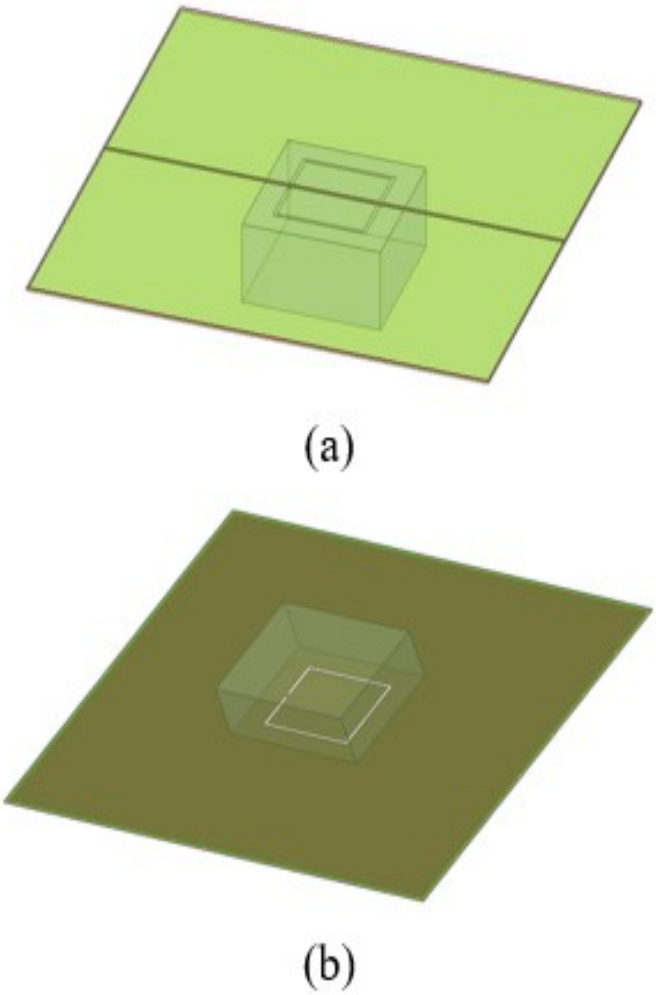

Figure 4.1 (a) Top (b) bottom view of the general sensors' setup. The etched resonator in this figure is a single CSRR with cross-polarization excitation. The MUT appears as a semi-transparent cube attached to the ground plane. (Reprinted from [110], © IEEE [2019])

4.2.1 CSRR Excitation: Pure Electric Vs. Electric/Magnetic

CSRR loaded to a waveguide can be excited using electric and/or magnetic excitations [7]. However, CSRR loaded to MTL has limited excitation choices as pure

magnetic excitation is not realizable. Excitation's strength and type can be controlled by rotating the CSRR's magnetic wall (i.e. line of symmetry for a square CSRR) with respect to the axis of the MTL conducting strip. CSRR is excited using electric excitation when its magnetic wall is orthogonal with respect to the MTL conducting strip. On the other hand, CSRR is excited using electric/magnetic excitation when its magnetic wall is not orthogonal with respect to the MTL strip. As a special case, when the magnetic wall of the loaded CSRR is parallel with respect to the MTL conducting strip, then the CSRR will be excited with maximum electric/magnetic excitation. This type of excitation is also called cross-polarization excitation [112]. In this chapter we will refer to electric excitation as pure electric excitation to further stress that the magnetic field effect in this type of excitation is negligible.

Four cases were simulated to extract the relative permittivity of the MUT using a 6-mm square CSRR with identical MUTs. The aim of these cases is to study the influence of the CSRR's excitation scheme on the sensors' sensitivity. For each case, the utilized MTL has a 0.125-mm substrate thickness with a dielectric constant of 2.9 and a strip width of 0.267mm. The relative permittivity of the MUT was varied from 1 to 10 with a 0.25-step. A single CSRR was used for the first two cases with pure electric excitation in one case as shown in Fig.4.2(a) and a maximum electric/magnetic (cross-polarization) excitation in the other one as shown in Fig.4.2(b). A double CSRR was used for the third and fourth cases with pure electric excitation in one case as shown in Fig.4.2(c) and maximum electric/magnetic (cross-polarization) excitation in the other one as shown in Fig.4.2(d).

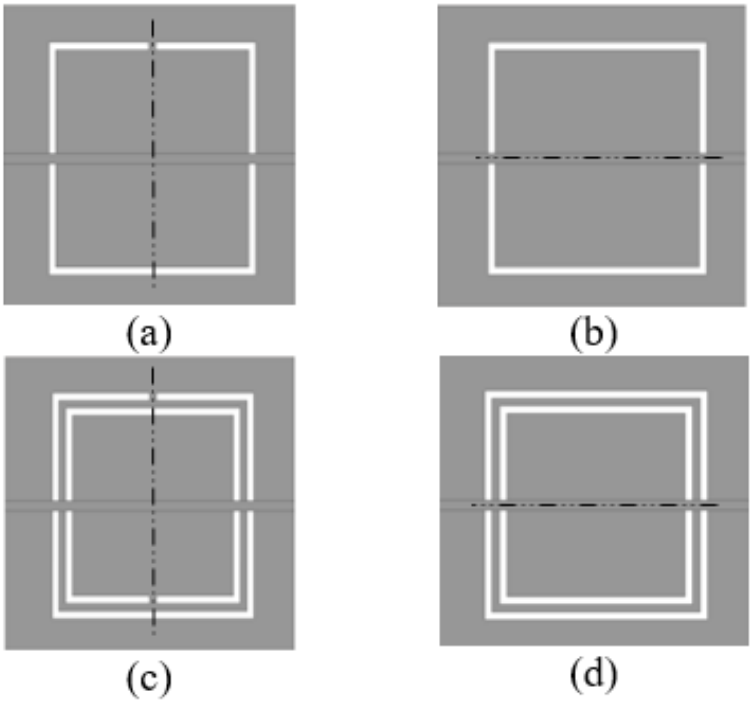

Figure 4.2 Top view of MTL loaded with square (a) single CSRR with pure electric excitation (b) single CSRR with cross-polarization excitation (c) double CSRR with pure electric excitation (d) double CSRR with cross-polarization excitation. The dashed lines show the magnetic wall of the loaded CSRR. (Reprinted from [110], © IEEE [2019])

The sensitivity of the four simulated sensors was compared based on the change in the minimum transmission frequency as defined by (4.3). Fig.4.3 shows the results of the first two cases while Fig.4.4 shows the results of the third and fourth cases. The obtained results show higher sensitivity for the sensors with maximum electric/magnetic (cross-polarization) excitation compared to the ones with pure electric excitation for either single or double CSRR.

To further investigate the influential factor that causes this superiority, a fifth simulation case was added. In this case a single 6-mm square CSRR based sensor was used with seven excitation schemes ranging from pure electric to maximum electric/magnetic

(cross-polarization) excitation. The seven schemes were realized by rotating the CSRR's magnetic wall from its reference position (0°) (i.e. Fig.4.2(a)) which corresponds to pure electric excitation toward (90°) (i.e. Fig.4.2(b)) which corresponds to maximum electric/magnetic (cross-polarization) excitation using a 15-degree step. It should be noted that as the rotation angle increases from 0° to 90°, the influence of the exciting magnetic field increases [43].

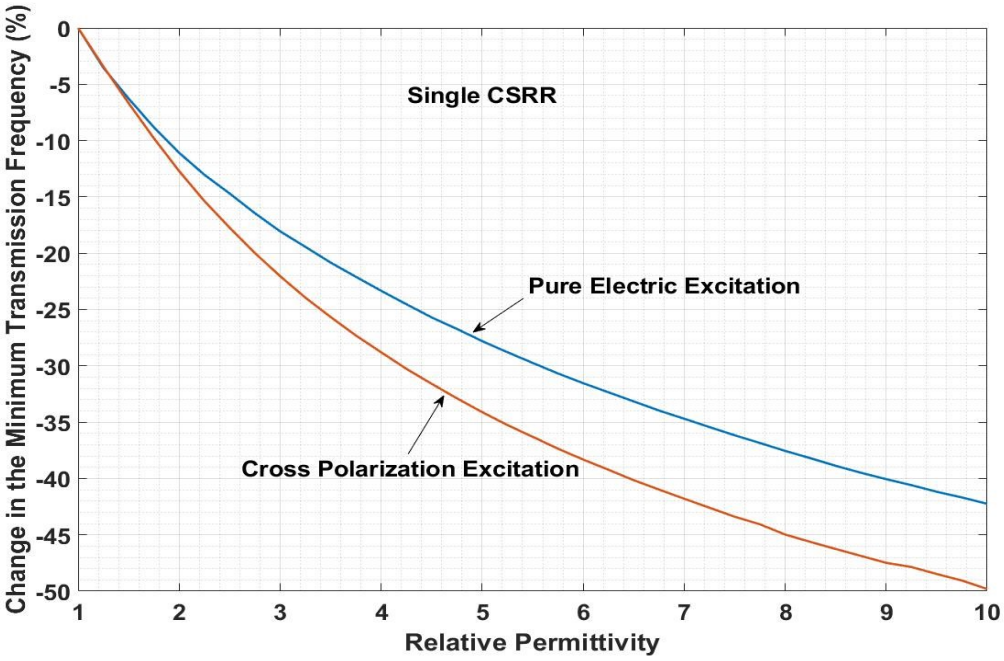

Figure 4.3 Change in the minimum transmission frequency versus MUT's relative permittivity for single CSRR with pure electric (blue) and cross-polarization (red) excitation. (Reprinted from [110], © IEEE [2019])

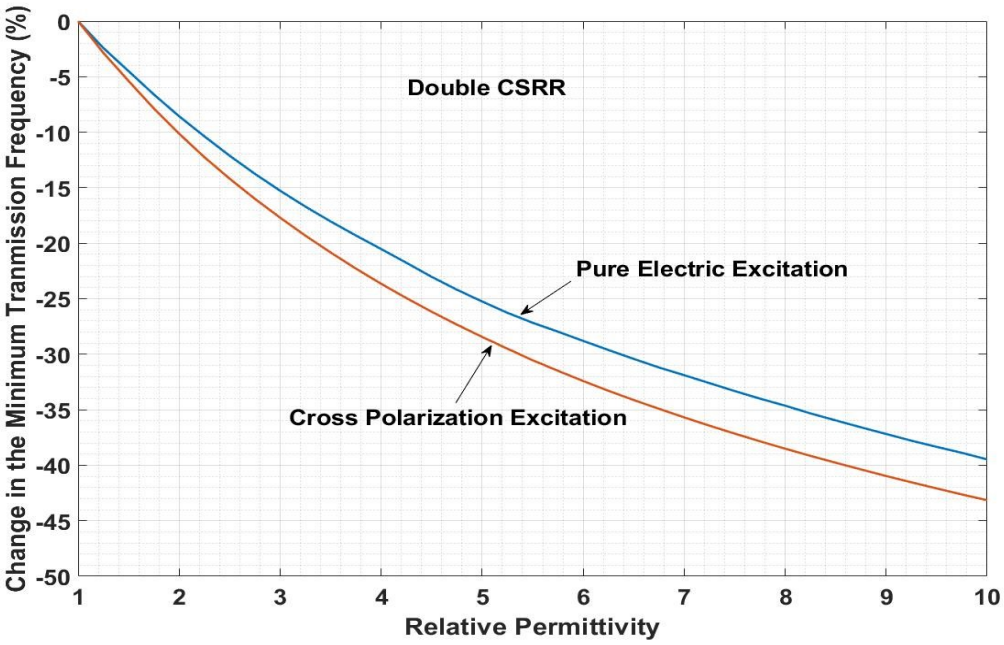

Figure 4.4 Change in the minimum transmission frequency versus MUT's relative permittivity for double CSRR with pure electric (blue) and cross-polarization (red) excitation. (Reprinted from [110], © IEEE [2019])

Fig.4.5 shows the minimum transmission frequency for the seven excitation schemes while Fig.4.6 shows the variation of the minimum transmission frequency for the same cases. These figures show almost identical minimum transmission frequency for the sensors with CSRRs at 0^{o} (pure electric excitation), 15^{o} and 30^{o} (both have different levels of electric/magnetic excitation). This indicates that the exciting magnetic field or more specifically its induced currents do not have a noticeable contribution to the equivalent inductance and capacitance of the CSRR and consequently do not alter its minimum transmission frequency. However, as the excitation gradually moves toward a higher electric/magnetic excitation scheme, the sensors' sensitivity starts to vary. From 30^{o} angle upward, the exciting magnetic field begins to have a noticeable influence which is revealed by the gradual increase in the free space minimum transmission frequency as shown in Fig.4.5 as well as the gradual rise in the sensors' sensitivity as shown in Fig.4.6. Based on

(4.1), the gradual increase in the free space minimum transmission frequency is a sign of a reduction in the combined CSRR equivalent reactive elements term ($L_{CSRR} \times C_{CSRR}$). Such reduction increases the dependence of the minimum transmission frequency on the ($L_{CSRR} \times C_{MUT}$) term or more specifically on the loaded MUT permittivity that is modeled by C_{MUT}. This justifies the superiority of CSRR based sensors with maximum electric/magnetic (cross-polarization) excitation scheme with respect to other excitation schemes.

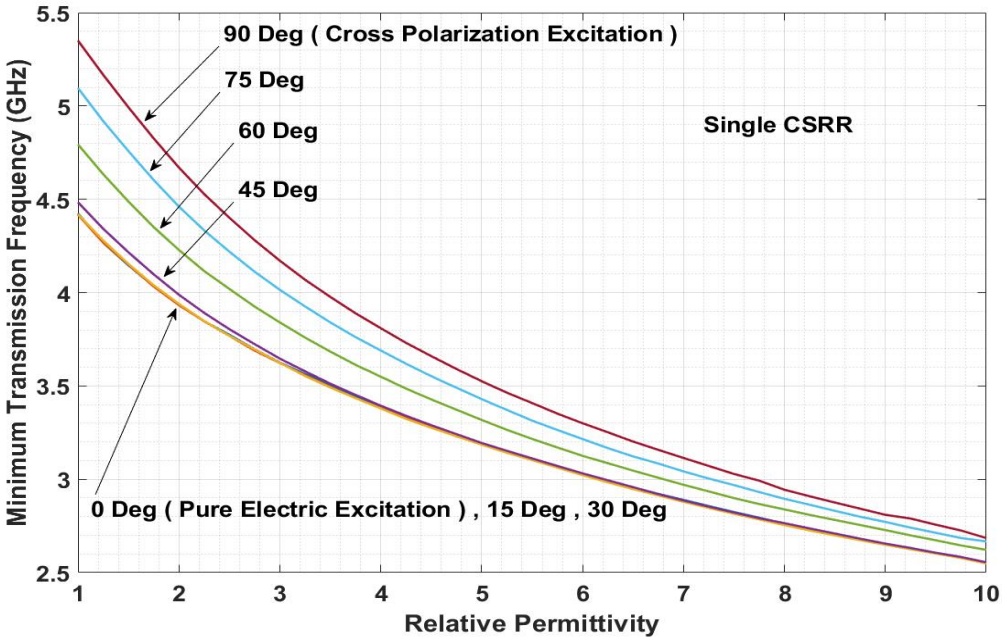

Figure 4.5 Minimum transmission frequency versus MUT's relative permittivity for single CSRR with seven excitations ranging from pure electric (0º) to cross-polarization (90º) excitation using a 15- degree step. (Reprinted from [110], © IEEE [2019])

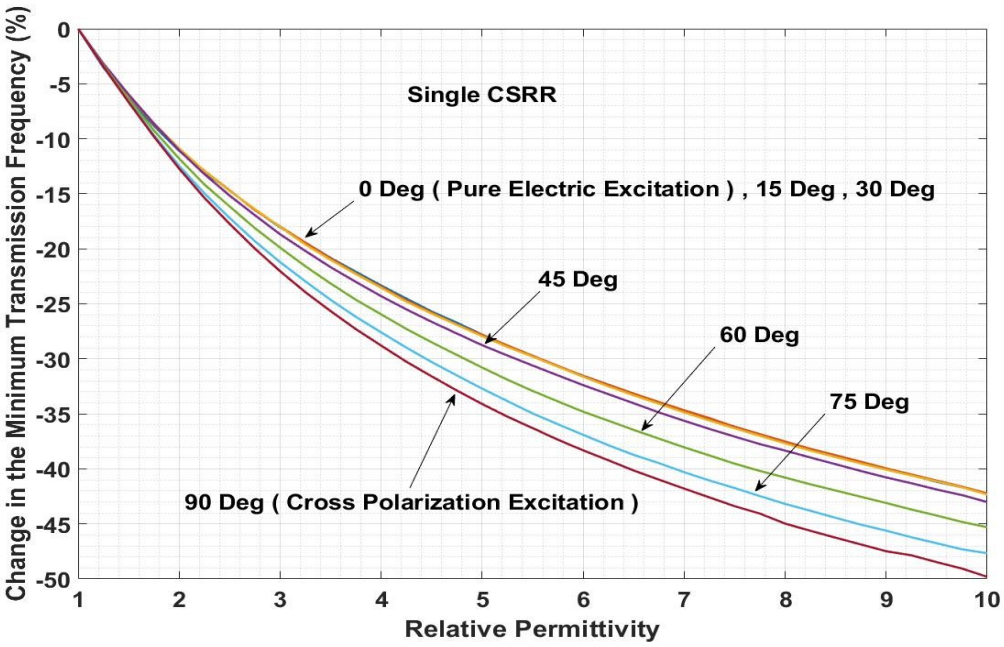

Figure 4.6 Change in the minimum transmission frequency versus MUT's relative permittivity for single CSRR with seven excitations ranging from pure electric (0º) to cross-polarization (90º) excitation using a 15- degree step. (Reprinted from [110], © IEEE [2019])

4.2.2 Single Vs. Double CSRR

The reported studies in the introduction utilized either single or double CSRR for materials characterization. To the best knowledge of the authors, the optimum choice of either single or double CSRR for material characterization using MTL based sensors has not been investigated before. Here we are performing a systematic sensitivity comparison between two sensors with identical substrate and MUTs. The first one uses a single 6-mm square CSRR while the other one uses a double 6-mm square CSRR. Four cases were simulated to extract the relative permittivity of loaded MUTs using the specified sensors. In each case the relative permittivity of the MUTs were varied from 1 to 10 with a 0.25-step. In the first two cases a single and a double CSRR with pure electric excitation were used. The third and fourth cases have a single and a double CSRR with maximum

electric/magnetic (cross-polarization) excitation. Fig.4.7 shows the results of the first two cases while Fig.4.8 shows the results of the third and fourth cases. The results confirm the superiority of the MTL sensors with single CSRR over the ones with double CSRR for relative permittivity measurements. This superiority is irrespective of the used excitation scheme, as the single CSRR sensors were more sensitive in both excitation schemes. The obtained results are expected as double CSRR has two concentric rings with a very small separation between the inner and the outer rings. This configuration increases the equivalent capacitance of the resonator, which consequently reduces the dependence of the sensor's minimum transmission frequency on the MUT's equivalent capacitance.

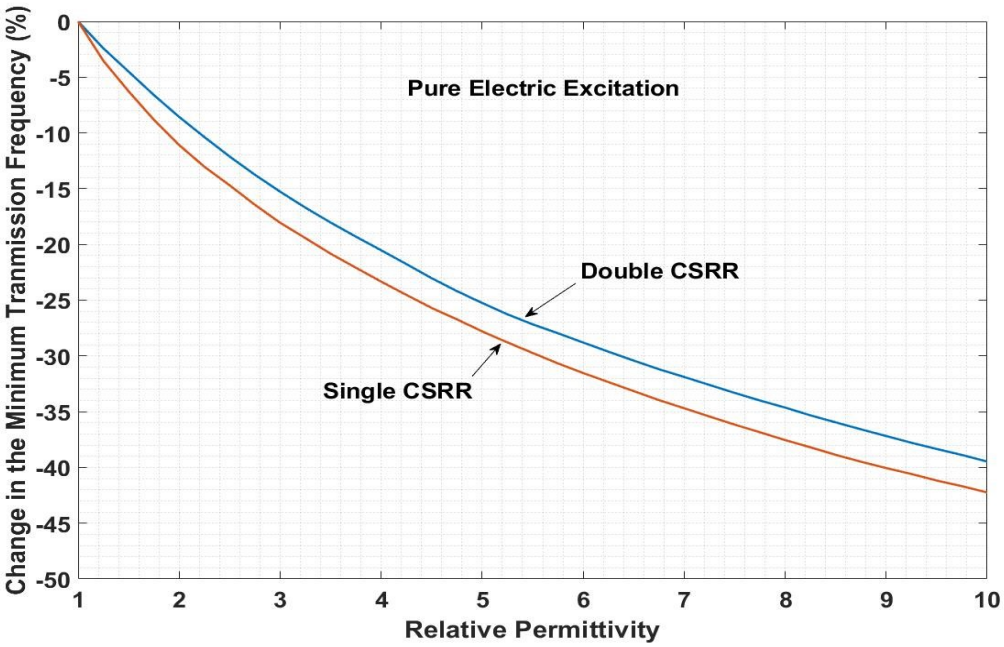

Figure 4.7 Change in the minimum transmission frequency versus MUT's relative permittivity for single (red) and double (blue) CSRR with pure electric excitation. (Reprinted from [110], © IEEE [2019])

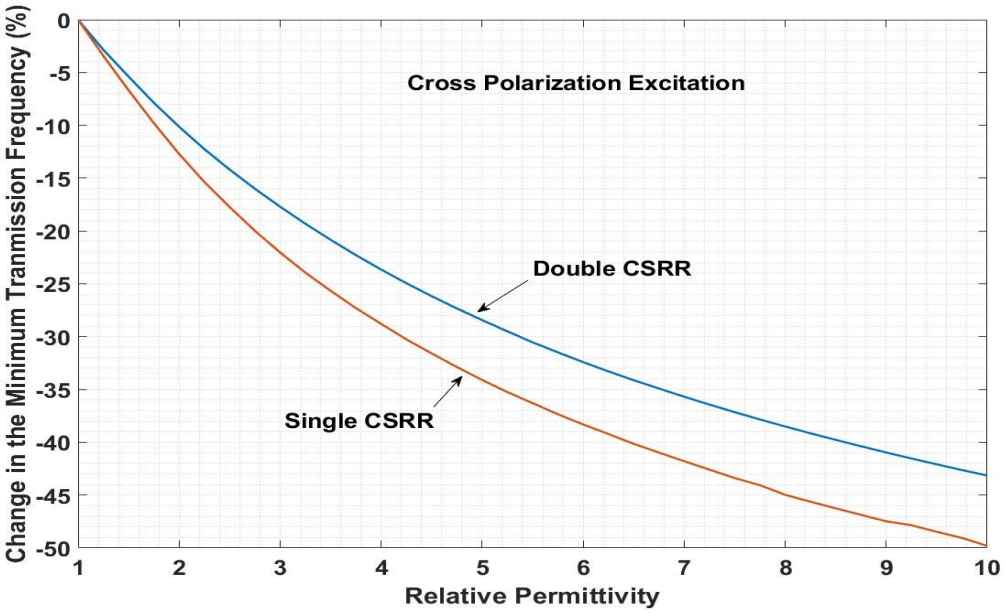

Figure 4.8 Change in the minimum transmission frequency versus MUT's relative permittivity for single (red) and double (blue) CSRR with cross-polarization excitation. (Reprinted from [110], © IEEE [2019])

4.2.3 Substrate Thickness Effect

The dielectric substrate is a medium through which a substantial portion of the guided EM waves propagates in electrically thick MTL. When a given structure resonates, the resonating electric field polarizes the surrounding dielectrics. Each homogenous polarized dielectric can be represented by an equivalent capacitance. Thus, for a given MTL that is loaded with a CSRR, the resonating electric field polarizes a portion of the MTL substrate and a portion of the loaded MUT if any. C_{CSRR} and C_{MUT} depend on the polarized portion of the substrate and the polarized portion of the loaded MUT, respectively. Reducing the polarized portion of the MUT, decreases the dependence of the minimum transmission frequency on C_{MUT} and decreases the sensor's sensitivity. For this reason, the used MUTs in this chapter have a 5-mm height to ensure efficient interaction with the resonating electric field. Furthermore, reducing the polarized portion of the

substrate increases the polarized portion of the loaded MUT which consequently increases the dependence of the minimum transmission frequency on C_{MUT} and increases the sensor's sensitivity. Reducing the polarized portion of the substrate can be achieved by reducing the portion of the substrate that falls under the influence of the resonating electric field. This reduction can be realized by reducing the thickness of the substrate.

Eight cases were considered where we studied the sensitivity of various CSRR based sensors with different substrate thicknesses. In each case a single 6-mm square CSRR with cross-polarization excitation was utilized as a sensor's resonator. Eight different sensors with eight different substrate thicknesses were considered. The dielectric constant of the used substrates is 2.9. Each sensor has a different MTL strip width to match its impedance to the feeding network impedance (i.e.50-ohm). For each case, the relative permittivity of the loaded MUT was varied from 1 to 10 with a 0.25-step. The results of the considered cases are shown in Fig.4.9 and Fig.4.10. The utilized thicknesses are also shown in the figures. The obtained results show that the free space minimum transmission frequency is higher for CSRR based sensors with thinner substrates. As per (3), this indicates that the combined CSRR equivalent reactive elements term ($L_{CSRR} \times C_{CSRR}$) is smaller for thinner substrates which consequently increases the dependence of the minimum transmission frequency on the loaded MUT. Thus, the sensitivity of the sensor with the thinnest substrate used in these cases (i.e. 0.125mm) has the highest sensitivity as shown in Fig.4.10. It should also be noted that for relatively thicker substrates (i.e. 1mm and 1.28mm in these cases), the minimum transmission frequency and the sensor's sensitivity of a CSRR based sensor do not depend on the substrate thickness. This can be understood based on the discussed polarization mechanism in the previous paragraph. As

the thickness of the substrate increases, the polarized substrate portion increases which increases C_{CSRR}. At a certain thickness, the substrate portion which is close to the CSRR will be completely polarized and the C_{CSRR} will be fixed. Any increment in the substrate thickness will add additional substrate or additional dielectric layers which will not be under the influence of the resonating electric field and consequently will not affect the minimum transmission frequency and the sensor's sensitivity as it will not change the equivalent capacitance of the CSRR.

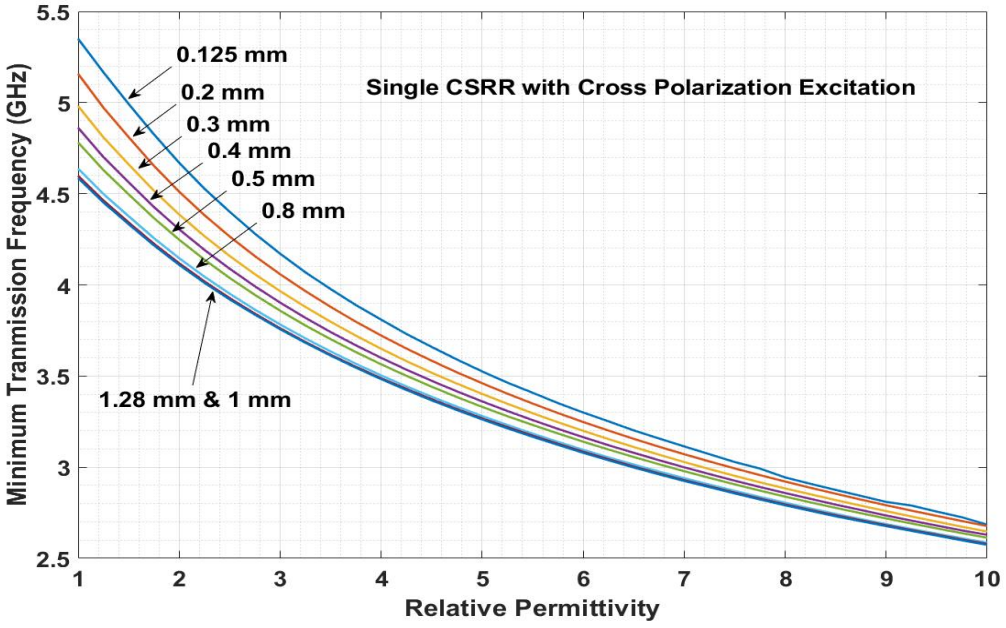

Figure 4.9 Minimum transmission frequency versus MUT's relative permittivity for CSRR based sensors with different substrate thicknesses. (Reprinted from [110], © IEEE [2019])

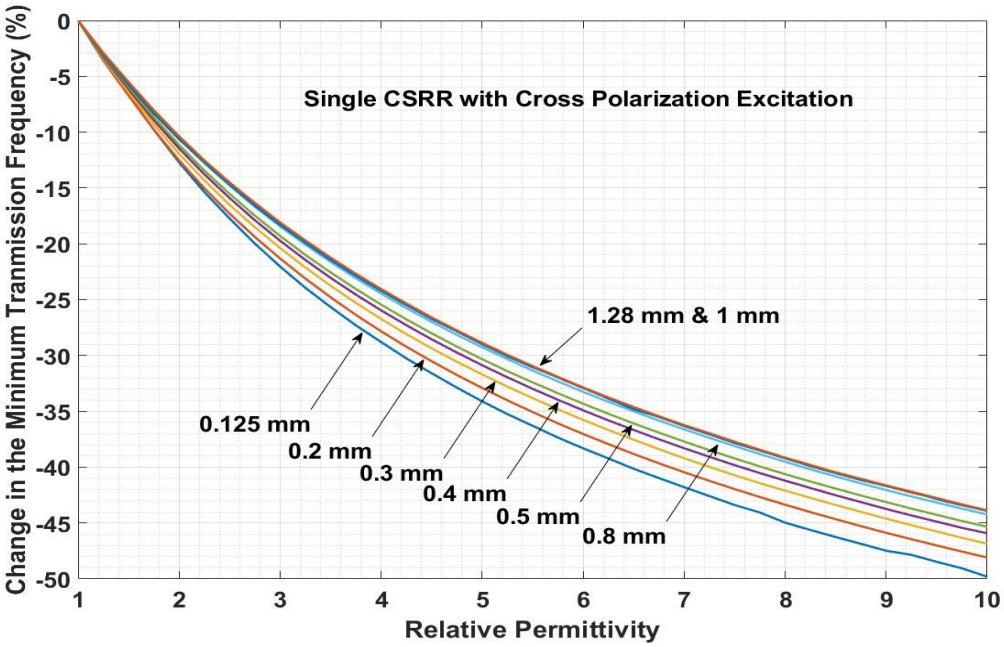

Figure 4.10 Change in the minimum transmission frequency versus MUT's relative permittivity for CSRR based sensors with different substrate thicknesses. (Reprinted from [110], © IEEE [2019])

4.2.4 Sensitivity Uniformity

Relative permittivity is a frequency-dependent parameter. A single sensor that operates within a specific band of frequency is required to extract material's relative permittivity within a specified band. However, if the characterization is going to be conducted over different frequency bands, different sensors are needed where each sensor has its own frequency range of operation and its own sensitivity. Therefore, if the sensitivity of the utilized sensors is different, the obtained relative permittivities will not be consistent. To overcome this problem, a general condition of sensitivity uniformity is presented in this dissertation (Appendix A) for CSRR based sensors that are utilized for relative permittivity measurement. For completeness, another general condition of sensitivity uniformity is also presented for relative permeability measurement

The minimum transmission frequency of MTL based resonator can be varied by varying the substrate's thickness, its dielectric constant or the resonator's design parameters. Changing a substrate thickness and/or it's dielectric constant may require an associated change of the MTL strip width to match it to the feeding network impedance. Uncontrolled variation of all or some of these three parameters may result in an unpleasant disorder of wave confinement within the MTL substrate which drastically reduces the amount of the fields at the resonator vicinity and consequently reduces its sensitivity. It will also cause different sensitivity for different frequency bands due to the variation of wave confinements within the MTL substrate. Therefore, changing one or more of the resonator's parameters (i.e. the size of CSRR in this chapter) would be a better option to vary the minimum transmission frequency which will consequently change the frequency band of operation. Sensitivity uniformity across a large spectrum could be achieved using the condition of sensitivity uniformity which is derived in Appendix A.

Sixteen cases were considered to study the sensitivity uniformity of a thin substrate MTL loaded with a single square CSRR and excited using cross-polarization excitation. Each case, has a specific CSRR size, MUT size and frequency band of operation. To vary the frequency of operation, the size of the loaded CSRR was varied by varying its side length from 3mm to 18mm with a 1-mm step. To maintain a uniform sensitivity, the ratio between C_{CSRR} and C_{MUT} maintained constant (see Appendix A). Thus, for each scaled CSRR, the width and length of the MUT assumed to be identical and to be two times higher than the side length of the scaled CSRR. For example, for a CSRR with a 3-mm side length the loaded MUT has a length and width of 6-mm. For each case, the relative permittivity of the loaded MUT was varied from 1 to 10 with a 0.25-step.

The minimum transmission frequency and corresponding sensitivity of the tested sensors are presented in Fig.4.11 and Fig.4.12, respectively. The presented results declare excellent sensitivity uniformity throughout [0.90-10.90] GHz band for each relative permittivity and each utilized sensor. As this band encompasses all used bands in the previously proposed sensors in [8,40-43], these results verify the superiority of the proposed sensors' sensitivity over previously reported ones even within their bands.

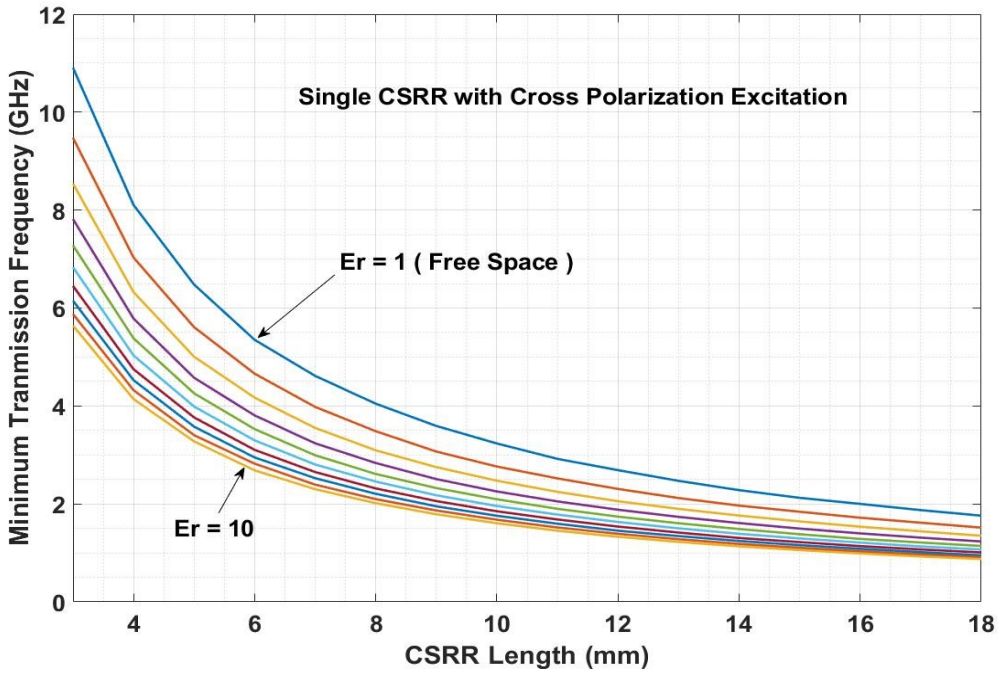

Figure 4.11 Minimum transmission frequency versus CSRR side length for MUTs with relative permittivity ranging from Er=1 to Er=10. The curves are in sequence from top to bottom starting from Er=1 (at the top) to Er=10 (at the bottom). (Reprinted from [110], © IEEE [2019])

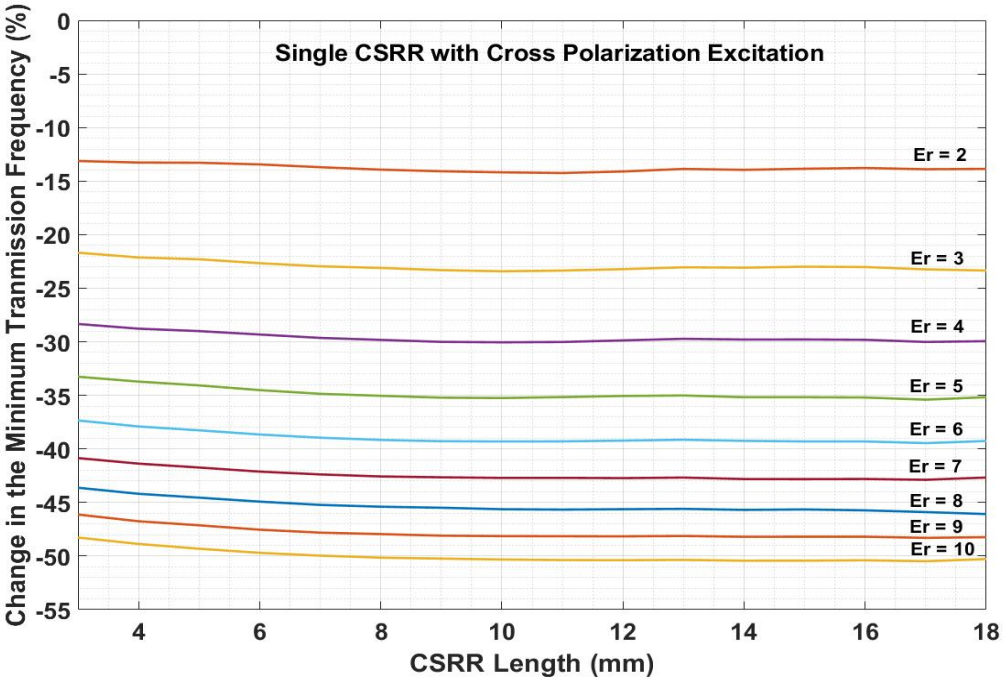

Figure 4.12 Change in the minimum transmission frequency versus CSRR side length for MUTs with relative permittivity ranging from Er=2 to Er=10. The curves are in sequence from top to bottom starting from Er=2 (at the top) to Er=10 (at the bottom). (Reprinted from [110], © IEEE [2019])

Here is another advantage of the condition of sensitivity uniformity. Previous studies estimated MUT's permittivity using a single equation that relates MUT's permittivity to the measured magnitude of change in the minimum transmission frequency (i.e. eq.4.2) rather than the percentage of change (i.e. eq.4.3) [8,40-43]. Following such procedure for a multi-band sensor requires the extraction of a unique equation for each frequency band. However, when the sensor's sensitivity is independent of the frequency band of operation, we can extract a single equation that can be utilized over a large spectrum by relating the MUT's permittivity to the measured change in the minimum transmission frequency ratio or percentage (i.e. eq.4.3) rather than frequency shift magnitude (i.e. measured in GHz as per eq.4.2). This is a vital feature especially when such

sensors are utilized as sensing spots for massive sensors network applications such as IoT where networks' computational power is limited [1]. The relation between the free space minimum transmission frequency and the side length of the square CSRR is given in (4.4). A single relation that relates the MUT's relative permittivity to the change in the minimum transmission frequency for all considered sensors that operate at different frequency bands is given in (4.5).

$$f_{free}^{tmin} = 0.00058 \times Length_{CSRR}^{4} - 0.03 \times Length_{CSRR}^{3} + 0.57 \times Length_{CSRR}^{2} - 5 \times Length_{CSRR} + 19 \quad (4.4)$$

$$\varepsilon_{MUT0} = -6.7 \times 10^{-5} \times \left(\Delta f^{tmin}\,\%\right)^{3} - 0.0016 \times \left(\Delta f^{tmin}\,\%\right)^{2} - 0.096 \times \Delta f^{tmin}\,\% + 0.94 \quad (4.5)$$

Where f_{free}^{tmin} is the free space minimum transmission frequency in (GHz), $Length_{CSRR}$ is the CSRR side length in (mm), ε_{MUT0} is the estimated MUT's relative permittivity and $\Delta f^{tmin}\,\%$ is the change in the minimum transmission frequency.

4.3 Sensors Design

This section summarizes the design of the proposed sensors. Each proposed sensing platform is composed of a 30-mm by 30-mm MTL loaded with a single square CSRR. The resonator line of symmetry coincides with the MTL strip projection on the ground plane as shown in Fig.4.1(b). This CSRR/MTL strip configuration ensures the resonator's excitation with maximum electric/magnetic (cross-polarization) excitation. The MTL is expected to be fed with a coaxial cable with a 50-ohm impedance. To match the MTL to the impedance of the feeding network, the conducting strip is designed with a 0.267 mm

strip width. CSRR path width is 0.2 mm. CSRR split length is identical to its path width (i.e.0.2 mm). The used substrate has a 0.125 mm thickness with a dielectric constant of 2.9. The size of the loaded CSRR can be scaled to vary the minimum transmission frequency and the associated frequency band of operation as per Fig.4.11. In this study the side length of the square CSRR was scaled from 3mm to 18mm with a 1-mm step for performance verification. The corresponding frequency band of operation for MUT with relative permittivity ranging from 1 to 10 is [0.90 to 10.90] GHz. It should be noted that the proposed sensors' can also be utilized outside this range with larger CSRRs or with MUTs with higher relative permittivity. However, this range is the range through which the performance of the proposed sensors' was studied.

The following steps summarize the required procedure to measure MUT's relative permittivity using the proposed sensors:

1. Identify the band of operation based on the MUT intended application.
2. Select a CSRR side length ($Length_{CSRR}$) that better fits the identified band of operation using Fig.4.11 and Fig.4.12.
3. Use the selected ($Length_{CSRR}$) to calculate the free space minimum transmission frequency (f_{free}^{tmin}) using (4.4).
4. Fabricate the sensor using the selected ($Length_{CSRR}$) and the detailed MTL specifications then measure its (f_{free}^{tmin}) experimentally and confirm that it matches the calculated one from step (3).
5. Load the sensor with a MUT then measure the new minimum transmission frequency (f_{MUT0}^{tmin}).

6. Calculate the change in the minimum transmission frequency (Δf^{tmin} %) by substituting the measured (f_{free}^{tmin}) and (f_{MUT0}^{tmin}) using (4.3).
7. Use (7) and the calculated (Δf^{tmin} %) from step (6) to calculate MUT's relative permittivity (ε_{MUT0}).

4.4 Experimental Measurements

To verify the performance of the proposed sensors experimentally, a prototype sensor was fabricated using a 30-mm by 30-mm low loss flexible substrate. The dielectric constant of the substrate is 2.9 with a 0.116 mm thickness. This substrate is slightly thinner than the used one in the previous sections (i.e. 0.125mm) however, such fabrication error is expected for thin substrates. A single square CSRR with a 6-mm side length was etched in the ground plane. The CSRR excited using cross-polarization excitation. The path width as well as the split length is 0.2mm. The planar sensor is fed with a 50-ohm coaxial cable. The obtained free space minimum transmission frequency is 5.39 GHz. This frequency is almost in the middle of the sensors' free space minimum transmission frequencies. Hence, the selection of this sensor is an optimal choice for experimental verification. Three cubic MUTs were fabricated using Roger substrates RO3003, RO3006 and RO3010. The nominal relative permittivities of these substrates are 3, 6.15 and 10.2, respectively. Each MUT was constructed by vertically stacking four layers of corresponding copper-free substrate. Each layer is a 15 mm by 15mm layer. Fig.4.13 shows the fabricated porotype and the constructed MUTs. Four measurements were obtained. The first one is the free space minimum transmission frequency. The other three are the minimum transmission frequencies of the RO3003, RO3006 and RO3010 MUTs. The MUTs minimum

transmission frequencies were obtained by placing each MUT directly underneath the MTL with direct contact with the CSRR to interrupt its resonating fields. Fig.4.14 shows the obtained experimental measurements as well as the corresponding numerical results. The experimental and numerical results are in a good match. The simulation results presented in Fig.4.14 are extracted using a 0.116 mm substrate. The little mismatch is caused by the air gap between the MUTs layers which reduces their corresponding effective permittivity. Another source of error is the air gap layer between the CSRR footprint and the MUTs. This effect is discussed in the next section.

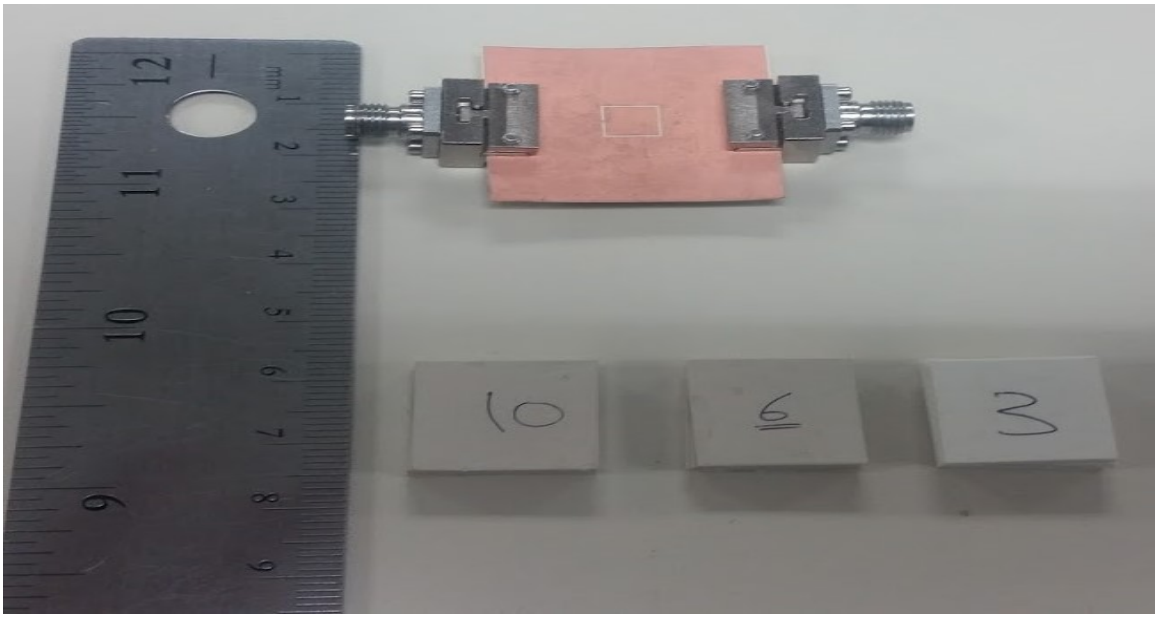

Figure 4.13 Fabricated sensor and three MUTs fabricated using Roger substrates RO3003, RO3006 and RO3010. (Reprinted from [110], © IEEE [2019])

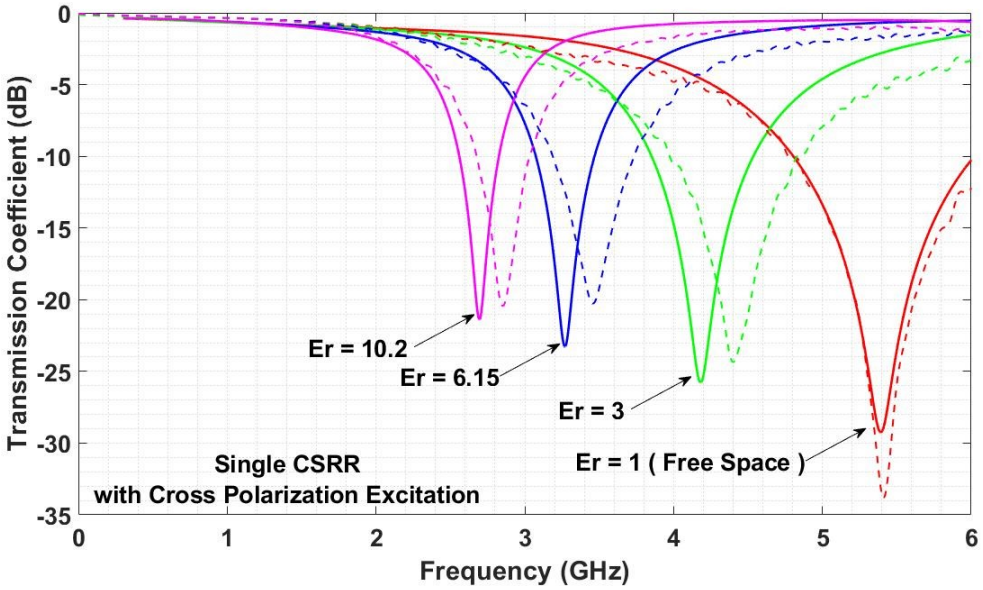

Figure 4.14 Comparison between numerical (solid line) and experimental (dashed lines) results for the 6-mm CSRR based sensor. The red curve for Er=1.The used MUTs have relative permittivities of Er=3 (green), Er=6.15 (blue) and Er=10.2 (pink). (Reprinted from [110], © IEEE [2019])

4.5 Air Gap Effect

Previous numerical results assumed direct contact between the CSRR footprint and the loaded MUT. This setup ensures perfect coupling as the CSRR's resonating fields are in a sole interaction with the MUT at the sensing zone. However, in practice an air layer may exist between the two objects forming an air gap. The presence of an air gap alters the equivalent resonator's load capacitance which consequently introduces an error in the obtained measurements. The introduced error is directly proportional to the air layer's thickness and the MUT relative permittivity.

For a permittivity sensor with a uniform air layer (i.e. air layer with a constant thickness all over the CSRR footprint), the air gap can be modeled with two equivalent capacitances in series with the MUT's equivalent capacitance [113]. As the thickness of

the air gap increases its equivalent capacitance decreases consequently the resonator's load formed by the three series capacitances (i.e. air gap /MUT/air gap) decreases. Similarly, for a non-zero fixed air layer thickness, as the MUT's relative permittivity increases the resonator's load formed by the three series capacitances decreases. Therefore, as the air gap widens the coupling between the sensor and the MUT is minimized. Consequently, a large air layer vanishes the coupling between the sensor and the loaded MUT a case at which the sensor's minimum transmission frequency becomes independent of the loaded MUT.

A case was considered and studied numerically to extract the relative permittivity of a loaded MUT at the presence of variable air gap layers using a 6-mm CSRR based sensor. The air gap layer in the considered case was varied from 0 mm to 100 um with a 10-um step. The relation of the change in the minimum transmission frequency magnitude and percentages ($\Delta f_{air\_gap}^{tmin}$), ($\Delta f_{air\_gap}^{tmin}$ %) are shown in (4.6) and (4.7), respectively. In these two relations, (f_{MUT0}^{tmin}) refers to minimum transmission frequency with a 0-mm air gap while (f_{MUT1}^{tmin}) refers to the minimum transmission frequency when an air gap exists between the CSRR and the loaded MUT. Fig.4.15 shows the change in the minimum transmission frequency with respect to the air gap thickness and the MUT's relative permittivity. The figure verifies the discussed air gap effect. The positive frequency shift percentages indicate that the change in the minimum transmission frequency moves toward the free space the change in the minimum transmission frequency as the air layer thickness and/or the MUT permittivity increase(s) which implicitly indicate that the coupling between the sensor and the loaded MUT decreases in either case.

$$\Delta f_{air\_gap}^{tmin} = f_{MUT1}^{tmin} - f_{MUT0}^{tmin} \quad (4.6)$$

$$\Delta f_{air\_gap}^{tmin}\ \% = \left(\frac{f_{MUT1}^{tmin} - f_{MUT0}^{tmin}}{f_{MUT0}^{tmin}}\right) \times 100 \quad (4.7)$$

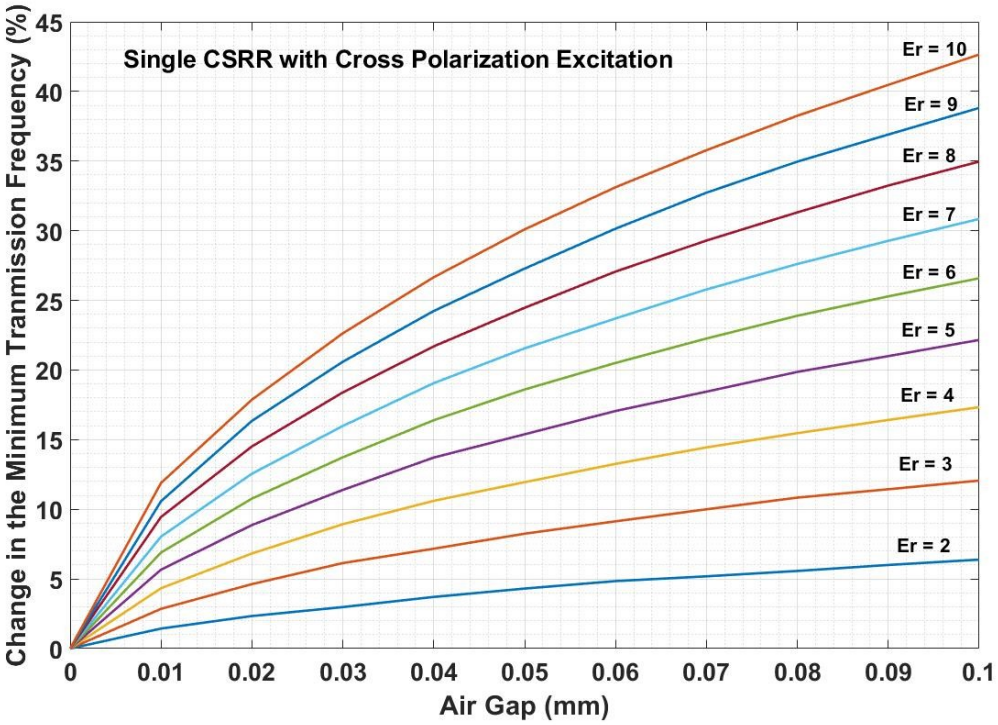

Figure 4.15 Change in the minimum transmission frequency versus air layer thickness for MUTs with relative permittivity ranging from Er=2 to Er=10. The curves are in sequence from bottom to the top starting from Er=2 (at the bottom) to Er=10 (at the top). (Reprinted from [110], © IEEE [2019])

CHAPTER 5. SECTORIAL CSRR BASED SENSOR

5.1 Introduction

This chapter proposes miniaturized, lightweight and ultrasensitive planar metamaterial sensor for relative permittivity measurement. The proposed sensor is designed using a thin-substrate microstrip line loaded with tapered sectorial Complementary Split Ring Resonator (CSRR). Compared to similar state-of-the-art sensors, the proposed one is least (60)% more sensitive with a wide dynamic range of the sensing related frequency. Moreover, unlike previously proposed sensors, the relative permittivity of a dielectric sample can be estimated using the variation of the minimum transmission frequency as well as the variation of the 10-dB sensor's bandwidth which increases the integrity and accuracy of the obtained results. The minimum transmission frequency of the proposed sensor shifts by almost 7.6 GHz with a percentage change of (61)% when the relative permittivity of the material under test (MUT) changes from 1 to 10. In addition, the 10-dB bandwidth is reduced by almost 7.7 GHz for the same MUT relative permittivity changes. Experimental measurements are in good agreement with the numerical findings. The chapter includes a comprehensive sensitivity analysis that investigates the effect of resonator's split length as well as its path width on the sensitivity and dynamic range of CSRR based sensors. Finally, the proposed sensor was used for biomedical microfluidic sensing to further demonstrate its practicality using different samples with different electrical properties. The sensor was able to provide distinct features for three different eye drops. The proposed sensor can be utilized as an effective

permittivity sensor for various sensing applications such as displacement, nondestructive and biomedical sensing.

The chapter is organized as follows. Section 5.2 provides an overview of the proposed sensor design and sensing mechanism. Section 5.3 presents a comprehensive sensitivity analysis that discusses the effect of the path width and split length variation on the sensors' sensitivity. It also illustrates how we can increase the sensitivity of the proposed sensor using two dielectric test samples instead of one. The experimental results are presented in section 5.4. Section 5.5 and section 5.6 provide the required proof of concept for the sensor practicality as they demonstrate how we can utilize the proposed sensor as a microfluidic or crack sensor.

5.2 Sensor Design

The proposed sensor in this chapter is designed using a planar transmission line that is loaded with a passive resonator. Meta-resonator is an electrically small resonator that can be modeled by lumped circuit elements. It can be modeled by equivalent resonator' capacitance and equivalent resonator' inductance. These two circuit elements control the minimum transmission frequency and the bandwidth of the meta-resonator.

For sensing applications, the loaded meta-resonator should have efficient interaction with the loaded MUT. This interaction results in additional parallel equivalent MUT's capacitance for a permittivity sensor or parallel equivalent MUT's inductance for a permeability sensor. The change in the minimum transmission frequency of the composite structure (meta-resonator/MUT) is directly proportional to the equivalent MUT's capacitance for a permittivity sensor or equivalent MUT's inductance for a

permeability sensor. Thus, the selected resonator should be able to induce a strong electric field (magnetic field) within the loaded MUT to create a high enough equivalent capacitance (inductance) for permittivity (permeability) sensor.

At resonance, SRR creates a normal magnetic dipole that can induce a magnetic field within the interacted MUT while CSRR creates a normal electric dipole that can induce an electric field within the interacted MUT. Since we are proposing a sensor for relative permittivity measurement, CSRR is used in this chapter. MTL is selected as the hosting transmission line as CSRR can be optimally designed with a vertical time-varying electric field [7].

Minimum transmission frequency was used to define the sensitivity of the proposed sensors. The minimum transmission frequency of MTL loaded with a CSRR is given by (5.1) [111]. The change in the minimum transmission frequency was calculated based on (5.2). The sensitivity of a CSRR based sensor at each studied case was calculated based on the percentage change in the minimum transmission frequency as given by (5.3).

$$f_{MUT0}^{tmin} = \frac{1}{2\pi\sqrt{L_{CSRR}(C_{CSRR} + C_{MUT})}} \qquad (5.1)$$

$$\Delta f^{tmin} = f_{MUT0}^{tmin} - f_{free}^{tmin} \qquad (5.2)$$

$$\Delta f^{tmin}\,\% = \left(\frac{f_{MUT0}^{tmin} - f_{free}^{tmin}}{f_{free}^{tmin}}\right) \times 100 \qquad (5.3)$$

where f_{MUT0}^{tmin} is the minimum transmission frequency at the presence of MUT with a 0-mm air gap . L_{CSRR} and C_{CSRR} are the equivalent inductance and capacitance of the

loaded CSRR, respectively. C_{MUT} is the equivalent capacitance of the loaded MUT. f_{free}^{tmin} is the free space minimum transmission frequency (i.e. $f_{free}^{tmin} = f_{MUT0}^{tmin}$ with $C_{MUT} = 0$) Δf^{tmin} is the change in the minimum transmission frequency in GHz. Δf^{tmin} % is the percentage change in the minimum transmission frequency.

From these equations, we can conclude that a reduction in the equivalent CSRR capacitance results in better sensitivity. Another important parameter for the design of a permittivity sensor is the determination of the dynamic range of the required sensor. MUT could be solid or liquid samples. Some liquid samples have distinct properties in a specific band of frequency compared to other bands. Moreover, some applications that use a permittivity sensor to measure the effective permittivity of the surrounding environment (i.e. displacement or velocity sensor) require sensors with high dynamic range. The dynamic range of a meta-resonator based sensor depends on the equivalent capacitance and equivalent inductance of the loaded resonator. In our case as we are using a CSRR based sensor, the dynamic range of the sensor for a specific MUT's permittivity range can be calculated using (5.2) and can be varied by varying the free space minimum transmission frequency which is a function of the L_{CSRR} and C_{CSRR}.

The previous chapter study optimized the sensitivity of a CSRR based sensor using thin substrate MTL, with cross-polarized single CSRR. The previous study didn't address the contribution of the CSRR's path width as well as the CSRR's split length on the sensitivity and dynamic range. The effect of these two parameters is studied in this chapter.

As per (5.1), decreasing the equivalent capacitance of the CSRR (C_{CSRR}) increases the free space minimum transmission frequency as well as the sensitivity of the sensor. The

path width of a CSRR controls C_{CSRR}. As the path width of the CSRR increases, C_{CSRR} as well as the quality factor of the resonator decreases. In addition as the path width of the CSRR increases, its bandwidth increases. This is due to the fact that more electrical paths are afforded to the resonating displacement currents compared to a resonating CSRR with a narrower path width. When a dielectric MUT is loaded to a CSRR with a large path width (tapered CSRR), the permittivity of the loaded MUT increases the effective capacitance of the sensor (i.e. increases the term$(C_{CSRR} + C_{MUT})$) which decreases the minimum transmission frequency and consequently increases the sensitivity compared to the sensitivity of a non-tapered CSRR sensor. Moreover, the loaded MUT varies the resonating current velocity as it varies the electrical length of resonating structure which is composed of the CSRR as well as the interacting portion of the loaded MUT. This in turn, varies the quality factor as well as the bandwidth of the resonating structure.

As per (5.1), decreasing the equivalent inductance of the CSRR (L_{CSRR}) increases free space minimum transmission frequency. L_{CSRR} is a strong function of the CSRR split length. It has an influence on the sensor's sensitivity however, this influence (for permittivity sensor) is not equivalent to the influence of the C_{CSRR}. As the split length of the CSRR increases, L_{CSRR} and the quality factor of the sensor decrease while the bandwidth and sensitivity of the sensor increase. When a dielectric MUT is loaded to a CSRR with a large split length, the permittivity of the loaded MUT increases the effective inductance of the sensor as it increases the current flow from the ground plane to the CSRR internal island which decreases the minimum transmission frequency and consequently increases the sensitivity compared to the sensitivity of non-tapered CSRR sensor.

5.3 Sensitivity Analysis

This section presents a comprehensive numerical study that discusses the influence of the meta-resonator's path width and split length on the sensitivity of a meta-resonator relative permittivity sensor. Many scenarios were simulated to extract the scattering parameters and analyze the contribution of the two meta-resonator parameters on the sensitivity of the proposed sensor. The study was conducted using the full-wave numerical simulation package ANSYS HFSS. The used sensing platform (sensor) consists of a thin-substrate MTL loaded with a case-specific meta-resonator. For all simulated scenarios, the properties of the MTL and its substrate were fixed. The substrate's dielectric constant and thickness are 2.9 and 0.125mm, respectively. The MTL strip width is 0.267 mm to match the sensing platform to a 50-ohm feeding network.

The simulated scenarios can be categorized into two categories. In the first category, the sensor is assumed to be loaded with a single cubic dielectric sample (single MUT) in direct contact with the meta-resonator (i.e. loaded to the sensor from the ground plane side). In the second category, the sensor is loaded with two cubic dielectric samples (two MUTs) one of them is in direct contact with the meta-resonator while the other is placed above the MTL strip. For all simulated cases, the used MUT is a rectangular cube dielectric material with a 5-mm cube height and 15mm length and width. The MUT relative permittivity was varied for each simulated case as detailed in the upcoming subsections. Fig.5.1 shows the general setup of the used sensor and MUTs.

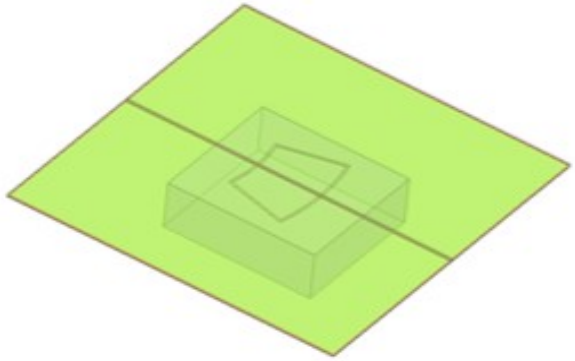

(a)

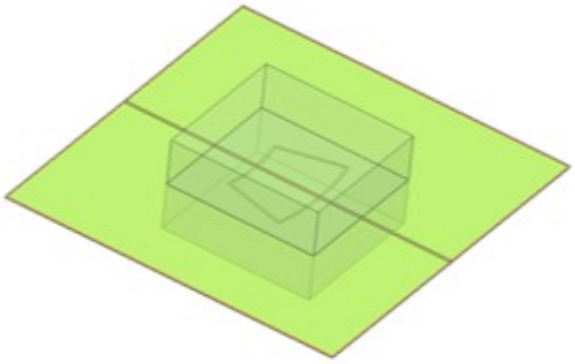

(b)

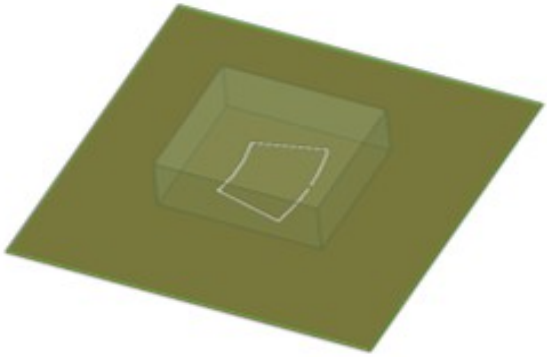

(c)

Figure 5.1 (a) Top view of the general sensor's setup with one MUT (b) top view of the general sensor's setup with two MUTs (c) bottom view of the general sensor's setup for both categories. The etched resonator in the figure is a non-tapered CSRRB. The MUT appears as a semi-transparent cube attached to the ground plane.

Two sectorial CSRRs were used interchangeably as the sensor's meta-resonator. They are both sectorial CSRR where one of them has a CSRR's split on the bigger arc (CSRRB) while the other has a CSRR's split on the smaller arc (CSRRS). For each CSRR, the length of the outer bigger arc, outer smaller arc and side length are 9 mm, 6 mm and 6 mm, respectively. Fig.5.2 shows the used CSRRs. Each of the sectorial CSRR was utilized with each category of the simulated scenarios. The loaded CSRR is excited using cross-polarization excitation as it is the optimum excitation scheme for a permittivity sensor. The path width and the split length of the utilized sectorial CSRR were varied based on the case requirement as detailed in the upcoming subsections.

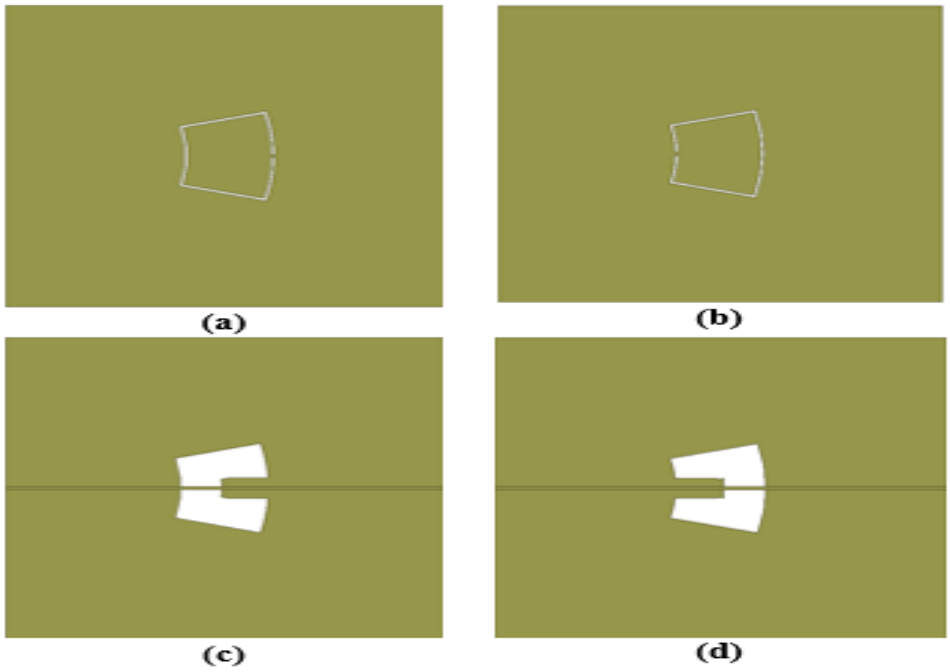

Figure 5.2 (a) Top view of the sensor with non-tapered CSRRB. (b) Top view of the sensor with non-tapered CSRRS. (c) Top view of the sensor with tapered CSRRB (d) Top view of the sensor with tapered CSRRS. The substrate was removed for more clarity. The MTL strip

5.3.1 One MUT

In this category of the simulated scenarios, CSRRB and CSRRS based sensors were used with a single MUT. The CSRR's path width was varied from 0.2 mm to 2.8 mm with a 0.2 mm step. Also, the CSRR's split length was varied from 0.2 mm to 2.0 mm with a 0.2 mm step. The used MUT has a relative permittivity of either 1 or 10.

Fig.5.3 shows the free space minimum transmission frequency of the CSRRB based sensor while Fig.5.4 shows the free space minimum transmission frequency of the CSRRS based sensor.

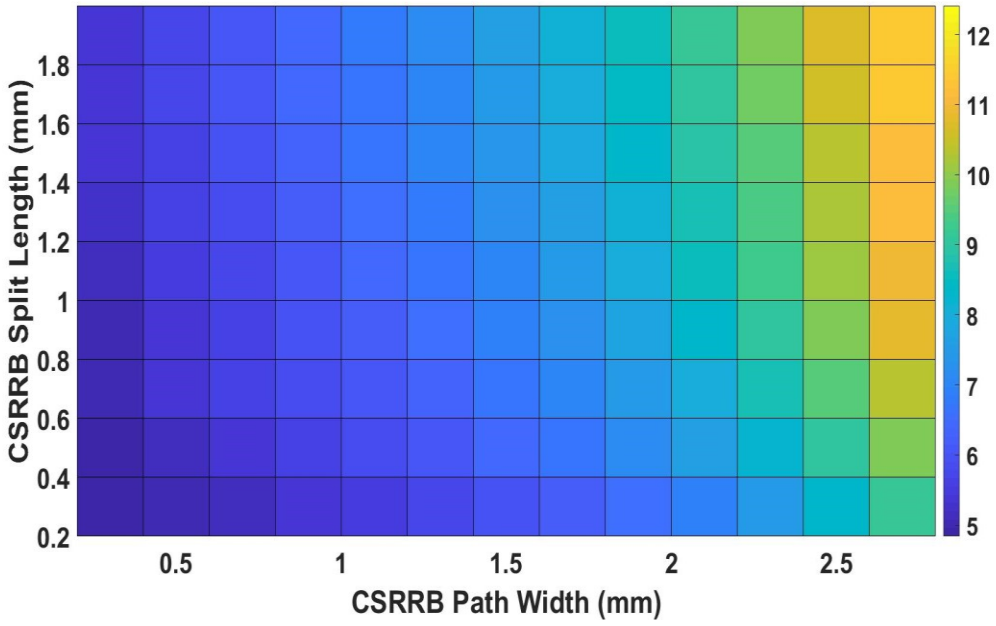

Figure 5.3 Free space minimum transmission frequency of the CSRRB based sensor in (GHz) versus CSRRB's path width and split length in (mm)

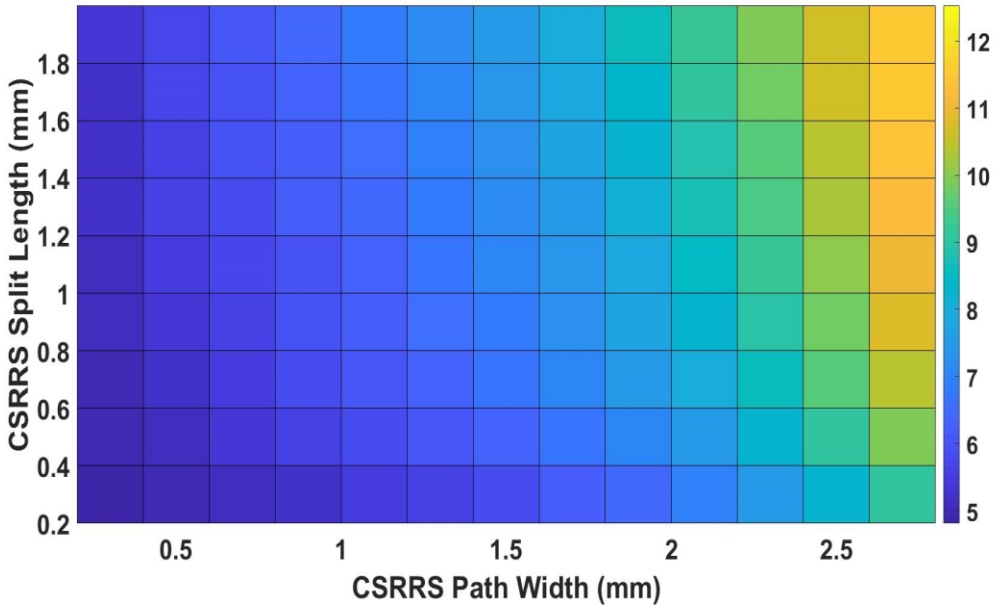

Figure 5.4 Free space minimum transmission frequency of the CSRRS based sensor in (GHz) versus CSRRS's path width and split length in (mm)

As per these two figures, the minimum transmission frequency of the CSRRB or CSRRS sensors increases with the increase of the CSRR's path width or with the increase of the CSRR's split length. However, it should be noted from the same figures that the rate of increase in the free space minimum transmission frequency for both CSRRs is higher when the path width of the CSRR increases for fixed split length compared to the rate of increase when the split length increases for fixed path width. This indicates that the rate of the equivalent CSRR's capacitance reduction in (5.1) is higher than the rate of the equivalent CSRR's inductance reduction in the same relation. Also, based on (5.1) and these figures, CSRRs with 2 mm split length and 2.8 mm path width (tapered CSRR), has the minimum equivalent CSRR's inductance and capacitance while CSRRs with 0.2 mm split length and 0.2 mm path width has the maximum equivalent CSRR's inductance and capacitance.

To quantify the rate of increase in the free space minimum transmission frequency, all minimum transmission frequencies in the two figures were normalized using the lowest minimum transmission frequency (i.e the minimum transmission frequency of the CSRRs with 0.2 mm split length and 0.2 mm path width). Fig. 5.5 and Fig. 5.6 show the normalized free space minimum transmission frequency of the two sensors.

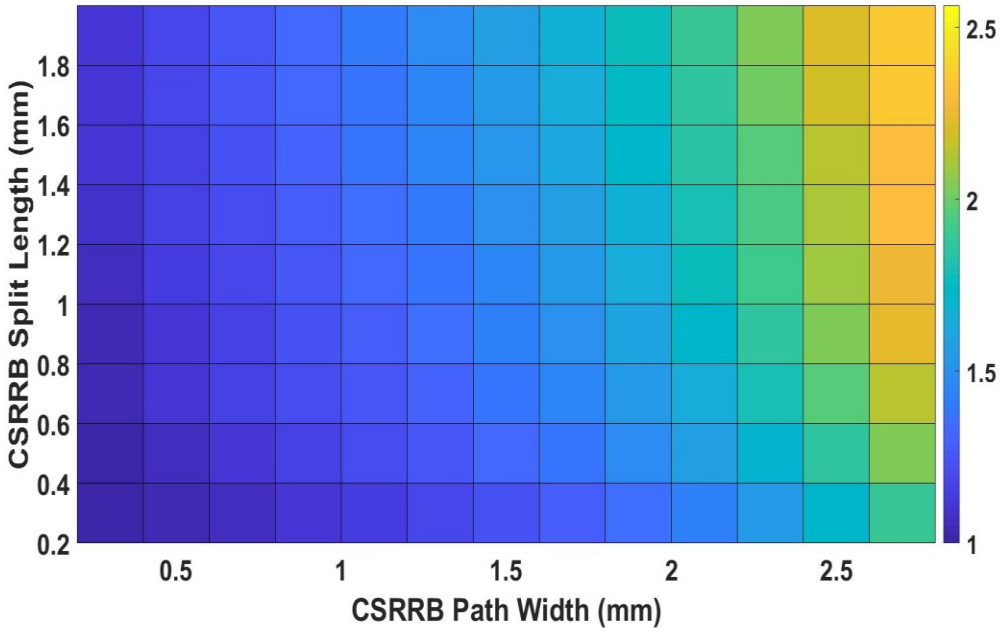

Figure 5.5 Normalized free space minimum transmission frequency of the CSRRB based sensor versus CSRRB's path width and split length in (mm)

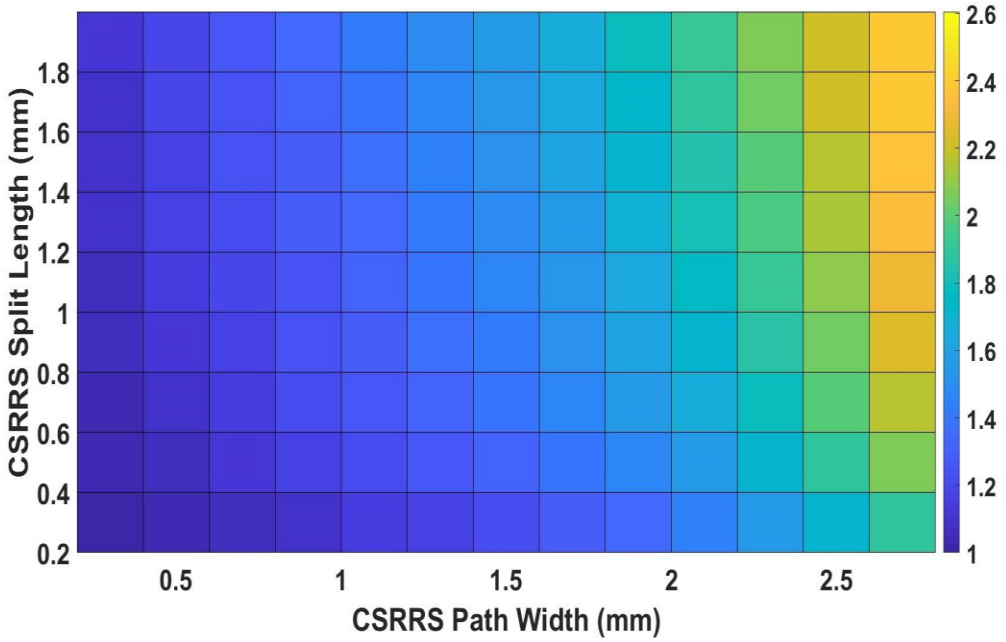

Figure 5.6 Normalized free space minimum transmission frequency of the CSRRS based sensor versus CSRRS's path width and split length in (mm)

As shown, the minimum transmission frequency of the CSRRs' sensors with 2 mm split length and 2.8 mm path width (tapered CSRR) is almost 2.6 times the minimum transmission frequency of the CSRRs with 0.2 mm split length and path width. As the minimum transmission frequency is controlled by the effective permittivity of the CSRR and MUT if any, and based on the mentioned factors it is expected that the dynamic range and sensitivity of the tapered CSRR are going to be higher than the dynamic range and sensitivity of the non-tapered one. This is verified by the upcoming figures and simulated cases.

Fig.5.7 and Fig.5.8 show the change in the minimum transmission frequency of the CSRRB and CSRRS sensors, respectively in GHz when the relative permittivity of the loaded MUT was changed from 1 to 10. These two figures are utilized to define the dynamic range of the two sensors. Fig.9 and Fig.10 show the percentage change in the

minimum transmission frequency for the same cases. These two figures are utilized to calculate the sensitivity of the considered CSRRs sensors.

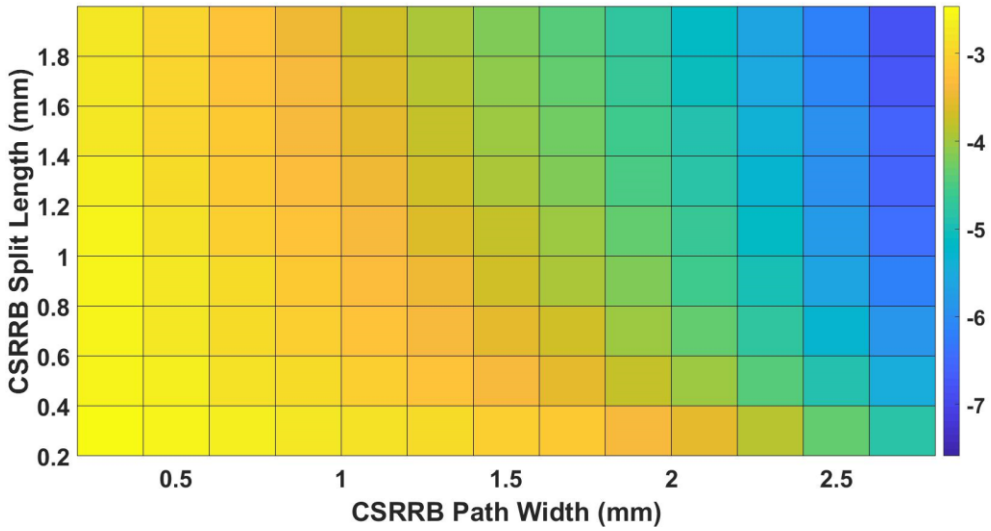

Figure 5.7 Change in the minimum transmission frequency for the CSRRB based sensor in (GHz) when the relative permittivity of the loaded MUT changes from 1 to 10 versus CSRRB's path width and split length in (mm)

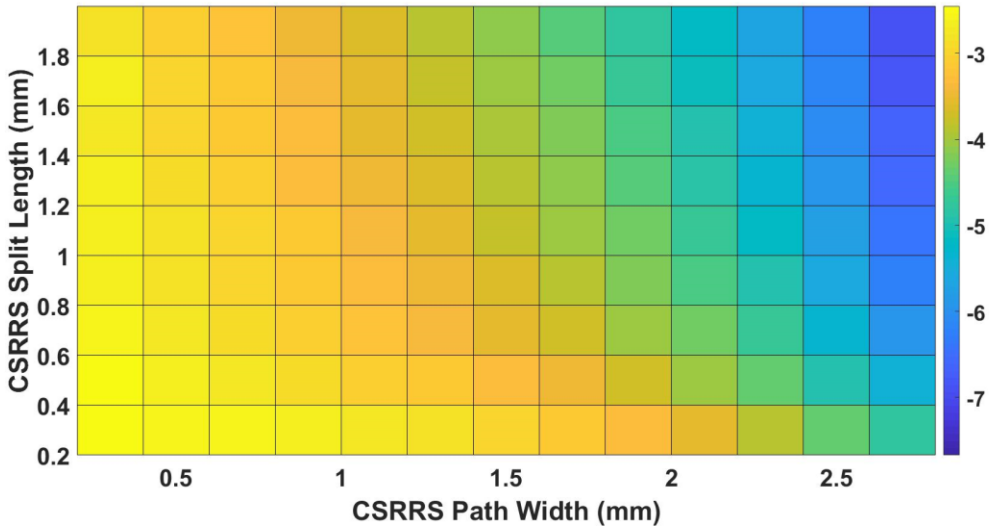

Figure 5.8 Change in the minimum transmission frequency for the CSRRS based sensor in (GHz) when the relative permittivity of the loaded MUT changes from 1 to 10 versus CSRRS's path width and split length in (mm)

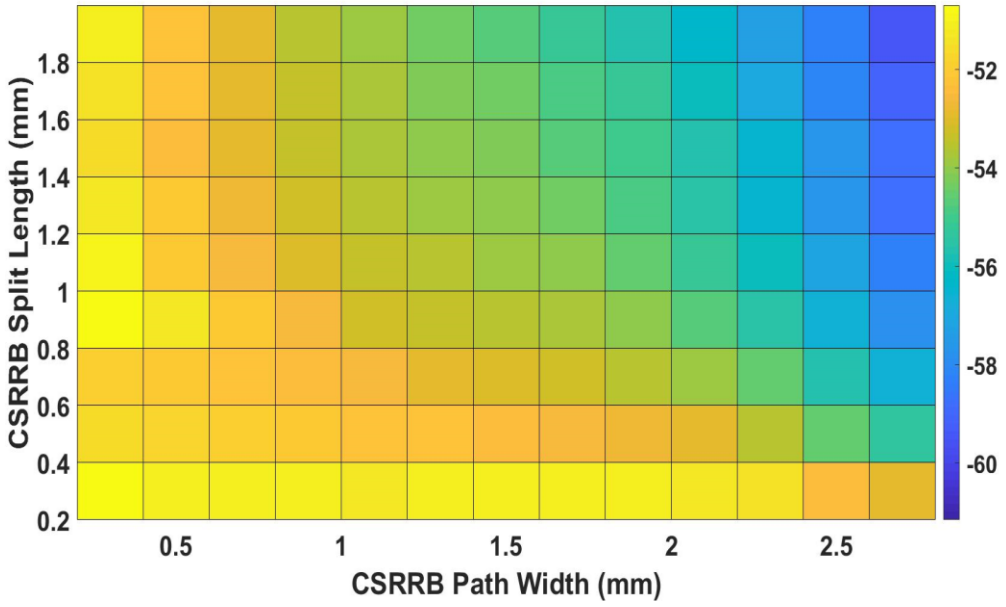

Figure 5.9 Change in the minimum transmission frequency for the CSRRB based sensor in (%) when the relative permittivity of the loaded MUT changes from 1 to 10 versus CSRRB's path width and split length in (mm)

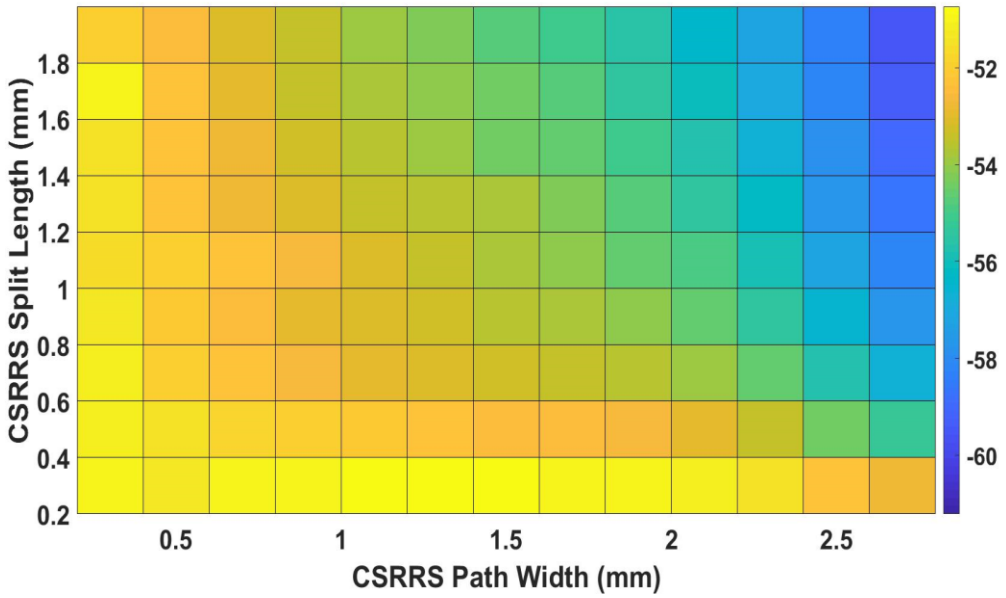

Figure 5.10 Change in the minimum transmission frequency for the CSRRS based sensor in (%) when the relative permittivity of the loaded MUT changes from 1 to 10 versus CSRRS's path width and split length in (mm)

As per these four figures, the change in the minimum transmission frequency of the two sensors is similar. The dynamic range and sensitivity of the considered CSRR sensors, increase with the increase of the CSRR's path width or with the increase of the CSRR's split length. It is also noticed that the rate of increase is higher when the path width of the CSRR increases for fixed split length compared to the rate of increase when the split length increases for fixed path width. The dynamic range of the CSRRB and CSRRS sensors with 2 mm split length and 2.8 mm path width (tapered CSRR) are almost 7.59 GHz and 7.67 GHz, respectively. The dynamic range of the CSRRB and CSRRS sensors with 0.2 mm split length and path width are almost identical and equal to 2.5 GHz. Moreover, the sensitivity of the two tapered sensors is 61% while the sensitivity of the non-tapered ones is 50%. Thus, the tapering technique improves the dynamic range and the sensitivity of the sensor by more than 300% and 22%, respectively. Fig. 5.11 and Fig.5.12 show specific sensitivity and resolution comparison between the non-tapered and tapered CSRRB and CSRRS sensors when the relative permittivity of the loaded MUT was varied from 1 to 10 with a 0.25- step. The figures show the superiority of the tapered CSRRs based sensors in terms of sensitivity and resolution.

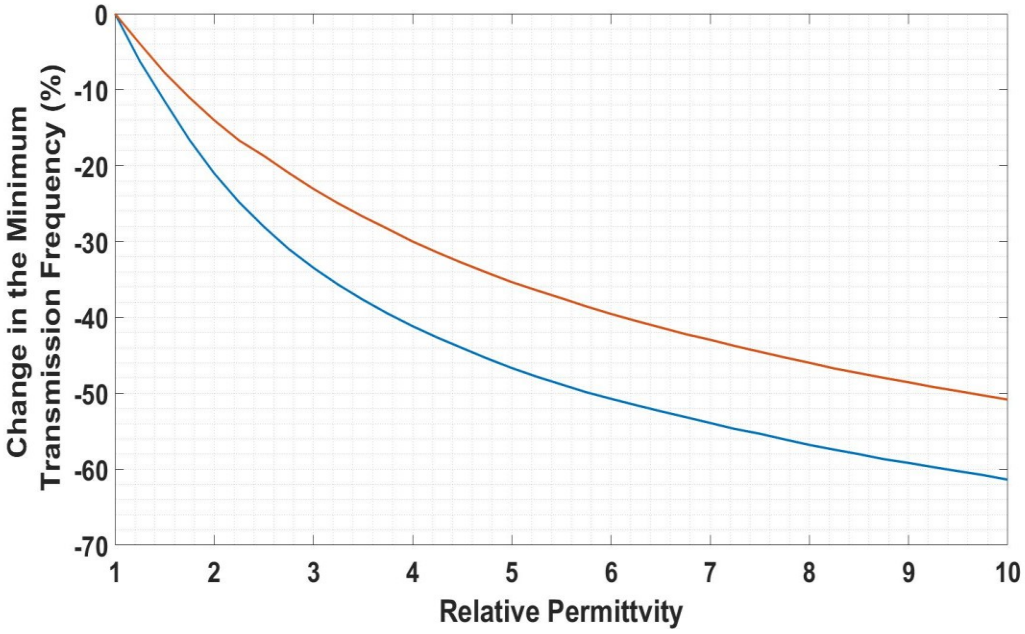

Figure 5.11 Change in the minimum transmission frequency versus MUT's relative permittivity for the non-tapered CSRRB (red) and tapered CSRRB (blue) based sensors.

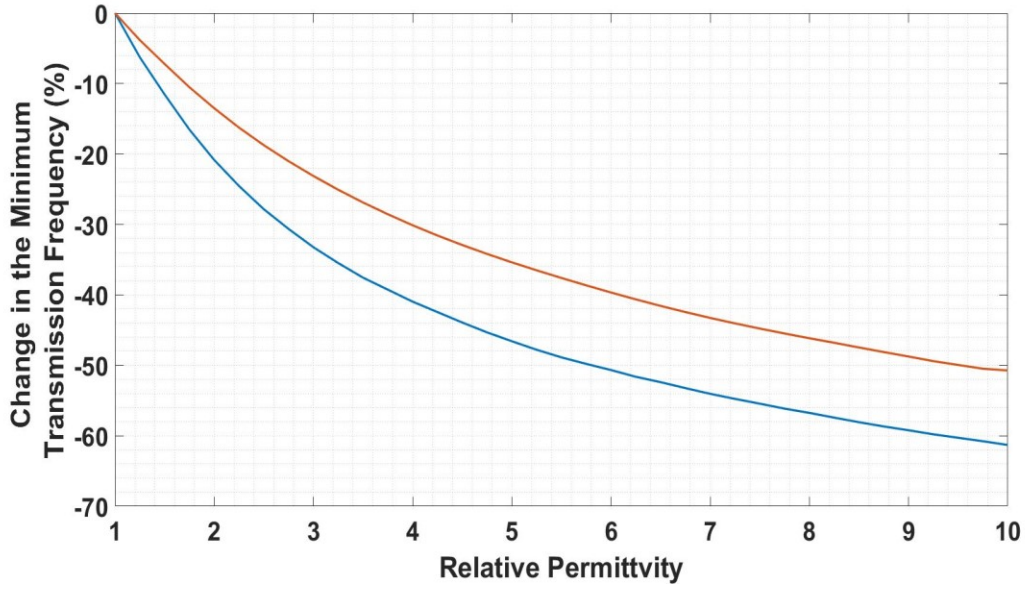

Figure 5.12 Change in the minimum transmission frequency versus MUT's relative permittivity for the non-tapered CSRRS (red) and tapered CSRRS (blue) based sensors.

The relative permittivity of the loaded MUT can be estimated using the below formula which utilizes the variation of the minimum transmission frequency of the CSRRB based sensor

$$\varepsilon_{MUT} = 8.6 \times 10^{-7} \times \left(\Delta f^{tmin}\,\%\right)^4 + 4.5 \times 10^{-5} \times \left(\Delta f^{tmin}\,\%\right)^3 + 0.0014 \times \left(\Delta f^{tmin}\,\%\right)^2 - 0.03 \times \Delta f^{tmin}\,\% \; + 1 \qquad (5.4)$$

Where ε_{MUT} is the estimated MUT's relative permittivity and $\Delta f^{tmin}\,\%$ is the change in the minimum transmission frequency.

Tapered CSRR allows more circulating currents to circulate at different path lengths which consequently increases the number of circulating currents' wavelengths and increases the dispersion. This in turn, increases the difference between the loaded and unloaded CSRR. Thus, in principle, the bandwidth of the sensor with tapered CSRR can be utilized to estimate the relative permittivity of the loaded MUT. The following figures provide the required validation of this hypothesis.

Fig 5.13 shows the free space 10-dB stopband bandwidth of the CSRRB based sensor while Fig 5.14 shows the free space 10-dB stopband bandwidth of the CSRRS based sensor.

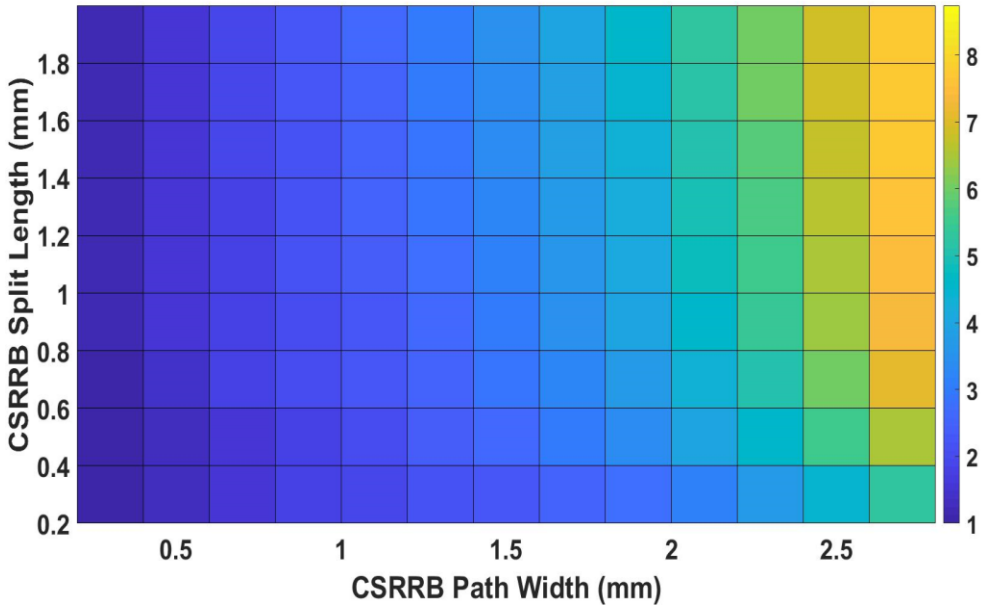

Figure 5.13 Free space 10-dB stopband bandwidth of the CSRRB based sensor in (GHz) versus CSRRB's path width and split length in (mm)

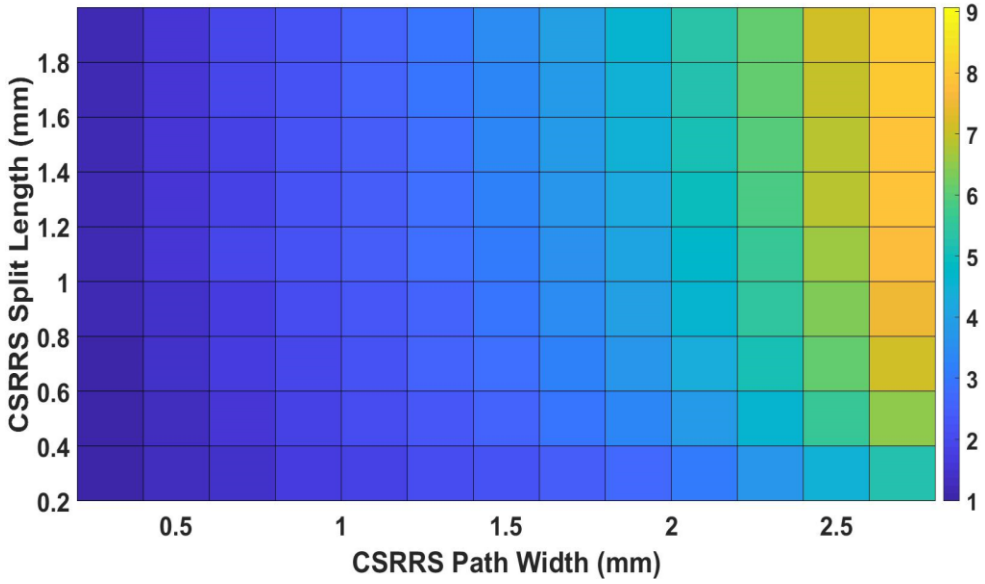

Figure 5.14 Free space 10-dB stopband bandwidth of the CSRRS based sensor in (GHz) versus CSRRS's path width and split length in (mm)

As per these two figures, the free space 10-dB stopband bandwidth of the CSRRB and CSRRS sensors increases with the increase of the CSRR's path width or with the increase of the CSRR's split length. However, it should be noted from the same figures that the rate of increase in the free space 10-dB stopband bandwidth for both CSRRs is higher when the path width of the CSRR increases for fixed split length compared to the rate of increase when the split length increases for fixed path width. The free space 10-dB stopband bandwidths of the CSRRB and CSRRS sensor with 2 mm split length and 2.8 mm path width (tapered CSRRs) are almost 8.88 GHz and 8.6 GHz, respectively. However, the free space 10-dB stopband bandwidths of the CSRRB and CSRRS sensor with 0.2 mm split length and 0.2 mm path width (non-tapered CSRRs) are almost identical and equal to 1 GHz.

Fig.5.15 and Fig.5.16 show the change in the stopband bandwidth of the CSRRB and CSRRS sensors, respectively in GHz when the relative permittivity of the loaded MUT was changed from 1 to 10.

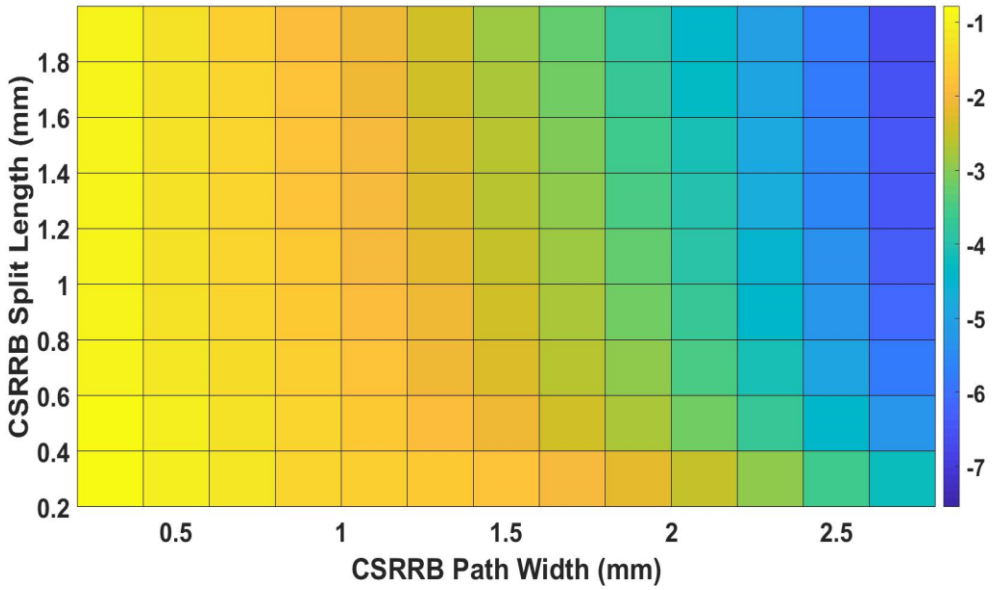

Figure 5.15 Change in the 10-dB stopband bandwidth for the CSRRB based sensor in (GHz) when the relative permittivity of the loaded MUT changes from 1 to 10 versus CSRRB's path width and split length in (mm)

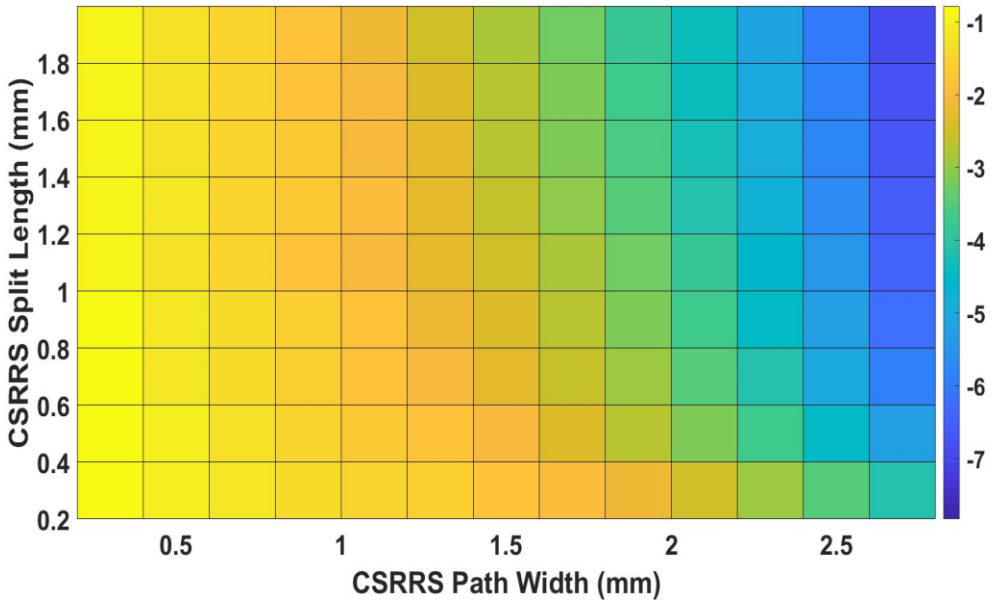

Figure 5.16 Change in the 10-dB stopband bandwidth for the CSRRS based sensor in (GHz) when the relative permittivity of the loaded MUT changes from 1 to 10 versus CSRRS's path width and split length in (mm)

As per these figures, the transmission bandwidth of the tapered CSRRB and the tapered CSRRS sensors reduces by 7.51GHz and 7.72 GHz, respectively. The corresponding reduction of the non-tapered CSRRB and CSRRS are almost identical and equal to 0.78 GHz. Thus, the tapered CSRR sensor reduces the stopband bandwidth of the sensor almost nine times the corresponding reduction by the non-tapered CSRR based sensor. The little difference in the change of bandwidths between the tapered CSRRB and tapered CSRRS is due to the fact that the equivalent capacitance in the CSRRB is defined by smaller arc compared to the equivalent capacitance in the CSRRS which consequently allow higher interaction between the loaded MUT and the CSRRS based sensor compared to the interaction between the MUT and the CSRRB sensor.

Fig. 5.17 and Fig.5.18 show the change in the 10-dB stopband bandwidth between the tapered and non-tapered CSRRB and CSRRS sensors when the relative permittivity of the loaded MUT was varied from 1 to 10 with a 0.25-step. These figures indicate that the tapering technique allows the designer to estimate the relative permittivity of unknown samples with higher integrity and resolution.

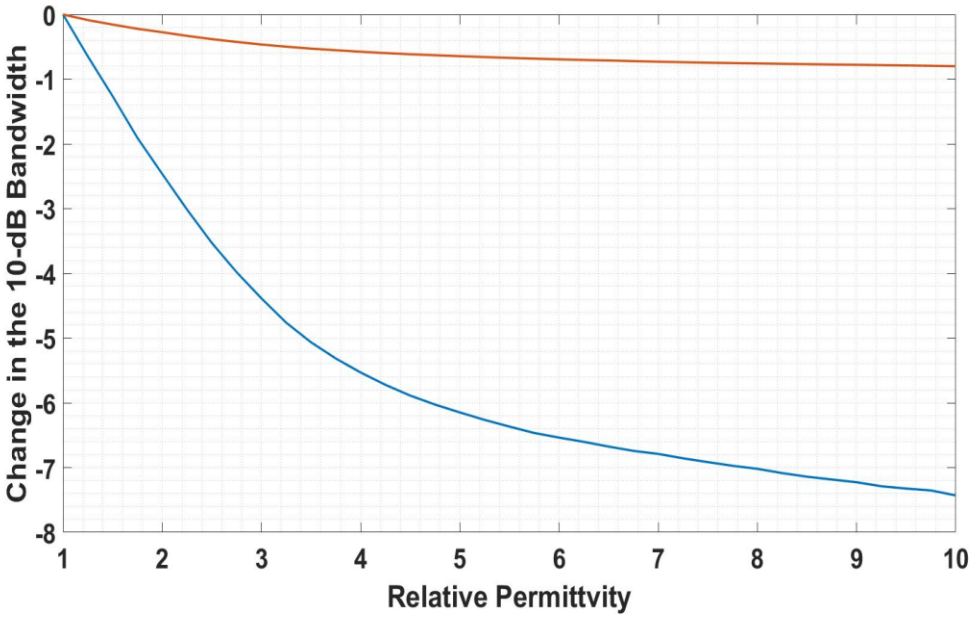

Figure 5.17 Change in the 10-dB stopband bandwidth versus MUT's relative permittivity for the non-tapered CSRRB (red) and tapered CSRRB (blue) based sensors.

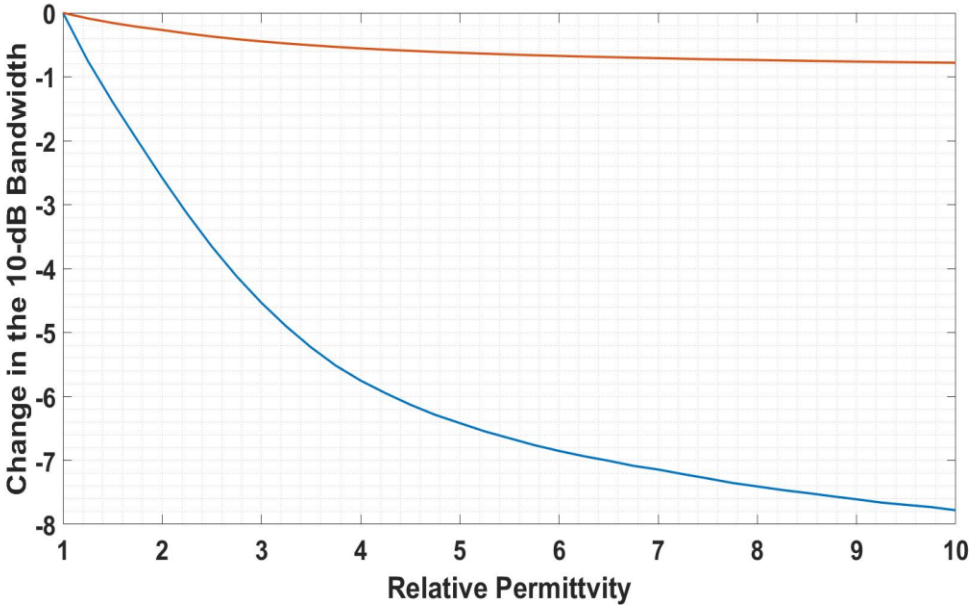

Figure 5.18 Change in the 10-dB stopband bandwidth versus MUT's relative permittivity for the non-tapered CSRRS (red) and tapered CSRRS (blue) based sensors.

The relative permittivity of the loaded MUT can be estimated using the below formula which utilizes the variation of the 10-dB stopband bandwidth of the CSRRB based sensor

$$\varepsilon_{MUT} = -0.0019 \times (\Delta bw^t)^5 - 0.022 \times (\Delta bw^t)^4 - 0.088 \times (\Delta bw^t)^3 - 0.12 \times (\Delta bw^t)^2 - 0.43 \times \Delta bw^t + 1 \quad (5.5)$$

Where ε_{MUT} is the estimated MUT's relative permittivity and Δbw^t % is the change in the 10-dB stopband bandwidth in (GHz).

5.3.2 Two MUTs

A thin-substrate MTL disperses most of the transmitted wave as it has limited ability to firmly guide the wave within its electrically thin substrate. The wave dispersion is caused by the variation of the effective permittivity seen by the wave. The effective permittivity of MTL is a ratio between the surrounding medium (i.e. air) permittivity and the dielectric constant of the substrate. For electrically thick substrate, a large portion of the transmitted wave is guided within the substrate and the effective permittivity of the transmission line is almost the same as the dielectric constant of the line's substrate. As the substrate thickness reduces, the wave starts to travel through the substrate and the surrounding medium, the effective permittivity in this case is less than the dielectric constant of the substrate if the surrounding medium is air. Thus, for sensing applications, a thin-substrate allows more interaction between the MUT and the dispersed wave even without the presence of a resonator. The MUT interacts with the dispersed wave more from the top side of the MTL around the MTL strip. To make use of the dispersion feature of a thin-

substrate transmission line sensor, the previous analysis was repeated with the placement of another MUT above the MTL strip in the presence of MUT with similar relative permittivity in the ground plane as shown in Fig.5.1b. An additional 6% and 3% shift in the minimum transmission frequency of the non-tapered and tapered CSRRS sensors were noticed, respectively. The additional variation in the 10-dB bandwidth for the two sensors were negligible. Fig 5.19 and Fig 5.20 show specific sensitivity and resolution comparison between the non-tapered and tapered CSRRB and CSRRS sensors when the relative permittivity of the loaded MUTs was varied from 1 to 10 with a 0.25-step.

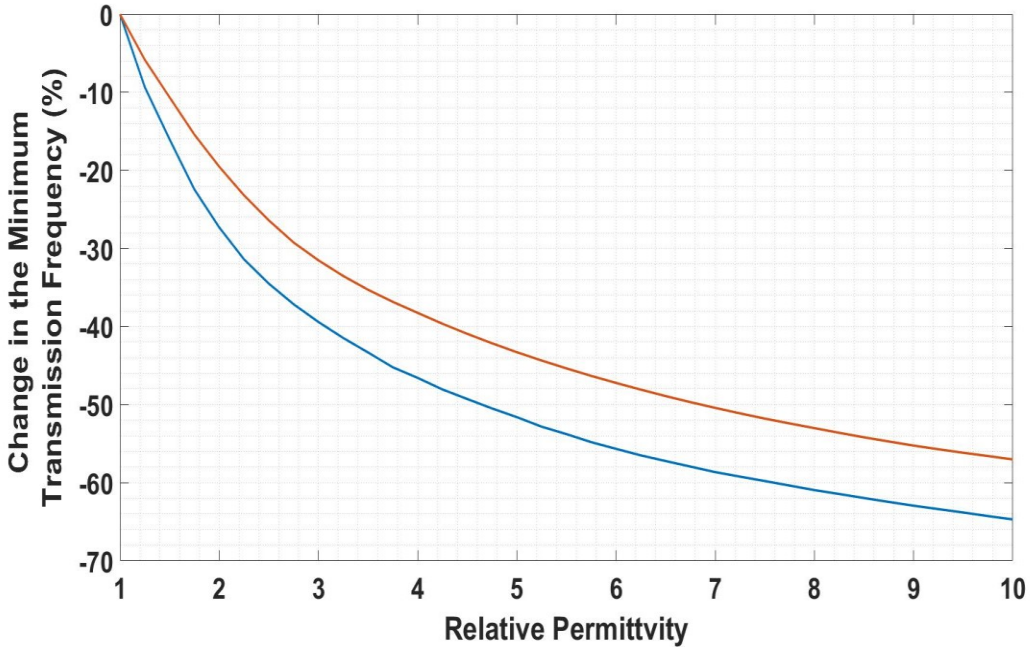

Figure 5.19 Change in the minimum transmission frequency versus MUT's relative permittivity for the non-tapered CSRRB (red) and tapered CSRRB (blue) based sensors. The sensors were loaded with two identical MUTs.

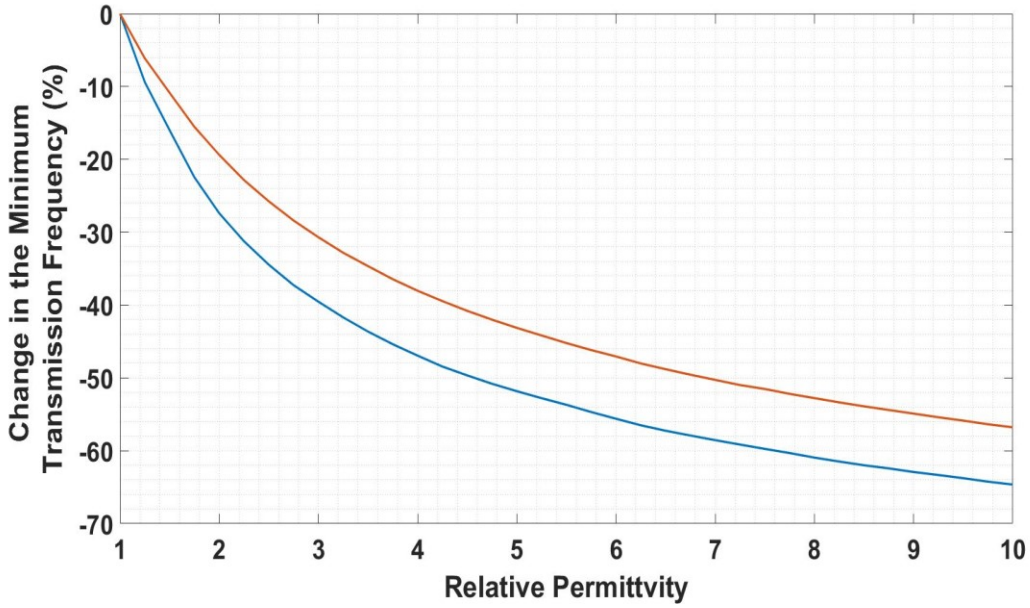

Figure 5.20 Change in the minimum transmission frequency versus MUT's relative permittivity for the non-tapered CSRRS (red) and tapered CSRRS (blue) based sensors. The sensors were loaded with two identical MUTs.

5.3.3 Similarities Between CSRRB and CSRRS Based Sensors

The reader might noticed the great similarities between the results of the CSRRB and CSRRS based sensors despite the fact that the spilt of each one of them is placed in a different arc with different width and length. In fact, the verification of these similarities is one of the comparison goals in this chapter. For such miniaturized meta-resonator, the two sensors are almost similar and these specific design details don't noticeably vary the performance of the sensors and consequently don't alter their equivalent inductance and/or capacitance significantly. Note that the shown similarities are related only to the magnitude of the transmission coefficients and the two sensors might not be similar when other parameters are considered. For example, the two sensors are non-reciprocal sensors and consequently their transmission and reflection phase are not similar.

5.4 Experimental Measurements

Previous sections showed high similarities between the CSRRB and CSRRS based sensors, thus the performance of the proposed sensors can be verified by either one. The CSRRB was utilized in this section to verify the performance of the proposed sensor experimentally with a single MUT. A flexible liquid crystal polymer (LCP) substrate was used to fabricate the sensor. The dielectric constant of the substrate is 2.9, with a substrate thickness of 0.116mm. A 30 by 30 mm prototype was fabricated. The fabricated sensor is shown in Fig.5.21. Three cubic dielectric samples were fabricated using Roger substrates RO3003, RO3006 and RO3010. The nominal relative permittivity of these substrates is approximately 3, 6 and 10, respectively. Each MUT has a height of 5mm with length and width of 15mm. The samples are similar to the ones in the previous chapter. Fig.5.22 shows the obtained experimental results as well as the simulated ones for the three cubic samples and free space minimum transmission frequency. The obtained measurements are in good agreement with the simulated ones. The little mismatch is due to the presence of air gaps between the sensor and the MUT as well as the air gap between the stacked Roger substrate layers that were utilized to fabricate the MUTs. To further verify the validity of the proposed estimation techniques and equations, Table 5.1 shows the calculated relative permittivity for each tested MUT using the experimental results and equations (5.4) and (5.5). The two equations provide a similar estimation for the tested MUTs. It is also noted that the obtained results for the third MUT with approximate relative permittivity of 10 have a higher mismatch. This is due to the fact that estimation of relative permittivity using stopband bandwidth is highly sensitive to little variation in the bandwidth for MUT with relative permittivity beyond 10.

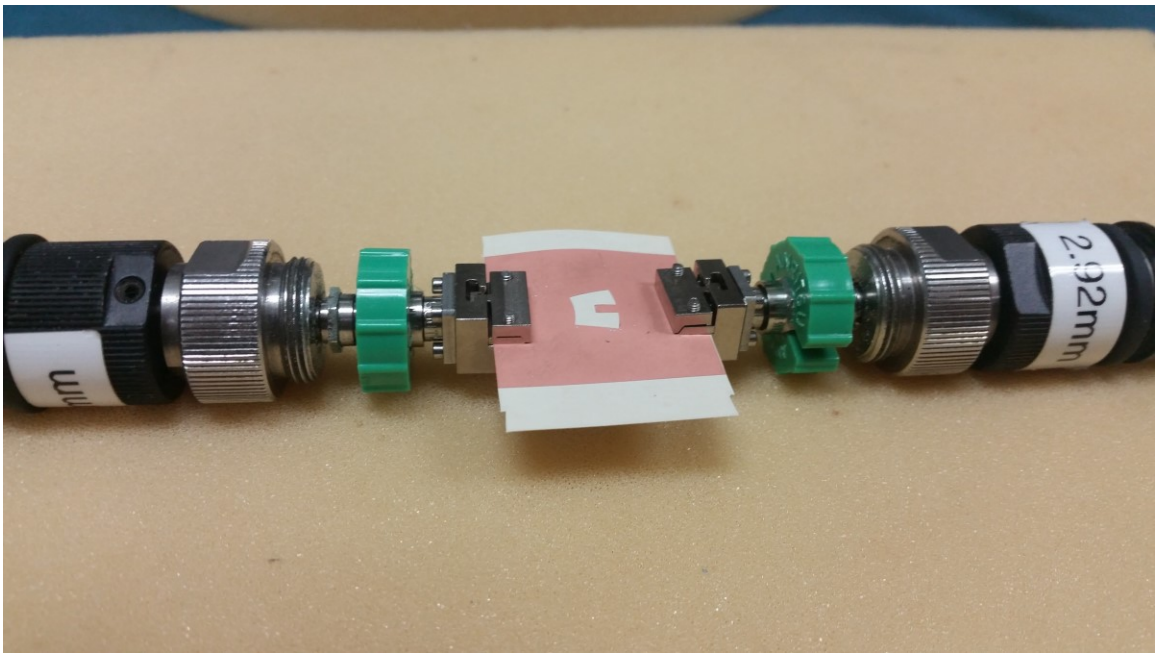

Figure 5.21 Fabricated CSRRB based sensor.

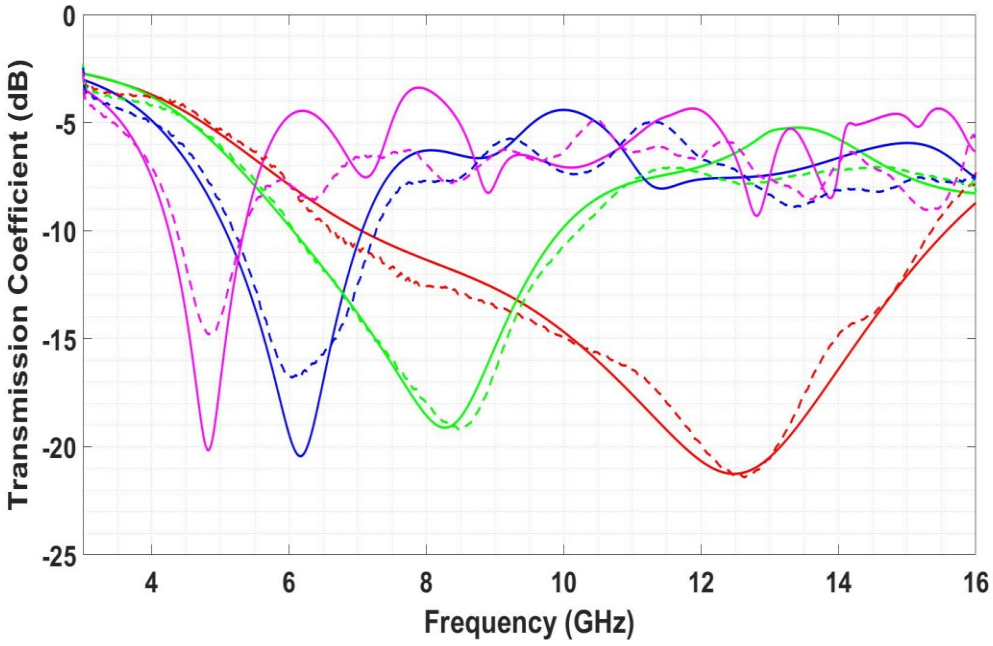

Figure 5.22 Comparison between numerical (solid line) and experimental (dashed lines) results for the CSRRB based sensor. The red curve for Er=1.The used MUTs have relative permittivity of Er=3 (green), Er=6 (blue) and Er=10 (pink).

Table 5-1 Extracted Relative Permittivity using (5.4) and (5.5)

Eq.	Tested Sample		
	RO3003	RO3006	RO3010
(5.4)	2.9190	6.1143	10.1106
(5.5)	3.0850	6.2875	12.2802

5.5 Application: Biomedical Microfluidic Sensing

The designed sensor can be utilized to estimate the relative permittivity of a homogenous dielectric sample or utilized to estimate the effective permittivity of a given sample that is placed in the sensing zone. Thus, this type of sensor can be used for a wide range of practical applications such as crack detection in a dielectric cube or object displacement estimation. It can also be utilized to estimate the effective permittivity of a microfluidic sample hosted in a dielectric container.

In this section the fabricated sensor is utilized to estimate the effective permittivity of three biomedical eye drops from three different manufacturers and with three different active ingredients. The test of each eye drop involves two steps. In the first step the empty drop's dropper is tested to estimate the relative permittivity of the dropper alone. In the second step the filled eye drop is tested to estimate the effective permittivity of the dropper/microfluidic. The first eye drop has a 1.4% polyvinyl alcohol. The second eye drop is a lubricant eye drop with 0.5% carboxymethylcellulose sodium. The third drop is an eye drop called (Restasis) with 0.05% cyclosporine. The three drops are shown in Fig 5.23. The experimental results are shown in Fig. 5.24. As seen in Fig. 5.23, the dropper of the first drop has a flat surface while the dropper of the second and third drops have an uneven structure. Thus, the dropper of the first drop has better contact and less air gap with the

sensor's surface compared to the other droppers. This justifies the obtained results in Fig.5.24 where the effective permittivity of the second and third dropper is closer to free space permittivity compared to the dropper of the first drop. Table 5.2 shows the calculated effective permittivity for each tested drop using the experimental results and equations (5.4) and (5.5).

Figure 5.23 The first, second and third eye drops utilized in this section. The drops are in a sequence from left to right.

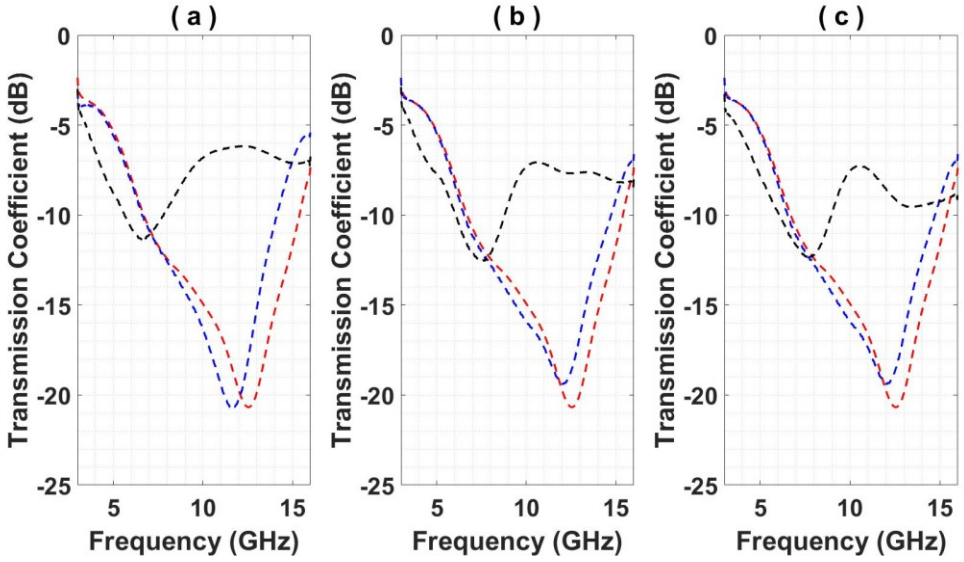

Figure 5.24 Comparison between measured free space (red dashed lines), empty dropper (blue dashed lines) and filled drop (black dashed lines). (a) Measurement using the first drop. (b) Measurement using the second drop. (c) Measurement using the third drop.

Table 5-2 Extracted Relative Permittivity using (5.4) and (5.5)

Eq.	First Drop		Second Drop		Third Drop	
	Empty	Filled	Empty	Filled	Empty	Filled
(5.4)	1.266	5.599	1.158	3.768	1.158	3.530
(5.5)	1.469	6.472	1.198	4.534	1.198	4.263

The results in Table 5.2 show good agreement with almost ± 0.7 mismatches between the results obtained from eq. (5.4) and the ones obtained from eq. (5.5). This mismatch is due to the limited surface contact between the used MUT (dropper in this case) and the CSRRB footprint. As the dropper surface is not wide enough to cover the CSRRB footprint, the dropper was placed in the area with the highest electric field (i.e. smaller arc). Thus, almost half of the upper part of the CSRRB is covered with the dropper while the other half is covered by air layers. The estimation of the relative permittivity using the bandwidth is less sensitive to the presence of air layers as it estimates the permittivity using the dispersion properties of the circulating current. However, the minimum transmission

frequency is affected more by the overall capacitive load seen by the CSRRB, which is composed of the air layers' equivalent capacitance and the dropper's equivalent capacitance. This is also supported by the increment in the estimated effective permittivity using (5.5) compared to the ones estimated using (5.4).

From this practical example and the previous three cubic dielectric samples that cover the whole CSRRB's footprint we can conclude that for a better matching between the two estimations the user should utilize samples with a surface area equal to or more than the surface area of the used meta-resonator.

5.6 Application: Crack Sensing

Oil and gas operating facilities contain hundreds of metallic and non-metallic pipelines, pressure vessels and tanks. These assets are subject to numerous types of defects and corrosion mechanisms during fabrication, shipment, installation and while they are in service. Thus, continuous inspections and assets' evaluations using conventional and advanced techniques are essential for the insurance of uninterrupted and safe operations. In addition, it is always preferred to conduct the required equipment inspection and evaluation without equipment shutdown to increase profitability and to avoid complicated and lengthy equipment return to service procedure.

Crack is one of the most frequent and serious defects that takes place in several types of mechanical equipment. It is initiated due to the presence of highly localized stresses in a relatively weak portion within the equipment. The latter is the main reason for crack initiation however, there are other factors that may increase the probability of crack presence and initiation. For example, in oil and gas industry pressure vessels and

process piping host several chemicals that operate at wide range of temperatures and stress levels which increase the corrosion rate and consequently increase the possibility of equipment failure caused by crack presence.

Crack occurs in metallic and non-metallic surfaces. It also may occur below the surface of the equipment a case at which the crack is considered as an embedded crack that can't be detected with a visual inspection. It should be noted that several inspection procedures and acceptance criteria, don't allow utilization of any mechanical equipment that has a single crack with any dimensions in the weld joints or the internal walls.

There are several conventional and advanced techniques that are used to detect and characterize cracks. These techniques vary based on their complexity, inspection time and result integrity. Liquid Penetrate Testing (PT) and Magnetic Particles Testing (MT) are two of the main conventional techniques that are commonly used for surface crack detection. These two methods are simple and don't need sophisticated training. However, they involve the utilization of toxic chemical materials that need to be handled and disposed with specific precautions. In addition, these two methods are slow as they involve utilization of dwell time to allow the utilized liquid to penetrate within the cracked surface. Conventional and advanced Ultrasonic Testing (UT) are also utilized for surface and subsurface crack detections and characterization. In fact, advanced UT is nowadays the standard technique for metallic equipment embedded crack detection and characterization. This method is accurate and gained high popularity in the last two decades. However, it uses excessive high viscous couplants between the UT probe and the MUT as it uses high-frequency mechanical waves. Moreover, advanced UT depends heavily on advanced signal processing techniques that require a huge amount of data and memory.

In principle, the electromagnetic waves can be utilized to detect a surface crack in metallic surfaces as well as surface and non-surface cracks in non-metallic structures. Microwave doesn't propagate through metallic structures, thus it can't be utilized to detect internal anomalies. Several microwave techniques have been proposed for crack detection and characterization in metallic surfaces using waveguides [103-105]. However, these techniques involve the utilization of bulky waveguides, high-frequency testing equipment and require large testing setup and space which are not usually affordable.

Based on this discussion transmission line based metamaterials are good candidates for crack detection and characterization. In fact, the proposed sensor in this chapter can be integrated with a smart structural health monitoring (SSHM) system to provide online, precise and reliable measurements. The interpretation of the sensor's result is simple and doesn't need a sophisticated signal processing tool. The insertion loss of the loaded resonator is used to test the sample. When the tested sample is defect-free, the insertion loss will have a single minimum transmission frequency located at a specific frequency within the frequency band of operation. However, the presence of surface defects reduces the effective permittivity seen by the sensor and consequently increases the minimum transmission frequency of the sensor. The crack length, width and depth can be extracted based on the correlation between the obtained test results. Crack is a type of defect that has an irregular shape, thus using a resonator with a curved side at the maximum electric field location increases the probability of detection (POD) and consequently increases the sensor integrity.

The proposed sectorial CSRR based sensor in this chapter was redesigned with slight dimension differences to extract the relative permittivity of a 3D printed sample and then to detect crack presence within three different 3D printed samples that were printed

with artificial cracks. The length of the longer arc of the tapered sectorial CSRR is 9 mm. The width of each edge of the sectorial CSRR is 2 mm with a split width of 2mm as well.

Three 3D printed samples were designed with longitudinal slots to simulate longitudinal surface cracks as shown in Fig.5.25, which also includes a defect-free sample (reference sample). Two of the four samples have one crack each with similar depth (3mm) and different width (500um and 1mm, respectively). The third sample has two cracks with a 1-mm width and a 3-mm depth each and separated by 1-mm. Fig.5.26 and Fig.5.27 show the obtained test results. The sensor was able to detect a 500-um width longitudinal surface crack with a 277 MHz shift in the minimum transmission resonance frequency from the reference case, which corresponds to a 12% frequency shift.

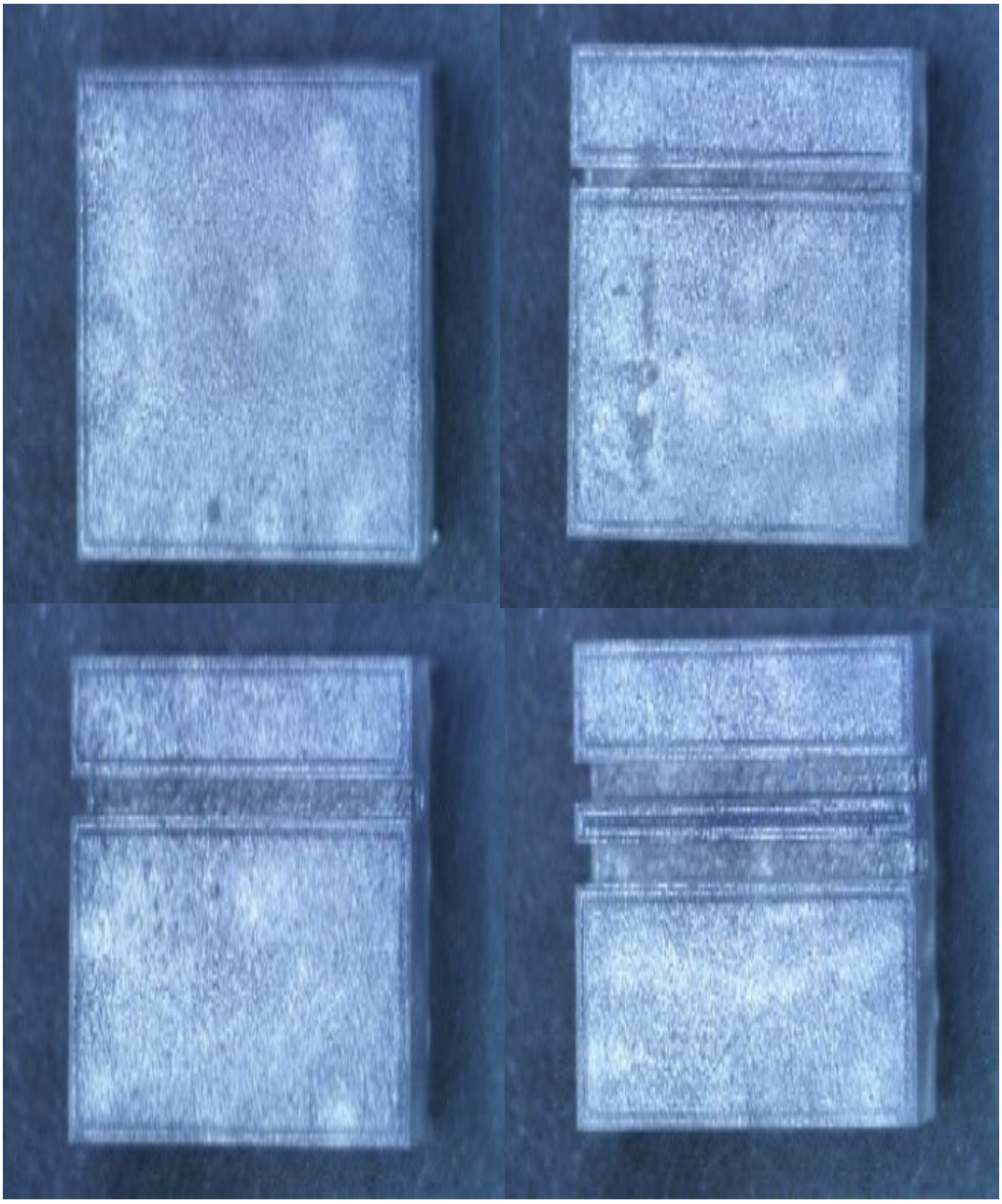

Figure 5.25 Four 3D printed samples (Reprinted from [115], © IEEE [2019])

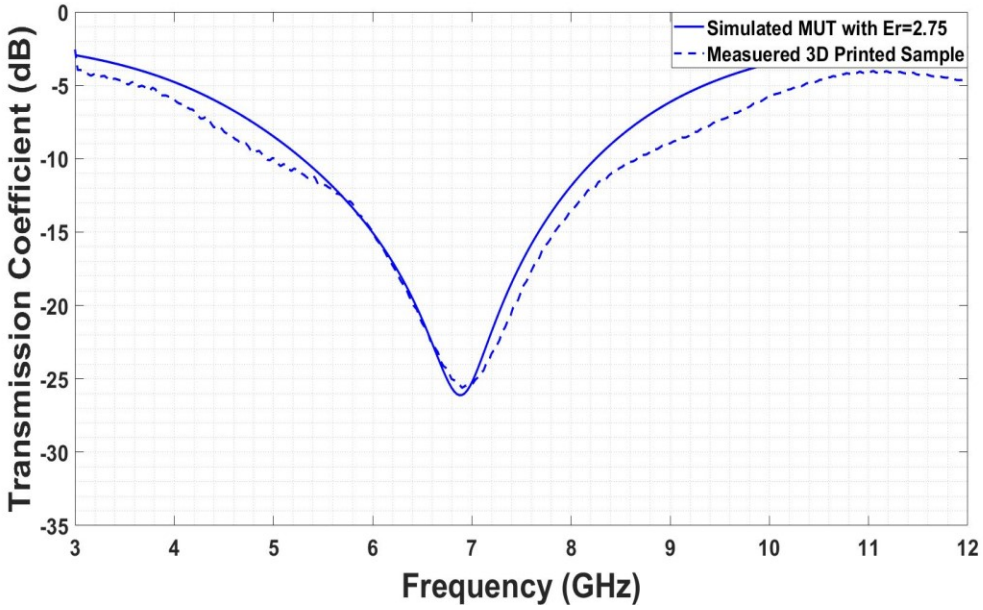

Figure 5.26 Transmission coefficient of the simulated MUT (solid line) and the measured one for a 3D printed sample (dashed line) (Reprinted from [115], © IEEE [2019])

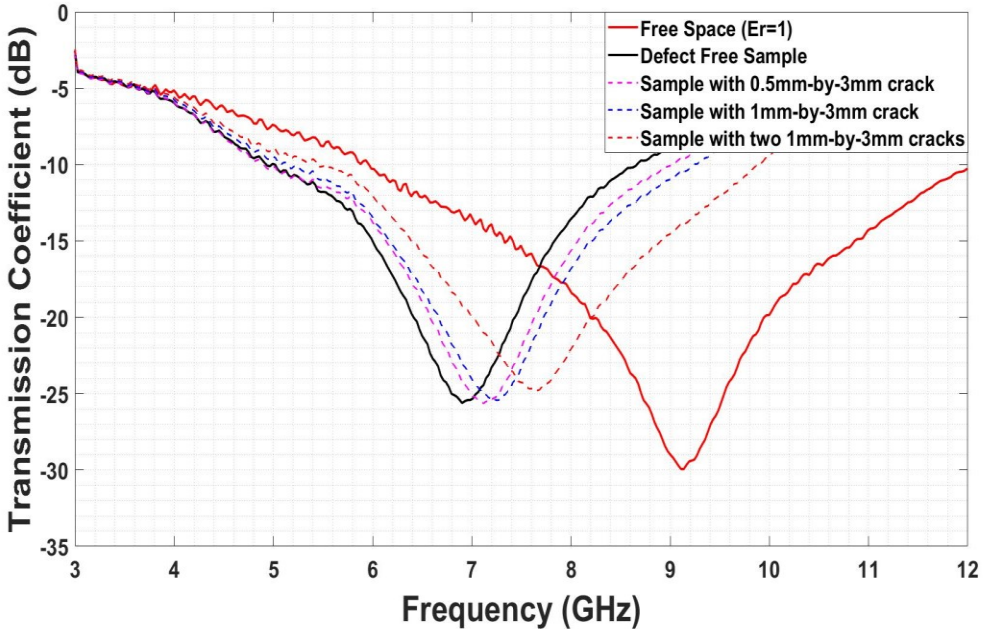

Figure 5.27 Measured transmission of free space (solid-red), defect-free sample (solid-black) and cracked 3D printed samples (dashed lines) (Reprinted from [115], © IEEE [2019])

CHAPTER 6. CONCLUSION

Microwave sensing nodes are fundamental components in the microwave sensing network. They are the front ends of any sensing network and consequently they have a strong influence on the network integrity, practicality and robustness. Future sensing networks will consist of millions sensing nodes that are spatially distributed and connected through pre-defined communication protocols. Thus, for optimized network performance, each sensing node needs to meet stringent design criteria such as minimum power usage, response consistency and design parameters flexibility. Furthermore, they need to be designed and fabricated with simple procedures and at a low cost.

Transmission line based metamaterials have distinct sensing capabilities and other features that fulfill and supersede the outlined criteria for future network sensing nodes. The main objective of this research is to perform a deliberate, comprehensive and systematic study that leads to the design of low power, miniaturized, ultrasensitive microwave planar metamaterial based sensors, evaluate their performance and then utilize them for bulk materials' constitutive parameters extraction and other practical applications with a narrower scope such as nondestructive and microfluidic sensing. The following sections outline the major outcomes and contributions of this dissertation. They also list future works and author's journals and conferences publications.

6.1 Major Outcomes

The below points summarize the major outcomes of this research:

1- This dissertation presents a comprehensive sensitivity analysis that investigates the effect of the meta-resonator's excitation scheme, its order (i.e. single or double CSRR), resonator's path width, split length and transmission line's substrate thickness on the sensitivity of transmission line based metamaterials. The analysis includes in-depth physical interpretations for the causes of the noticed effects based on the field profiles of the exciting fields, currents as well as applicable models.

2- For the first time, this dissertation investigates the effect of meta-resonator scalability on the consistency of the transmission line based metamaterials over a different band of operation. This investigation leads to the proposal of sensitivity uniformity condition.

3- Unlike previous studies that utilized only single dielectric test sample, this study discusses the added advantage of the utilization of two dielectric test samples for relative permittivity estimation.

4- This dissertation discusses in detail and for the first time the variation of transmission line based metamaterials stopband bandwidth with respect to meta-resonator split length, path width and MUT's relative permittivity.

5- Finally, the dissertation presents the design and verification of ultrasensitive, miniaturized and lightweight transmission line based metamaterials for material characterization with improved and uniform sensitivity.

6.2 Major Contributions

1- Novel transmission line based planar metamaterials with different topologies and operating frequencies were designed and used for relative permittivity extractions of low loss, isotropic and nondispersive materials. The designed planar metamaterials reduce the resonator's equivalent reactive elements dramatically which improves the sensitivity of the used metamaterials by almost 60% compared to similar state-of-the-art sensors.

2- For the first time, this dissertation estimates the relative permittivity of a dielectric sample using the variation of the minimum transmission frequency as well as the variation of the 10-dB sensor's bandwidth which increases the integrity and accuracy of the obtained results.

3- To further demonstrate the practicality of the proposed sensing nodes in this dissertation, the designed metamaterials were utilized for practical applications such as the extraction of the relative permittivity of unknown 3D printed samples, crack detection and microfluidic sensing.

4- This dissertation proposes a condition of sensitivity uniformity over a large spectrum for relative permittivity and relative permeability sensors. The proposed condition is a crucial condition for the integrity and consistency of the sensors reading over different frequency band of operations.

6.3 Future Work

Based on the research outcomes and contributions, the below points summarize the expected future work:

1- The future works in this field should consider the utilization of a meta-resonator based sensor with non-traditional transmission lines that offer better excitation to the loaded meta-resonator which consequently leads to better sensitivity.
2- Meta-resonator varies the velocity of the microwave, thus the relation between the phase difference, meta-resonator parameters as well as the MUT's relative permittivity should be thoroughly investigated.
3- The air gap is one of the main sources of error for any near field sensor. The future works should consider the utilization of a new setup, hosting transmission lines or meta-resonator design to mitigate the effect of air gap presence.
4- Future works should design a metamaterial-based sensor that can estimate the electrical and magnetic properties of anisotropic materials.

6.4 Publications

This is a list of papers that were published or submitted by the author.

6.4.1 Journal papers

1- Alotaibi, S. A., Cui, Y., & Tentzeris, M. M. (2019). CSRR Based Sensors for Relative Permittivity Measurement with Improved and Uniform Sensitivity throughout [0.9-10.9] GHz Band. *IEEE Sensors Journal*.

2- Alotaibi, S. A., Cui, Y., & Tentzeris, M. M.. Ultrasensitive Tapered CSRR Based Sensor for Relative Permittivity Measurement with Application to Biomedical Microfluidic Sensing. *Submitted*

6.4.2 Conference papers

1- Alotaibi, Salem A., Yepu Cui, and Manos M. Tentzeris. "Ultrasensitive Planar Metamaterials for Material Characterization Using Tapered CSRR with Application to NDT of 3D Printed Structures." *2019 49th European Microwave Conference (EuMC)*. IEEE, 2019.

2- Al-Otaibi, Salem A., and Manos M. Tentzeris. "Development of Surface Crack Sensors using Fractal Geometries of Complementary Split Ring Resonators." *ASNT Annual Conference 2017*. 2017.

3- Al-Otaibi, Salem A., and Manos M. Tentzeris. "Metasurface Based Surface Crack Sensor using Asymmetric Complementary Split Ring Resonator." In *27th ASNT Research Symposium*, pp. 12-19. 2018.

APPENDIX A: DERIVATION OF SENSITIVITY UNIFORMITY CONDITIONS

In this appendix a sensitivity uniformity condition is extracted for CSRR based permittivity sensor and for CSRR based permeability sensor.

AA.1 CSRR Based Permittivity Sensor

A necessary condition for uniform sensitivity is to have

$$\Delta f_1^{tmin}\,\% = \Delta f_2^{tmin}\,\% \qquad \text{AA.1}$$

where Δf_1^{tmin} % and Δf_2^{tmin} % are the change in the minimum transmission frequencies of the first and second sensors with two different CSRR sizes, respectively.

Dividing both sides by 100 and using (4.1) and (4.3), (AA.1) can be rewritten as

$$\frac{\dfrac{1}{2\pi\sqrt{L_{CSRR1}(C_{CSRR1}+C_{MUT1})}}-\dfrac{1}{2\pi\sqrt{L_{CSRR1}C_{CSRR1})}}}{\dfrac{1}{2\pi\sqrt{L_{CSRR1}(C_{CSRR1}+C_{MUT1})}}}$$

$$=\frac{\dfrac{1}{2\pi\sqrt{L_{CSRR2}(C_{CSRR2}+C_{MUT2})}}-\dfrac{1}{2\pi\sqrt{L_{CSRR2}C_{CSRR2})}}}{\dfrac{1}{2\pi\sqrt{L_{CSRR2}(C_{CSRR2}+C_{MUT2})}}} \qquad \text{AA. 2}$$

where L_{CSRR1} and L_{CSRR2} are the equivalent inductances of the first and second CSRR based sensors, C_{CSRR1} and C_{CSRR2} are the equivalent capacitances of the first and second

CSRR based sensors, C_{MUT1} and C_{MUT2} are the equivalent capacitances of the loaded MUT of the first and second CSRR based sensors, respectively.

Multiplying numerator and denominator of both sides by (2π), multiplying numerator and denominator of the left side by $\left(\sqrt{L_{CSRR1}}\right)$ and multiplying numerator and denominator of the right side by$\left(\sqrt{L_{CSRR2}}\right)$, (AA.2) can be simplified to

$$1-\frac{\sqrt{(C_{CSRR1}+C_{MUT1})}}{\sqrt{(C_{CSRR1})}}=1-\frac{\sqrt{(C_{CSRR2}+C_{MUT2})}}{\sqrt{(C_{CSRR2})}} \qquad \text{AA. 3}$$

which is equivalent to

$$\sqrt{1+\frac{C_{MUT1}}{C_{CSRR1}}}=\sqrt{1+\frac{C_{MUT2}}{C_{CSRR2}}} \qquad \text{AA. 4}$$

From which the condition of uniform sensitivity for CSRR based permittivity sensors is

$$\frac{C_{MUT1}}{C_{CSRR1}}=\frac{C_{MUT2}}{C_{CSRR2}} \qquad \text{AA. 5}$$

AA.2 CSRR Based Permeability Sensor

A necessary condition for uniform sensitivity is to have

$$\Delta f_1^{tmin}\,\% = \Delta f_2^{tmin}\,\% \qquad \text{AA.1}$$

where Δf_1^{tmin} % and Δf_2^{tmin} % are the change in the minimum transmission frequencies of the first and second sensors with two different CSRR sizes, respectively.

Dividing both sides by 100 and using equations similar to (4.1) and (4.3), (AA.1) can be rewritten as

$$\frac{\frac{1}{2\pi\sqrt{C_{CSRR1}(L_{CSRR1}+L_{MUT1})}}-\frac{1}{2\pi\sqrt{C_{CSRR1}L_{CSRR1})}}}{\frac{1}{2\pi\sqrt{C_{CSRR1}(L_{CSRR1}+L_{MUT1})}}}$$

$$=\frac{\frac{1}{2\pi\sqrt{C_{CSRR2}(L_{CSRR2}+L_{MUT2})}}-\frac{1}{2\pi\sqrt{C_{CSRR2}L_{CSRR2})}}}{\frac{1}{2\pi\sqrt{C_{CSRR2}(L_{CSRR2}+L_{MUT2})}}} \qquad \text{AA. 6}$$

where L_{CSRR1} and L_{CSRR2} are the equivalent inductances of the first and second CSRR based sensors, C_{CSRR1} and C_{CSRR2} are the equivalent capacitances of the first and second CSRR based sensors, L_{MUT1} and L_{MUT2} are the equivalent inductances of the loaded MUT of the first and second CSRR based sensors, respectively.

Multiplying numerator and denominator of both sides by (2π) , multiplying numerator and denominator of the left side by $\left(\sqrt{C_{CSRR1}}\right)$ and multiplying numerator and denominator of the right side by$\left(\sqrt{C_{CSRR2}}\right)$, (AA.6) can be simplified to

$$1-\frac{\sqrt{(L_{CSRR1}+L_{MUT1})}}{\sqrt{(L_{CSRR1})}}=1-\frac{\sqrt{(L_{CSRR2}+L_{MUT2})}}{\sqrt{(L_{CSRR2})}} \qquad \text{AA. 7}$$

which is equivalent to

$$\sqrt{1+\frac{L_{MUT1}}{L_{CSRR1}}}=\sqrt{1+\frac{L_{MUT2}}{L_{CSRR2}}} \qquad \text{AA. 8}$$

From which the condition of uniform sensitivity for CSRR based permeability sensors is

$$\frac{L_{MUT1}}{L_{CSRR1}} = \frac{L_{MUT2}}{L_{CSRR2}} \qquad \text{AA. 9}$$

(AA.5) and (AA.9) indicate that for a uniform sensitivity over different bands of frequency, if the CSRR is scaled to vary the operation frequency, a corresponding MUT's scaling by the same ratio shall also be implemented to vary its equivalent reactive element of interest (equivalent capacitance for a permittivity sensor and equivalent inductance for a permeability sensor).

In chapter 4, the width and length of the MUT that are interfaced with the CSRR footprint were identical and assumed to be two times higher than the side length of the square CSRR to meet the derived uniformity condition.

REFERENCES

[1] Yaqoob, I., Ahmed, E., Hashem, I. A. T., Ahmed, A. I. A., Gani, A., Imran, M., & Guizani, M. (2017). Internet of things architecture: Recent advances, taxonomy, requirements, and open challenges. IEEE wireless communications, 24(3), 10-16

[2] Caloz, Christophe, and Tatsuo Itoh. Electromagnetic metamaterials: transmission line theory and microwave applications. John Wiley & Sons, 2005.

[3] Veselago, V. G. Electrodynamics of substances with simultaneously negative values of e and u. *Usp. Fiz. Nauk*, 1967, 92: 517

[4] Pendry, J. B., Holden, A. J., Robbins, D. J., & Stewart, W. J. (1999). Magnetism from conductors and enhanced nonlinear phenomena. *IEEE transactions on microwave theory and techniques*, *47*(11), 2075-2084.

[5] Shelby, R. A., Smith, D. R., & Schultz, S. (2001). Experimental verification of a negative index of refraction. *science*, *292*(5514), 77-79.

[6] Martın, F., Bonache, J., Falcone, F. A., Sorolla, M., & Marqués, R. (2003). Split ring resonator-based left-handed coplanar waveguide. *Applied Physics Letters*, *83*(22), 4652-4654.

[7] J. D. Baena, J. Bonache, F. Martín, R. Marqués, F. Falcone, T. Lopetegi, M. A. G. Laso, J. García–García, M. F. Portillo, and M. Sorolla, "Equivalent-circuit models for split-ring resonators and complementary split-ring resonators coupled to planar transmission lines," *IEEE Trans. Microw. Theory Tech*., vol. MTT-53, pp. 1451–1461, 2005.

[8] Boybay, Muhammed Said, and Omar M. Ramahi. "Material characterization using complementary split-ring resonators." *IEEE Transactions on Instrumentation and Measurement* 61.11 (2012): 3039-3046.

[9] Smith, D. R., Schultz, S., Markoš, P., & Soukoulis, C. M. (2002). Determination of effective permittivity and permeability of metamaterials from reflection and transmission coefficients. *Physical Review B*, *65*(19), 195104.

[10] Nicolson, A. M., and G. F. Ross. "Measurement of the intrinsic properties of materials by time-domain techniques." *IEEE Transactions on instrumentation and measurement* 19.4 (1970): 377-382.

[11] Smith, D. R., Vier, D. C., Koschny, T., & Soukoulis, C. M. (2005). Electromagnetic parameter retrieval from inhomogeneous metamaterials. *Physical review E*, *71*(3), 036617.

[12] Weir, W. B. (1974). Automatic measurement of complex dielectric constant and permeability at microwave frequencies. *Proceedings of the IEEE*, *62*(1), 33-36.

[13] Hoekstra, P., & Delaney, A. (1974). Dielectric properties of soils at UHF and microwave frequencies. *Journal of geophysical research*, *79*(11), 1699-1708.

[14] Stuchly, M. A., & Stuchly, S. S. (1980). Coaxial line reflection methods for measuring dielectric properties of biological substances at radio and microwave frequencies-A review. *IEEE Transactions on instrumentation and measurement*, *29*(3), 176-183.

[15] Afsar, M. N., Birch, J. R., Clarke, R. N., & Chantry, G. W. (1986). The measurement of the properties of materials. *Proceedings of the IEEE*, *74*(1), 183-199.

[16] Djordjevic, A. R., Biljié, R. M., Likar-Smiljanic, V. D., & Sarkar, T. K. (2001). Wideband frequency-domain characterization of FR-4 and time-domain causality. *IEEE Transactions on Electromagnetic Compatibility*, *43*(4), 662-667.

[17] Luukkonen, O., Maslovski, S. I., & Tretyakov, S. A. (2011). A stepwise Nicolson–Ross–Weir-based material parameter extraction method. *IEEE antennas and wireless propagation letters*, *10*, 1295-1298.

[18] Vanzura, E. J., Baker-Jarvis, J. R., Grosvenor, J. H., & Janezic, M. D. (1994). Intercomparison of permittivity measurements using the transmission/reflection method in 7-mm coaxial transmission lines. *IEEE transactions on microwave theory and techniques*, *42*(11), 2063-2070.

[19] Varadan, V. V., & Ro, R. (2007). Unique retrieval of complex permittivity and permeability of dispersive materials from reflection and transmitted fields by enforcing causality. *IEEE transactions on Microwave Theory and Techniques*, *55*(10), 2224-2230.

[20] Nozaki, R., & Bose, T. K. (1990). Broadband complex permittivity measurements by time-domain spectroscopy. *IEEE transactions on instrumentation and measurement*, *39*(6), 945-951.

[21] Cole, R. H. (1975). Evaluation of dielectric behavior by time domain spectroscopy. II. Complex permittivity. *The Journal of Physical Chemistry*, *79*(14), 1469-1474.

[22] Nelson, S. O. (1994). Measurement of microwave dielectric properties of particulate materials. *Journal of food engineering*, *21*(3), 365-384.

[23] Catala-Civera, J. M., Canos, A. J., Penaranda-Foix, F. L., & de los Reyes Davo, E. (2003). Accurate determination of the complex permittivity of materials with transmission reflection measurements in partially filled rectangular waveguides. *IEEE Transactions on Microwave Theory and Techniques*, *51*(1), 16-24.

[24] Chalapat, K., Sarvala, K., Li, J., & Paraoanu, G. S. (2009). Wideband reference-plane invariant method for measuring electromagnetic parameters of materials. *IEEE Transactions on Microwave Theory and Techniques*, *57*(9), 2257-2267.

[25] Courtney, C. C. (1998). Time-domain measurement of the electromagnetic properties of materials. *IEEE Transactions on Microwave Theory and Techniques*, *46*(5), 517-522.

[26] Ghodgaonkar, D. K., V. V. Varadan, and V. K. Varadan. "Free-space measurement of complex permittivity and complex permeability of magnetic materials at microwave frequencies." *IEEE Transactions on instrumentation and measurement* 39.2 (1990): 387-394.

[27] Courtney, William E. "Analysis and evaluation of a method of measuring the complex permittivity and permeability microwave insulators." *IEEE Transactions on Microwave Theory and Techniques* 18.8 (1970): 476-485.

[28] Baker-Jarvis, James, Eric J. Vanzura, and William A. Kissick. "Improved technique for determining complex permittivity with the transmission/reflection method." *IEEE Transactions on microwave theory and techniques* 38.8 (1990): 1096-1103.

[29] Kobayashi, Yoshio, and Masayuki Katoh. "Microwave measurement of dielectric properties of low-loss materials by the dielectric rod resonator method." *IEEE Transactions on Microwave Theory and Techniques* 33.7 (1985): 586-592.

[30] Belhadj-Tahar, N-E., Arlette Fourier-Lamer, and Helie De Chanterac. "Broad-band simultaneous measurement of complex permittivity and permeability using a coaxial discontinuity." *IEEE Transactions on Microwave Theory and Techniques* 38.1 (1990): 1-7.

[31] Ghodgaonkar, Deepak K., Vasundara V. Varadan, and Vijay K. Varadan. "A free-space method for measurement of dielectric constants and loss tangents at

microwave frequencies." *IEEE Transactions on Instrumentation and measurement* 38.3 (1989): 789-793.

[32] Bernard, P. A., and J. M. Gautray. "Measurement of dielectric constant using a microstrip ring resonator." *IEEE Transactions on Microwave Theory and Techniques* 39.3 (1991): 592-595.

[33] Blackham, David V., and Roger D. Pollard. "An improved technique for permittivity measurements using a coaxial probe." *IEEE Transactions on Instrumentation and Measurement* 46.5 (1997): 1093-1099.

[34] Boughriet, A-H., Christian Legrand, and Alain Chapoton. "Noniterative stable transmission/reflection method for low-loss material complex permittivity determination."*IEEE Transactions on Microwave Theory and Techniques* 45.1 (1997): 52-57.

[35] Janezic, Michael D., and Jeffrey A. Jargon. "Complex permittivity determination from propagation constant measurements." *IEEE Microwave and Guided Wave Letters* 9.2 (1999): 76-78.

[36] Ebrahimi, Amir, James Scott, and Kamran Ghorbani. "Transmission Lines Terminated With LC Resonators for Differential Permittivity Sensing." *IEEE Microwave and Wireless Components Letters* 28.12 (2018): 1149-1151.

[37] Baker-Jarvis, James, Richard G. Geyer, J. H. Grosvenor, Michael D. Janezic, Chriss A. Jones, Bill Riddle, Claude M. Weil, and J. Krupka. "Dielectric characterization of low-loss materials a comparison of techniques." *IEEE Transactions on Dielectrics and Electrical insulation* 5, no. 4 (1998): 571-577.

[38] Tabib-Azar, Massood, Neil S. Shoemaker, and Stephen Harris. "Non-destructive characterization of materials by evanescent microwaves." *Measurement science and technology* 4.5 (1993): 583.

[39] Tabib-Azar, M., P. S. Pathak, G. Ponchak, and S. LeClair. "Nondestructive super resolution imaging of defects and nonuniformities in metals, semiconductors, dielectrics, composites, and plants using evanescent microwaves." *Review of Scientific Instruments* 70, no. 6 (1999): 2783-2792.

[40] Lee, Chieh-Sen, and Chin-Lung Yang. "Complementary split-ring resonators for measuring dielectric constants and loss tangents." *IEEE Microwave and Wireless Components Letters* 24.8 (2014): 563-565.

[41] Lee, Chieh-Sen, and Chin-Lung Yang. "Single-compound complementary split-ring resonator for simultaneously measuring the permittivity and thickness of dual-layer dielectric materials." *IEEE Transactions on Microwave Theory and Techniques* 63.6 (2015): 2010-2023.

[42] Ansari, Mohammad Arif Hussain, Abhishek Kumar Jha, and Mohammad Jaleel Akhtar. "Design and application of the CSRR-based planar sensor for noninvasive measurement of complex permittivity." *IEEE Sensors Journal* 15.12 (2015): 7181-7189.

[43] Raj, A., Kumar Jha, A., Ansari, M. A. H., Akhtar, M. J., and Panda, S. "Metamaterial-inspired microwave sensor for measurement of complex permittivity of materials." *Microwave and Optical Technology Letters* 58.11 (2016): 2577-2581.

[44] Ebrahimi, Amir, James Scott, and Kamran Ghorbani. "Differential sensors using microstrip lines loaded with two split-ring resonators." *IEEE Sensors Journal* 18.14 (2018): 5786-5793

[45] Withayachumnankul, Withawat, Kata Jaruwongrungsee, Adisorn Tuantranont, Christophe Fumeaux, and Derek Abbott. "Metamaterial-based microfluidic sensor for dielectric characterization." *Sensors and Actuators A: Physical* 189 (2013): 233-237

[46] Ebrahimi, A., Withayachumnankul, W., Al-Sarawi, S., & Abbott, D. (2013). High-sensitivity metamaterial-inspired sensor for microfluidic dielectric characterization. *IEEE Sensors Journal*, *14*(5), 1345-1351.

[47] Abduljabar, A. A., Rowe, D. J., Porch, A., & Barrow, D. A. (2014). Novel microwave microfluidic sensor using a microstrip split-ring resonator. *IEEE Transactions on Microwave Theory and Techniques*, *62*(3), 679-688.

[48] Salim, A., & Lim, S. (2016). Complementary split-ring resonator-loaded microfluidic ethanol chemical sensor. *Sensors*, *16*(11), 1802.

[49] Vélez, P., Su, L., Grenier, K., Mata-Contreras, J., Dubuc, D., & Martín, F. (2017). Microwave microfluidic sensor based on a microstrip splitter/combiner configuration and split ring resonators (SRRs) for dielectric characterization of liquids. *IEEE Sensors Journal*, *17*(20), 6589-6598.

[50] Ebrahimi, A., Withayachumnankul, W., Al-Sarawi, S. F., & Abbott, D. (2015, November). Microwave microfluidic sensor for determination of glucose

concentration in water. In *2015 IEEE 15th Mediterranean Microwave Symposium (MMS)* (pp. 1-3). IEEE.

[51] Shih, K., Pitchappa, P., Manjappa, M., Ho, C. P., Singh, R., & Lee, C. (2017). Microfluidic metamaterial sensor: Selective trapping and remote sensing of microparticles. *Journal of Applied Physics*, *121*(2), 023102.

[52] Chahadih, A., Cresson, P. Y., Hamouda, Z., Gu, S., Mismer, C., & Lasri, T. (2015). Microwave/microfluidic sensor fabricated on a flexible kapton substrate for complex permittivity characterization of liquids. *Sensors and Actuators A: Physical*, *229*, 128-135.

[53] Abdolrazzaghi, M., Daneshmand, M., & Iyer, A. K. (2018). Strongly enhanced sensitivity in planar microwave sensors based on metamaterial coupling. *IEEE Transactions on Microwave Theory and Techniques*, *66*(4), 1843-1855.

[54] Sadeqi, A., Nejad, H. R., & Sonkusale, S. (2017). Low-cost metamaterial-on-paper chemical sensor. *Optics express*, *25*(14), 16092-16100.

[55] Zarifi, M. H., & Daneshmand, M. (2016). Wide dynamic range microwave planar coupled ring resonator for sensing applications. *Applied Physics Letters*, *108*(23), 232906.

[56] Jaruwongrungsee, K., Waiwijit, U., Withayachumnankul, W., Maturos, T., Phokaratkul, D., Tuantranont, A., ... & Wisitsoraat, A. (2015). Microfluidic-based split-ring-resonator sensor for real-time and label-free biosensing. *Procedia engineering*, *120*, 163-166.

[57] Su, W., Cook, B. S., & Tentzeris, M. M. (2016). Additively manufactured microfluidics-based "peel-and-replace" RF sensors for wearable applications. *IEEE Transactions on Microwave Theory and Techniques*, *64*(6), 1928-1936.

[58] Altintas, O., Aksoy, M., Akgol, O., Unal, E., Karaaslan, M., & Sabah, C. (2017). Fluid, strain and rotation sensing applications by using metamaterial based sensor. *Journal of The Electrochemical Society*, *164*(12), B567-B573.

[59] Abduljabar, A. A., Clark, N., Lees, J., & Porch, A. (2017). Dual mode microwave microfluidic sensor for temperature variant liquid characterization. *IEEE Transactions on Microwave Theory and Techniques*, *65*(7), 2572-2582.

[60] Su, L., Mata-Contreras, J., Vélez, P., Fernández-Prieto, A., & Martín, F. (2018). Analytical method to estimate the complex permittivity of oil samples. *Sensors*, *18*(4), 984.

[61] Abdolrazzaghi, M., Zarifi, M. H., & Daneshmand, M. (2016, October). Sensitivity enhancement of split ring resonator based liquid sensors. In *2016 IEEE SENSORS* (pp. 1-3). IEEE.

[62] Su, L., Naqui, J., Mata-Contreras, J., & Martín, F. (2016, May). Cascaded splitter/combiner microstrip sections loaded with complementary split ring resonators (CSRRs): Modeling, analysis and applications. In *2016 IEEE MTT-S International Microwave Symposium (IMS)* (pp. 1-4). IEEE.

[63] Chudpooti, N., Silavwe, E., Akkaraekthalin, P., Robertson, I. D., & Somjit, N. (2017). Nano-fluidic millimeter-wave lab-on-a-waveguide sensor for liquid-mixture characterization. *IEEE Sensors Journal*, *18*(1), 157-164.

[64] Velez, P., Grenier, K., Mata-Contreras, J., Dubuc, D., & Martín, F. (2018). Highly-sensitive microwave sensors based on open complementary split ring resonators (OCSRRs) for dielectric characterization and solute concentration measurement in liquids. *IEEE Access*, *6*, 48324-48338.

[65] Ye, D., Wang, W., Moline, D., Islam, M. S., Chen, F., & Wang, P. (2017). A microwave flow detector for gradient elution liquid chromatography. *Analytical chemistry*, *89*(20), 10761-10768.

[66] Karami, M., Rezaei, P., Kiani, S., & Sadeghzadeh, R. A. (2017). Modified planar sensor for measuring dielectric constant of liquid materials. *Electronics Letters*, *53*(19), 1300-1302.

[67] Jaruwongrungsee, K., Waiwijit, U., Withayachumnankul, W., Maturos, T., Phokaratkul, D., Tuantranont, A., & Wisitsoraat, A. (2015, July). Real-time and label-free biosensing with microfluidic-based split-ring-resonator sensor. In *2015 IEEE 15th International Conference on Nanotechnology (IEEE-NANO)* (pp. 1091-1094). IEEE.

[68] Koirala, G., Dhakal, R., Kim, E. S., Yao, Z., & Kim, N. Y. (2018). Radio frequency detection and characterization of water-ethanol solution through spiral-coupled passive micro-resonator sensor. *Sensors*, *18*(4), 1075.

[69] Chuma, E. L., Iano, Y., Fontgalland, G., & Roger, L. L. B. (2018). Microwave sensor for liquid dielectric characterization based on metamaterial complementary split ring resonator. *IEEE Sensors Journal*, *18*(24), 9978-9983.

[70] Vélez, P., Muñoz-Enano, J., Gil, M., Mata-Contreras, J., & Martín, F. (2019). Differential microfluidic sensors based on dumbbell-shaped defect ground structures in microstrip technology: Analysis, optimization, and applications. *Sensors*, *19*(14), 3189.

[71] Horestani, A. K., Fumeaux, C., Al-Sarawi, S. F., & Abbott, D. (2012). Displacement sensor based on diamond-shaped tapered split ring resonator. *IEEE Sensors Journal*, *13*(4), 1153-1160.

[72] Naqui, J., & Martı, F. (2013). Transmission lines loaded with bisymmetric resonators and their application to angular displacement and velocity sensors. *IEEE Transactions on Microwave Theory and Techniques*, *61*(12), 4700-4713.

[73] Horestani, A. K., Abbott, D., & Fumeaux, C. (2013). Rotation sensor based on horn-shaped split ring resonator. *IEEE Sensors Journal*, *13*(8), 3014-3015.

[74] Horestani, A. K., Naqui, J., Shaterian, Z., Abbott, D., Fumeaux, C., & Martín, F. (2014). Two-dimensional alignment and displacement sensor based on movable broadside-coupled split ring resonators. *Sensors and Actuators A: Physical*, *210*, 18-24.

[75] Horestani, A. K., Naqui, J., Abbott, D., Fumeaux, C., & Martín, F. (2014). Two-dimensional displacement and alignment sensor based on reflection coefficients of open microstrip lines loaded with split ring resonators. *Electronics letters*, *50*(8), 620-622.

[76] Naqui, J., & Martín, F. (2013). Angular displacement and velocity sensors based on electric-LC (ELC) loaded microstrip lines. *IEEE Sensors Journal*, *14*(4), 939-940.

[77] Ebrahimi, A., Withayachumnankul, W., Al-Sarawi, S. F., & Abbott, D. (2014). Metamaterial-inspired rotation sensor with wide dynamic range. *IEEE Sensors Journal*, *14*(8), 2609-2614.

[78] Naqui, J., Coromina, J., Karami-Horestani, A., Fumeaux, C., & Martín, F. (2015). Angular displacement and velocity sensors based on coplanar waveguides (CPWs) loaded with S-shaped split ring resonators (S-SRR). *Sensors*, *15*(5), 9628-9650.

[79] Mata-Contreras, J., Herrojo, C., & Martín, F. (2017). Application of split ring resonator (SRR) loaded transmission lines to the design of angular displacement and velocity sensors for space applications. *IEEE Transactions on Microwave Theory and Techniques*, *65*(11), 4450-4460.

[80] Joodaki, M., & Rezaee, M. (2016). Coplanar waveguide (CPW) loaded with an electromagnetic bandgap (EBG) structure: Modeling and application to displacement sensor. *IEEE Sensors Journal*, *16*(9), 3034-3040.

[81] Su, L., Mata-Contreras, J., Vélez, P., & Martín, F. (2017). A review of sensing strategies for microwave sensors based on metamaterial-inspired resonators: dielectric characterization, displacement, and angular velocity measurements for health diagnosis, telecommunication, and space applications. *International Journal of Antennas and Propagation*, *2017*.

[82] Gargari, A. M., Ozbey, B., Demir, H. V., Altintas, A., Albostan, U., Kurc, O., & Ertürk, V. B. (2018). A wireless metamaterial-inspired passive rotation sensor with submilliradian resolution. *IEEE Sensors Journal*, *18*(11), 4482-4490.

[83] Mata-Contreras, J., Herrojo, C., & Martín, F. (2018). Detecting the rotation direction in contactless angular velocity sensors implemented with rotors loaded with multiple chains of resonators. *IEEE Sensors Journal*, *18*(17), 7055-7065.

[84] Harnsoongnoen, S., & Angkawisittpan, N. (2016). Angular displacement sensor based on coplanar waveguide (CPWs) loaded with S-shaped golden spiral-tapered split ring resonators (SGS-SRRs). *Procedia Computer Science*, *86*, 75-78.

[85] Horestani, A. K., Shaterian, Z., & Martín, F. (2019, September). Detection Modalities of Displacement Sensors Based on Split Ring Resonators: Pros and Cons. In *2019 International Conference on Electromagnetics in Advanced Applications (ICEAA)* (pp. 0479-0484). IEEE.

[86] Albishi, Ali M., Muhammed S. Boybay, and Omar M. Ramahi. "Complementary split-ring resonator for crack detection in metallic surfaces." *IEEE Microwave and Wireless Components Letters* 22.6 (2012): 330-332.

[87] Albishi, A., & Ramahi, O. (2014). Detection of surface and subsurface cracks in metallic and non-metallic materials using a complementary split-ring resonator. *Sensors*, *14*(10), 19354-19370.

[88] Hu, B., Ren, Z., Boybay, M. S., & Ramahi, O. M. (2014). Waveguide probe loaded with split-ring resonators for crack detection in metallic surfaces. *IEEE Transactions on Microwave Theory and Techniques*, *62*(4), 871-878.

[89] Albishi, A. M., & Ramahi, O. M. (2016, April). Surface crack detection in metallic materials using sensitive microwave-based sensors. In *2016 IEEE 17th Annual Wireless and Microwave Technology Conference (WAMICON)* (pp. 1-3). IEEE.

[90] Albishi, A., & Ramahi, O. (2016, June). Ultrasensitive microwave near-field based sensors for crack detection in metallic materials. In *2016 IEEE International Symposium on Antennas and Propagation (APSURSI)* (pp. 1955-1956). IEEE.

[91] Alahnomi, R. A., Zakaria, Z., Yussof, Z. M., Sutikno, T., Alhegazi, A., & Abu-Khadrah, A. I. (2019). Enhanced symmetrical split ring resonator (SSRR) for metallic surface crack detection. *Telkomnika*, *17*(4).

[92] Albishi, Ali M., and Omar M. Ramahi. "Microwaves-based high sensitivity sensors for crack detection in metallic materials." *IEEE Transactions on Microwave Theory and Techniques* 65.5 (2017): 1864-1872.

[93] Yun, T., & Lim, S. (2014). High-Q and miniaturized complementary split ring resonator-loaded substrate integrated waveguide microwave sensor for crack detection in metallic materials. *Sensors and Actuators A: Physical*, *214*, 25-30.

[94] Rajni, R., Kaur, A., & Marwaha, A. (2015). Complementary split ring resonator based sensor for crack detection. *International Journal of Electrical and Computer Engineering*, *5*(5).

[95] Ali, A., El Badawe, M., & Ramahi, O. M. (2016). Microwave imaging of subsurface flaws in coated metallic structures using complementary split-ring resonators. *IEEE Sensors Journal*, *16*(18), 6890-6898.

[96] Ebrahimi, A., Scott, J., & Ghorbani, K. (2018). Differential sensors using microstrip lines loaded with two split-ring resonators. *IEEE Sensors Journal*, *18*(14), 5786-5793.

[97] Velez, P., Grenier, K., Mata-Contreras, J., Dubuc, D., & Martín, F. (2018). Highly-sensitive microwave sensors based on open complementary split ring resonators (OCSRRs) for dielectric characterization and solute concentration measurement in liquids. *IEEE Access*, *6*, 48324-48338.

[98] Vélez, P., Muñoz-Enano, J., Gil, M., Mata-Contreras, J., & Martín, F. (2019). Differential microfluidic sensors based on dumbbell-shaped defect ground structures in microstrip technology: Analysis, optimization, and applications. *Sensors*, *19*(14), 3189.

[99] Vélez, P., Muñoz-Enano, J., Grenier, K., Mata-Contreras, J., Dubuc, D., & Martín, F. (2018). Split Ring Resonator-Based Microwave Fluidic Sensors for Electrolyte Concentration Measurements. *IEEE Sensors Journal*, *19*(7), 2562-2569.

[100] Su, L., Mata-Contreras, J., Vélez, P., & Martín, F. (2016). Splitter/combiner microstrip sections loaded with pairs of complementary split ring resonators (CSRRs): Modeling and optimization for differential sensing applications. *IEEE Transactions on Microwave Theory and Techniques*, *64*(12), 4362-4370.

[101] Su, L., Mata-Contreras, J., Vélez, P., & Martín, F. (2017). A review of sensing strategies for microwave sensors based on metamaterial-inspired resonators: dielectric characterization, displacement, and angular velocity measurements for health diagnosis, telecommunication, and space applications. *International Journal of Antennas and Propagation*, *2017*.

[102] Velez, P., Su, L., Mata-Contreras, J., Martín, F., Grenier, K., & Dubuc, D. (2017, September). Modeling and analysis of pairs of open complementary split ring resonators (OCSRRs) for differential permittivity sensing. In *2017 IEEE MTT-S International Microwave Workshop Series on Advanced Materials and Processes for RF and THz Applications (IMWS-AMP)* (pp. 1-3). IEEE.

[103] Yeh, C. Y., & Zoughi, R. (1994). A novel microwave method for detection of long surface cracks in metals. *IEEE Transactions on Instrumentation and Measurement*, *43*(5), 719-725.

[104] Zoughi, R., Ganchev, S. I., & Huber, C. (1996, June). Measurement parameter optimization for surface crack detection in metals using an open-ended waveguide probe. In *Quality Measurement: The Indispensable Bridge between Theory and Reality (No Measurements? No Science! Joint Conference-1996: IEEE Instrumentation and Measurement Technology Conference and IMEKO Tec* (Vol. 2, pp. 1391-1394). IEEE.

[105] Zoughi, R., & Kharkovsky, S. (2008). Microwave and millimetre wave sensors for crack detection. *Fatigue & Fracture of Engineering Materials & Structures*, *31*(8), 695-713.

[106] Hansen, R. C., & Burke, M. (2000). Antennas with magneto-dielectrics. *Microwave and optical technology letters*, *26*(2), 75-78.

[107] Saadat-Safa, M., Nayyeri, V., Khanjarian, M., Soleimani, M., & Ramahi, O. M. (2019). A CSRR-Based Sensor for Full Characterization of Magneto-Dielectric Materials. *IEEE Transactions on Microwave Theory and Techniques*, *67*(2), 806-814.

[108] Preradovic, Stevan, and Nemai C. Karmakar. "Design of chipless RFID tag for operation on flexible laminates." *IEEE antennas and wireless propagation letters* 9 (2010): 207-210.

[109] Pozar, David M. Microwave engineering. John Wiley & Sons, 2009.

[110] Alotaibi, S. A., Cui, Y., & Tentzeris, M. M. (2019). CSRR Based Sensors for Relative Permittivity Measurement with Improved and Uniform Sensitivity throughout [0.9-10.9] GHz Band. *IEEE Sensors Journal*.

[111] Bonache, Jordi, Marta Gil, Ignacio Gil, Joan Garcia-Garcia, and Ferran Martin. "On the electrical characteristics of complementary metamaterial resonators." *IEEE Microwave and Wireless Components Letters* 16, no. 10 (2006): 543-545.

[112] Naqui, Jordi, Miguel Durán-Sindreu, and Ferran Martín. "Modeling split-ring resonator (SRR) and complementary split-ring resonator (CSRR) loaded transmission lines exhibiting cross-polarization effects." *IEEE Antennas and Wireless Propagation Letters* 12 (2013): 178-181

[113] Yang, Chin-Lung, Chieh-Sen Lee, Kuan-Wei Chen, and Kuan-Zhou Chen. "Noncontact measurement of complex permittivity and thickness by using planar resonators." *IEEE Transactions on Microwave Theory and Techniques* 64, no. 1 (2016): 247-257.

[114] Muñoz-Enano, Jonathan, et al. "An Analytical Method to Implement High Sensitivity Transmission Line Differential Sensors for Dielectric Constant Measurements." *IEEE Sensors Journal* (2019).

[115] Alotaibi, Salem A., Yepu Cui, and Manos M. Tentzeris. "Ultrasensitive Planar Metamaterials for Material Characterization Using Tapered CSRR with Application to NDT of 3D Printed Structures." *2019 49th European Microwave Conference (EuMC)*. IEEE, 2019.

VITA

Salem received B.Sc. and M.Sc. degrees in electrical engineering from King Fahd University of Petroleum and Minerals (KFUPM), Dhahran, Saudi Arabia in 2008 and 2012, respectively. He is currently pursuing the PhD degree at the School of Electrical and Computer Engineering, Georgia Institute of Technology, Atlanta, GA, USA.

Salem joined the Saudi Arabian Oil Company (Saudi Aramco) in 2008 where he served as Electrical Engineer, Group Leader, Radiation Protection Officer and Supervisor of Conventional NDT and Project Support Unit before his leave for PhD. He holds five ASNT NDT level III certificates in Radiographic Testing (RT), Ultrasonic Testing (UT), Magnetic Pericles Testing (MT), Liquid Penetrant Testing (PT) and Visual Testing (VT) methods. He also obtained PCN level II certificates in Ultrasonic Testing (UT), Phased Arrays Ultrasonic Testing (PAUT) and Time of Flight Diffraction Testing (ToFD). He is a member of Saudi Aramco NDT standard committee. Salem is currently a member of ATHENA research group. His research interests include computational electromagnetics and the design of microwave planar metamaterials for sensing applications.

Salem participated in many national NDT committees for the development of various NDT related research and educational programs. He was a member of Saudi Aramco-KACST committee which was formed to support the establishment of the first national center for NDT research in Riyadh. He also participated as an advisor in several visibility studies and NDT academic programs development for different academic institutions.